Development of Poly(Hindered Urea) Network for Self-healable Triboelectric Nanogenerators

Twinkalben Patel

A Thesis in the Department
of Chemistry and Biochemistry

Presented in Partial Fulfillment of the Requirements
For the Degree of
Doctor of Philosophy (Chemistry)
Concordia University
Montréal, Quebec, Canada

September 2023

CONCORDIA UNIVERSITY

SCHOOL OF GRADUATE STUDIES

This is to certify that the thesis prepared By: Twinkalben Patel

Entitled: **Development of Poly(Hindered Urea) Network for Self-healable Triboelectric Nanogenerators**

and submitted in partial fulfillment of the requirements for the degree of

Doctor Of Philosophy (Chemistry)

complies with the regulations of the University and meets the accepted standards with respect to originality and quality.

Signed by the final examining committee:

_____Chair
Dr. Isabelle Benoit Gelber

_____External Examiner
Dr. Audrey Laventure

_____External to Program
Dr. Nhat Truong Nguyen

_____Thesis Supervisor
Dr. Jung Kwon Oh

_____Examiner
Dr. Louis Cuccia

_____Examiner
Dr. Xianming Zhang

Approved by _____
Dr. Louis Cuccia, Graduate Program Director

9/05/2023 _____
Dr. Pascale Sicotte, Dean
Faculty of Arts and Science

Abstract

Development of Poly(Hindered Urea) Network for Self-healable Triboelectric Nanogenerators

Twinkalben Patel, Ph.D.
Concordia University, 2023

In recent years healable electronics have garnered significant attention for their scope in next-generation electronic devices. In particular, triboelectric nanogenerators (TENGs) which are capable of harvesting energies from mechanical motions have been explored as a promising power source for self-powered devices. TENGs possess the benefits of high performance, convenience, eco-friendliness, and low cost and require great strength and functionality to perform. The incorporation of self-healability into the design of TENG systems could improve their lifetime and durability as well as their energy harvesting capabilities. Dynamic covalent chemistries have been utilized extensively for the development of covalent adaptive networks exhibiting self-healability and reprocessability. However, most approaches require the use of external stimuli to establish the reversibility of broken networks. Therefore, the development of a new strategy for the synthesis of robust networks with the balanced properties of void-filling and mechanical strength is required for value-added applications such as flexible electronics.

Hindered urea bond (urea with a bulky substituent, attached to its nitrogen atom) is a promising dynamic covalent chemistry which undergoes dynamic exchange reaction at mild temperature, with no catalysts. The reaction of a bulky amine with isocyanate allows for a simple design of a polyurea self-healing network, further broadening the scope of applications for these materials.

My Ph.D. research has aimed to study self-healing mechanisms of hindered urea chemistry and to design and synthesize new materials that can undergo catalyst-free dynamic exchange reactions and thus autonomously repair cracks and starches at lower temperatures as well as exhibit reprocessability. Furthermore, the developed networks were evaluated for TENG performances to better understand the design principles of self-healable TENGs.

Acknowledgment

First and foremost, I would like to thank my supervisor, Dr. John Oh, for providing me with guidance and support throughout my graduate studies. His immense knowledge and experience have encouraged me in the time of my academic research life to always achieve great things. I would also like to thank him for providing me with the opportunity to collaborate with other researchers and expand my knowledge and develop collaborative works.

I am grateful to have two very knowledgeable committee members, Dr. Louis Cuccia and Dr. Zhibin Ye for their constructive feedback in the committee meetings. Special thanks to Dr. Louis Cuccia for being my interim supervisor and providing helpful knowledge about TENGs. Thanks to Dr. Nhat Truong Nguyen, Dr. Xianming Zhang and Dr. Audrey Laventure for accepting to be my defence examiners.

I would like to extend my appreciation towards Hyun Wook Jung and Hyunhyub Ko at Korea University and National Institute of Science and Technology respectively for their collaboration on self-healing and TENG properties analysis.

I would like to thank my collaborators in Oh research group for their contributions to my thesis projects, including Dr. Gandhi for his contribution to the fluorinated block co-polymer project as well as for always being available to provide insight. My deepest gratitude goes to the other members and former Oh members with whom I have unforgettable memories including, Dr. Sungmin, Sunghwa, Peter, Keaton, Arman, Kamal, Ge, Xiaolei, Chaitra, Newsha, Bakr, Yuanfeng, Kadambari, Sofia, and Brandon

I am also grateful to the technical staff who keep our facilities running: Dr. Alexy Denisov and Dr. Constantin Yannopoulos at Concordia NMR facility, Dr. Daniel Rosca and Dr. Heng Wang at Concordia Center of Composite (ConCom), Dr. Nooshin Movahed at Centre for NanoScience Research and Dr. Mohini Ramkaran at McGill University.

This work could not be done without funding from the funding agencies, including Mitacs, and the Faculty of arts and science graduate student award at Concordia University.

Finally, I would like to thank my parents for providing unfailing support and continuous encouragement throughout my years of study. I would like to thank my brother, Meet, for always being there to cheer me up and Pinank for always being there for support whenever needed.

Dedication

This thesis is dedicated to my parents for their endless love, support and encouragement.

Contribution of Authors

This thesis is an original work by the author of this thesis under the supervision of Dr. Jung Kwon (John) Oh. Chapters 2, 3, and 4 are reproduced in part or in whole with permission from the publishers, from the original articles. The author has conducted experimental design, data collection and analysis, and manuscription preparation and revision for all the chapters under guidance of Dr. Oh. The detailed contributions for each chapter are as follows:

Chapter 2: Dynamic Covalent Adaptive Polymer Network Materials based on Hindered Urea Bonds

The entire chapter 2 has been published as: T. Patel and J. K. Oh, *Journal of Macromolecular Science, Part A*, **2023** 60, 307-320

Chapter 3: Self-Healable Reprocessable Triboelectric Nanogenerators Fabricated with Vitrimeric Poly(hindered Urea) Networks

The entire chapter 3 has been published as: T. Patel, M.P, Kim, J. Park, T.H. Lee, P. Nellepalli, S.M. Noh, H.W. Jung, H. Ko, J.K. Oh, *ACS Nano* **2020**, 14, 9, 11442–11451

Contributions: Dr. Minsoo P. Kim conducted TENG studies, Junyoung Park conducted self-healing studies with NST/AFM. Dr. Pothana Gandhi Nellepalli assisted the preparation of Introduction and editing of manuscript.

Chapter 4: Self-healable triboelectric nanogenerators based on ionic poly(hindered urea) network materials cross-linked with fluorinated block copolymers

The entire chapter 5 has been published as: P. Nellepalli, T. Patel, M.P. Kim, J. Park, Z.Ye, H.W. Jung, H. Ko, J.K. Oh, *Polymer Chemistry* **2022**, 13, 4343-4351

Contributions: P. Nellepalli and T. Patel were equally contributed to this work. Dr. Pothana Gandhi Nellepalli conducted initial frame works on synthesis of FBCP and fabrication and characterization of PHU network materials . Dr. Minsoo P. Kim conducted TENG studies, Junyoung Park conducted self-healing studies with NST/AFM.

Chapter 5: **Heterogeneous Dynamic Poly(Hindered Urea) Network Materials Crosslinked with Methacrylate Polymer Crosslinker**

Contributions: Junyoung Park conducted self-healing studies with NST/AFM.

Table of Contents

List of Figures

List of Tables

List of Abbreviations

AFM	Atomic force microscopy
ARGET	Activators regenerated by electron transfer
ATRP	Atom transfer radical polymerization
DSC	Differential scanning calorimetry
FT-IR	Fourier transform infrared spectroscopy
GPC	Gel permeation chromatography
HUB	Hinder urea bond
IPDI	Isophorone diisocyanate
MEK	Methylethylketone
NMR	Nuclear magnetic resonance spectroscopy
PDMS	Bis(3-aminopropyl) terminated polydimethylsiloxane
PM	Polymethacrylate homopolymer
PHU	Poly(hindered) urea
PU	Polyurea
PUU	Polyurethane-urea
RAFT	Reversible addition fragmentation chain transfer
SH-TENG	Self-healable triboelectric nanogenerators
TBAEMA	2-(t-butylamino)ethyl methacrylate
TENG	Triboelectric nanogenerators
TGA	Thermogravimetric analysis
THF	Tetrahydrofuran

Chapter 1: Introduction

1.1 Energy Harvesting

Energy harvesting is the process of scavenging for sustainable electrical energy from wasted mechanical energy in nature or everyday life. These ambient energies are sourced from sunlight, wind, moving water, motion and geothermal energy. Depending on input energy, various energy harvesting technologies have been explored such as solar cells, wind power plants, and mechanical and thermal energy harvesting.

Mechanical energy harvesting in the industry is widely attractive as its presence is abundant, and moreover advantageous as they are not limited to any environmental condition such as weather. These mechanical energy sources range from vibration, ocean waves, structural noises, ultrasounds and sounds, as a function of the frequency. In general, mechanical energy sources are characterized by their frequencies, amplitudes, and acceleration levels, based on which potential power generation levels can be assessed. To convert mechanical energies into useful electricity, energy conversion mechanisms such as piezoelectric, triboelectric, and electromagnetic effects can be implemented. Depending on the energy conversion in use, triboelectric nanogenerators (TENGs),[13, 14] piezoelectric nanogenerators (PENGs),[15-17] electromagnetic nanogenerators (EMGs), and electrostatic nanogenerators [18] have been utilized.

1.2 Triboelectric Nanogenerators

TENGs have attracted significant attention from researchers as an effective technology for harvesting different types of mechanical energy due to multiple advantages such as versatile material choice, and simple and low-cost design process. TENGs have been reported to utilize energy from a vast number of environments, for instance, wind energy created by a passing high-speed train. This design not only utilizes the wasted wind energy but also offers the potential strategy for large-scale wind energy harvesting by TENGs.[19] Another source of green energy comes from sound, which is present everywhere. Multiple different designs of sound harvesting TENGs have been reported including a 3D-printed acoustic TENG for a self-powered edge sensing system for real-time speech recognition,[20] an electrospun PVDF polymer tube integrated with TENG for multifunctional sensing,[21] and self-powered TENG auditory sensor for constructing an

electronic auditory system and an architecture for an external hearing aid in intelligent robotic applications.[22] Structural vibration, which exists in people's daily lives from buildings, bridges, automobiles and industrial environments have abundant source of energy to harvest.[23] Variety of TENG devices have been demonstrated for structural vibration harvesting and applications, including a triple-cantilever based TENG for harvesting vibration energy,[24] a free-fixed TENG for train wheel energy harvesting and monitoring,[25] and a multiple-mode TENG for harvesting the freight train carriage joints and self-powered freight train monitoring.[26] Human body mechanical motions such as walking, running, and limb movement allow TENGs to be used for wearable and biomedical harvesting applications.[27, 28] Human gesture sensing and realtime clinical human vital sign monitoring have been successfully realized via various kinds of TENGs, including a breathable, waterproof fabric-based multifunctional TENG,[29] and a hierarchically designed high-performance stretchable TENG using ferroelectric barium-titanate-coupled 2D MXene ($Ti_3C_2T_x$) nanosheets.[30] TENGs offer a promising platform for sustainable power generation via converting various kinds of mechanical energy sources from wind, sound, structural vibrations, and human motions.

1.2.1 Fundamentals of TENGs

The fundamental theoretical origin of TENG is Maxwell's displacement current, where the term related to polarization-induced current $\partial P/\partial t$ is directly related to the output current of TENGs.[31] To date, four fundamental operational modes of TENG have been distinguished such as, vertical contact separation, lateral sliding, single-electrode and free-standing mode.[32] The most common is the contact separation mode which is composed of two oppositely charged tribo-materials and two electrodes (Figure 1.1a). A TENG relies on triboelectrification, also known as contact electrification. This phenomenon is the transfer of charge, when two different materials are charged after contact and separation from one another.[33]This situation is often found in nature in the example of lightening during a thunderstorm.

In the first step the surface charges on both the dielectric materials are equal in density due to contact electrification. Upon separation of these materials, it results in an electrostatic induction, caused by the localization of the opposite charges on the different surfaces, creating an electric field. This creates a potential difference between the two tribo-materials. When continuous force is applied by an external mechanical source, the repelled electrons in the negative dielectric

material flow to the opposite electrode producing alternating current (AC) according to the charge polarity, i.e., positive or negative. At the balanced state of TENGs, the device turns back to the initial state. When the two materials are brought into contact with each other by an applied external force, the inner surfaces produce opposite static charges with a charge density. Afterward, the release of the external force leads to the separation of the two tribo-materials, producing a potential difference (V) between both electrodes.[31]

While the concept of contact electrification has been greatly studied in the past millennium, the exact mechanism of contact electrification is still unknown and highly debated. To enhance triboelectrification it is important to improve output power by understanding the physics of the process. Extensive research has been focused on the triboelectrification between solid-solid rather than solid-liquid, solid-gas or liquid-gas contact. Since the first invention of TENG by Prof. Wang's group in 2012, most newly researched concepts involve solid-solid than that of other triboelectrification, therefore the underlying mechanism of non-solid based triboelectrification have yet been explored in-dept.[34] However, even in solid-solid triboelectrification, it is not exactly known which charge species are being transferred. It has been suggested that besides electron transfer, ions and material transfer models have also been proposed for charge transfer especially in systems with polymer materials.

The first proposed model was the electron transfer model, which indicates that the electrons carry the charge, which is transferred from one surface to the other during contact electrification (Figure 1.1b). It is believed that this is the dominating mechanism for metal-metal systems, where the work function and Fermi level define the amount of charge generated. The work function being the minimum amount of energy required to remove an electron from a solid surface.[35] For metal-dielectric material the electron transfer model is also probable for contact electrification. Researchers have found that besides work function, properties of the dielectric materials, such as electronic properties and electron affinity correlate to contact electrification. It has been found that the electron transfer may be occurring due to the thermionic emission effect at the surface as results show that decays at a faster rate with higher temperatures when contacting metal with SiO_2.[36] The mechanism of electron transfer during contact electrification between a dielectric material and another dielectric material is complex and still under debate among researchers.

As opposed to electron transfer model, ion transfer model has been proposed, where mobile ions could transfer between the materials, when they come into contact (Figure 1.1c), which results in one surface being positively charged and another being negatively charged. This model has been proposed to be the fundamental mechanism of contact electrification involving two dielectric materials. Surfaces functionalized with ionic groups showed that polarity of the charge after contact electrification was always the same as the polarity of the ionic functional groups, and the amount of charge generated was proportional to the surface area coated with ionic functional groups.[37] This model has also been proposed for dielectric material which does not contain ionic functional groups on the surface. This is possible since the surfaces have a tendency to adsorb water from the atmosphere, causing the transfer of water ions (H^+ and OH^-) from one surface to another.[38] The charge transfer is proportional to the zeta potential of the surfaces, which is defined by the tendency of the surfaces to adsorb aqueous ions. Other possible source of ion transfer may occur due to heterolytic cleavage of molecular bonds during contact electrification or even Lewis acidity/basicity of the contacting materials.[39]

The last mechanism is a material transfer (Figure 1.1d), which was proposed after the discovery of mosaic charge patterns between polymers.[40] The mosaic patterns were confirmed due to material transfer by characterization techniques such as confocal Raman spectroscopy and X-ray photoelectron spectroscopy. This discovery opened a new area of interest to researchers.

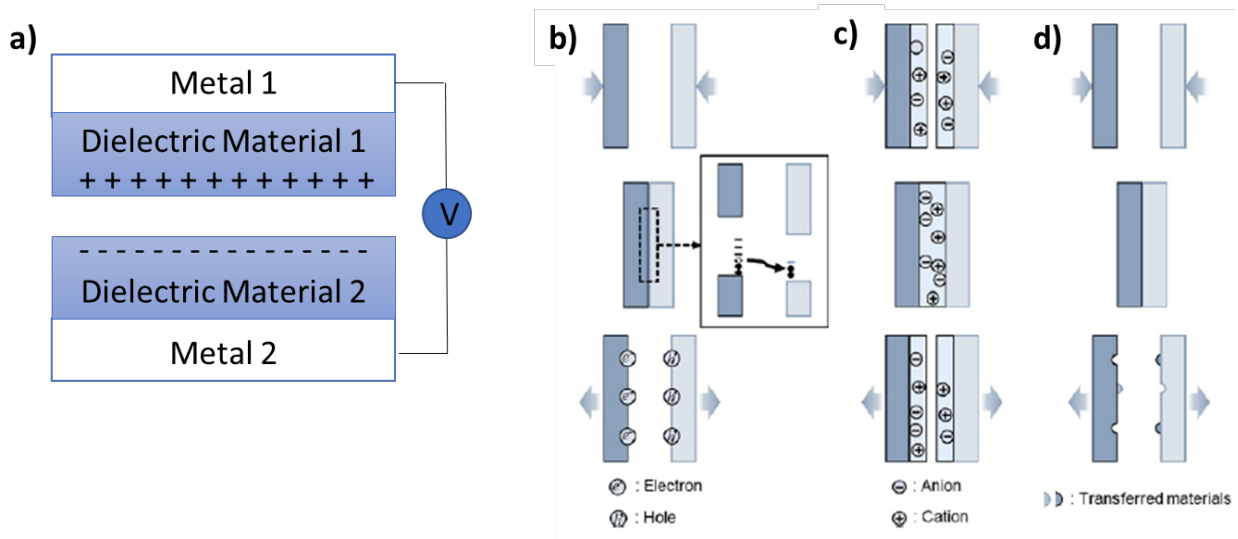

Figure 1.1 Schematic diagram of the vertical contact separation mode (a), model of electron transfer mechanism between two insulators (b), model of ion transfer between two insulators (c), model of material transfer between two insulators (d).[1]

1.2.2 Recent Trends of TENGs

The charge surface density is highly dependent on the properties of the material in the triboelectric series. Thus, numerous strategies have relied on the choice of materials in the triboelectric series, along with chemical and physical modifications, such as work function differences, stretchability, dielectric constant, surface roughness, and functionalization. Physical surface modification has been explored to achieve high output performance of TENGs, such as direct patterning,[41] surface attached nanoparticles,[42] and forming porous sponge structures.[43] All these techniques enlarge the contact surface area and roughness, consequently improving the surface charge density. For instance, sandpaper like micropattern on TENGs easily increases the surface contact thus enhancing the output.[44] Chemical modification of the surface could introduce, the possibility of fabricating diverse material surfaces, irrespective of their original triboelectric properties and allow the opportunity to change these properties. Multiple different techniques have been explored such as doping ions,[45] and utilizing functional molecules.[46] Shin et al. prepared multiple poly(ethylene terephthalate) films as substrate, which can be functionalized to be an electronegative and electropositive material, demonstrating atomic-level surface functionalization of a contact material.[47]

An important parameter for enhancing triboelectric properties is the dielectric constant (or relative permittivity). This is a factor where the applied electric field is decreased through the dielectric polarization of materials and can be enhanced by engineering dielectric materials through the introduction of dielectric additives. High permittivity nanoparticles are utilized to improve the dielectric constant of polymer nanocomposites, such as Ag nanowires,[48] CNTs,[49] and graphene.[50] The Polymeric network provides robust structural integrity. Natural polymers, such as protein and polysaccharides,[51] along with poly(vinyl alcohol)[52] and polyacrylamide hydrogel[53] have been used.

1.2.3 Challenges of Conventionally Designed TENGs

Since its initial discovery, TENG development has advanced drastically, however, the major issue of conventionally designed TENGs involves the failure of their self-charging power and the suppression of their output performance and lifetime. This is mainly because they are subjected to long-term mechanical impact and thus are susceptible to fracture and surface damage.

The promising solution to address this issue is the integration of dynamic (or reversible) linkages in the design of triboelectric materials, thus developing self-healing TENGs (SH-TENGs). Early approaches utilize weak supramolecular chemistry, however, the resultant SH-TENGs suffer from poor mechanical properties, which caused the output to worsen for robustness and durability upon damage.[54] A promising approach involves developing cross-linked polymers with reversible covalent bonds. Xu et al. developed a self-healable TENG using dynamic disulfide and hydrogen bond based healable PDMS-polyurethane with nickel magnetic balls. Upon damage to the surface, the hydrogen and disulfide bonds recovered when heated at 65 °C for 2 hrs. However, due to the bulkiness of the magnetic electrodes, the device was found to be non-stretchable, and prone to delamination from the matrix.[55] Other studies have explored imine chemistry,[56] aromatic disulfide metathesis,[57] and polysulfide elastomer[58] for SH-TENGs.

1.3 Covalent Adaptive Networks (CANs)

CANs were adopted due to the inability of crosslinked polymers or thermosets to be reprocessed or recycled. CANs are designed with dynamic covalent chemistries (DCCs). Well-developed CANs possess structural integrity and strength, while being reprocessable and recyclable. Given these features, CANs have been extensively explored as effective building blocks in the construction of various self-fabricating materials such as dynamic polymers, responsive sensors, adaptive membranes, and dynamic networks.[59, 60] Figure 1.2a shows typical DCCs that have been explored to be integrated in self-healable and reprocessable polymeric materials. They include Diels-Alder (DA)/retro-DA (rDA) adduct,[61] disulfide,[62] diselenide,[63] boronic ester,[64] and imine chemistries.[65]

DA/rDA chemistry involves the formation of a cycloadduct (or DA linkage) mostly through the cycloaddition of furan and maleimide groups even at ambient temperatures. Through rDA reaction at elevated temperature (>120 °C), the formed six-membered cycloadduct linkages are subjected to thermal cleavage to the corresponding furan and maleimide moieties, which can be rearranged to cycloadduct linkages upon cooling.[66] Disulfide bond (-SS-) undergoes dynamic exchange reaction through thiol-disulfide exchange or disulfide metathesis in the presence of base catalysts (such as phosphines or thiols), upon heating, or under UV irradiation.[67-69] Diselenide (Se-Se) undergoes dynamic exchange reactions under various conditions such as visible light, heat, and reduction. Diselenide possesses a lower bond energy (172 kJ/mol) than its counterpart of

disulfide (240 kJ/mol).[70] Compared with disulfide linkage that can undergo an exchange reaction under UV irradiation, diselenide metathesis can be induced by irradiation of visible light through radical mechanism.[71] Boronic esters in 5- or 6-membered rings undergo reversible exchange reaction or boronic ester metathesis under mild temperature conditions (>50 °C).[64] Imine (C=N) bond is generally formed by the condensation of an aldehyde and a primary amine in the presence of an acid catalyst as water is eliminated. The exchange reaction of imine bond, particularly benzoic imine, proceeds efficiently in the absence of external catalysts, but at elevated temperature.[65]

These CANs can be classified based on the mechanism of reversible exchange reaction. Dissociative mechanism relies on the covalent bond being broken and reformed due to thermodynamic equilibrium being shifted via stimulus (Figure 1.2b). The crosslinking density is changed. A typical example is dynamic DA/rDA chemistry. In contrast, associative exchange mechanism involves intermediates. The old bond is only broken when the new linkage is formed, ultimately the crosslinked density remains unchanged. Diselenide, disulfide, boronic ester and imine chemistry undergo associative mechanism.[72]

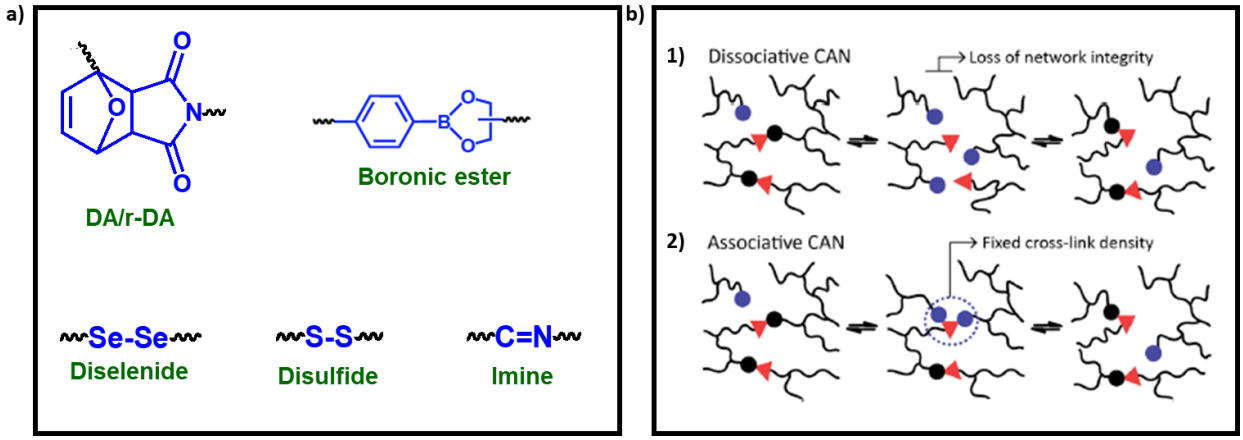

Figure 1.2 Typical dynamic covalent linkages include DA-rDA cycloadducts, disulfide, diselenide, imine, boronic ester, and hindered urea bonds (a). Schematic illustration of dissociative and associative mechanism for CANs (b).[72]

The ability of CANs to break and reform covalent crosslinks opens the possibility to bond multiple polymer networks after fabrication. CANs are known to completely recover their original mechanical properties despite the breaking of bonds during damage.[73] Utilizing CANs capability to form bonding and self-heal, will eventually allow for materials that were initially single use to

be restored. These materials can exhibit shape memory capabilities, allowing the material to be bent, folded wrapped or shaped into desired structures, when heated or appropriately stimulated. The material can either have a fixed temporary shape[74] or alternate between two or more shapes.[75]

1.4 Objective and Scope of My PhD Thesis

My PhD thesis focuses on the exploration of hindered urea chemistry, to study its self-healing abilities and to synthesize a variety of dynamic poly(hinderedurea) (PHU) networks crosslinked with bulky hindered urea bonds (HUBs) for TENG applications. To overcome self-charging power failure, SH-TENGs have been highly sought out for showing promising solutions to address this issue. Hindered urea chemistry is designed to take advantage of its key features of "dynamic" and "reversibility", which is highly beneficial in creating a self-healing material. These designed systems were characterized by their self-healing, thermal and mechanical properties as well as their TENG properties. The executive summary of each chapter of the thesis is listed below.

Chapter 2. Covalent adaptive polymeric networks are created by crosslinking polymers through dynamic covalent bonds that can undergo reversible exchange reactions. These networks possess excellent mechanical properties, dimensional stability, and solvent resistance similar to traditional thermoset materials. In addition, they exhibit unique properties such as self-healing, reprocessability, sustainability, and recyclability. One promising type of dynamic covalent bond for developing these network materials is the hindered urea bond (HUB), which involves a bulky group attached to one of the nitrogen atoms. HUB-bearing networks have found applications in diverse fields such as energy harvesting and storage, sensors, flexible and wearable electronics, and surface coatings, thanks to their dynamic characteristics. This review focuses on summarizing the advancement in strategies for fabricating dynamic polymer networks based on HUBs. It covers the design and synthesis of effective HUBs incorporating various bulky amino groups, as well as the synthesis of different polymeric materials used in these networks.

Chapter 3. In recent times, there has been a lot of excitement and promise surrounding the development of highly deformable and healable electronic devices, particularly in the context of next-generation technology. One area of interest is self-healable triboelectric nanogenerators (SH-TENGs), which offer great potential due to their ability to combine the triboelectric effect, electrostatic induction, and self-healing capabilities. However, most SH-TENGs have relied on weak polymeric networks that are healed using reversible supramolecular interactions or disulfide

bonds. Consequently, these materials suffer from poor mechanical properties and are prone to creeping. To overcome this challenge, we have successfully integrated a mechanically robust and self-healable poly(hindered urea) (PHU) network into the fabrication of efficient TENGs. The PHU network we designed possesses flexibility while exhibiting exceptional mechanical properties, including a high tensile strength of up to 1.7 MPa at the point of rupture. The network demonstrates rapid and repeatable self-healing capabilities, allowing for the complete recovery of triboelectric performance after the damaged surfaces have healed. Moreover, the enhancement of the dielectric constant induced by interfacial polarization gives our SH-TENG the highest triboelectric output performance (169.9 V/cm^2) reported among healable TENGs. This research opens up new possibilities for the development of mechanical energy-harvesting devices and self-powered sensors that offer excellent stretchability, high recoverability, and strong mechanical strength.

Chapter 4. The triboelectric nanogenerator (TENG) has gained attention as an affordable device for harvesting mechanical energy and converting it into electricity. Researchers have explored incorporating self-healing capabilities into TENGs to enhance their lifetime and functionality, alongside modifying the structural and functional properties of triboelectric materials. This study showcases the versatility of a reactive block copolymer method for creating ionic poly(hindered urea)-based covalent adaptive networks that contain pendant fluorinated species and utilize an ionic liquid as effective self-healable triboelectric materials. The reactive block copolymer used in this approach is precisely designed with a dynamic t-butylamino block to enable self-healing and a dielectric fluorinated block to enhance the triboelectric output. It serves as a multifunctional crosslinker. By employing a two-step polyaddition process in conjunction with physical blending with an ionic liquid, the resulting ionic fluorinated poly(hindered urea) networks, crosslinked with the reactive block copolymer, exhibit improved TENG outputs while maintaining good self-healing capabilities and mechanical strength. Remarkably, the damaged surfaces of these networks can recover over 90% of their triboelectric performance. This study highlights the versatility of the novel reactive block copolymer approach for fabricating dynamic PHU networks that possess desirable properties, making them valuable for advanced self-healing TENG-based energy harvesting devices and electronics.

Chapter 5. This study aimed to create dynamic hybrid network materials by utilizing a specific polymethacrylate homopolymer with t-butylaminoethyl pendants (PM) as a multifunctional crosslinker. The PM used in this work was a well-defined polymer with a narrow molecular weight distribution, synthesized through controlled radical polymerization. It was incorporated into the polyaddition process with a polyurea prepolymer. To investigate the relationship between structure and properties, a range of dynamic hybrid networks combining PHU (poly(hindered urea)) and PM in different proportions were prepared. These networks were then subjected to various tests to evaluate their optical, thermal, and mechanical characteristics. Additionally, their self-healing and reprocessability capabilities were assessed.

Chapter 6. The conclusions from my research project are summarized and future research directions are proposed.

Chapter 2. Dynamic Covalent Adaptive Polymer Network Materials Based on Hindered Urea Bonds

2.1 Introduction

Covalent adaptive networks (CANs) are covalently crosslinked polymer networks fabricated through the incorporation of dynamic covalent bonds that undergo reversible exchange reactions autonomously or in response to external stimuli such as changes in temperature and pH, irradiation of light or the presence of chemicals.[76-82] These networks differ from physically crosslinked networks containing dynamic noncovalent bonds which are based on supramolecular interactions such as hydrogen bonding and metal-ligand coordination as well as ionic, π-π, and host-guest interactions. Due to these features, CANs have been integrated into the development of conventional thermosets of various polymers including polyurethane, epoxy, polyester, poly(meth)acrylate, and their hybrids.[83-89] CAN-based thermosets retain the intrinsic properties of conventional thermosets such as good mechanical properties, dimensional stability, and solvent resistance. Furthermore, CAN-based thermosets possess built-in-ability that can repair damages and thus improve their lifetime as well as have reprocessability, sustainability and recyclability.[90-92]

Many dynamic covalent bonds and interactions typically including Diels-Alder (DA)/retro-DA adduct, disulfide, diselenide, imine, ester, and boronic ester bonds have been explored to develop self-healable reprocessable polymeric network materials.[92-95] Compared with these dynamic chemistries that require the introduction of heteroatoms such as sulfur and boron and hetero-bonds such as -C=N- bonds, hindered urea bond (HUB) is the essential building block for industrially-important polyureas (PUa) and polyurethanes (PUs). As illustrated in Figure 2.1, the HUB contains a bulky group on one of the two nitrogen atoms in a urea bond.[96] The HUB containing a bulkyamino group is generally formed by the reaction of an isocyanate (-NCO) with a secondary-bulkyamine (-NHR, R: bulky group). Because of the asymmetric geometry of the substituents (H and R) on the nitrogen atoms in the HUB, the carbon-nitrogen bond containing the bulky group is much weaker, compared with the other bond attached to the hydrogen atom. The asymmetric bond can be dissociated to the corresponding isocyanate and bulkyamino groups under a mild thermal condition, e.g. at lower and even ambient temperature, compared with DA/r-DA bond requiring elevated temperature (>120 °C) for the occurrence of r-DA reaction.[97-99] Consequently, HUB

undergoes a reversible exchange reaction, which allows for the HUB-bearing CANs to exhibit self-healability and reprocessability.

Given systematic investigation based on the dissociation rate constant (k_{-1}) and equilibrium constant ($K_{eq} = k_1/k_{-1}$) reported by Cheng's group (see Figure 2.1),[71] tertiary-butylamino group has been identified to be an effective bulkyamino group for the construction of efficient HUBs. Further to t-butylamino-based HUBs, other HUBs with different bulkyamino groups such as piperazine, isopropylamino, pyrazole, and phenylamino groups have been synthesized to fabricate a variety of dynamic polymer networks bearing HUBs. Because of the chemical route to synthesize HUBs by the reaction of isocyanate and amine groups, the fabrication of dynamic networks based on poly(urethane-urea) (PUU) or polyurea (PUa) bearing HUBs has been extensively exploited. Further, other polymer networks bearing HUBs such as epoxy resin, polysulfide, and poly(meth)acrylate have been developed.

This review describes recent advances in the development of effective strategies to fabricate dynamic polymer materials bearing HUBs that exhibit self-healability and reprocessability through the reversible exchange of dynamic HUBs. The strategies are focused on the design and synthesis of effective HUBs with various bulkyamino groups that undergo rapid bond exchange, thus enabling the synthesis of reversible networks to be diverse as step-growth networks of PUUs, PUas, epoxy resins, and polysulfides as well as chain-growth networks of poly(meth)acrylates.

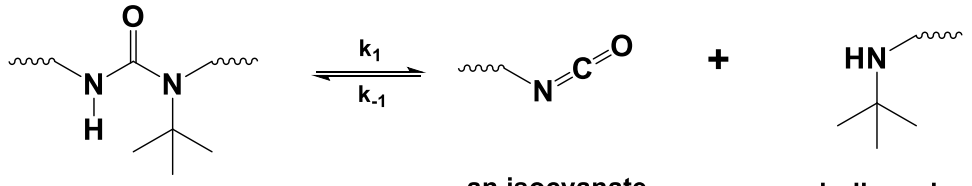

Figure 2.1. Schematic illustration of a HUB bearing t-butylamino group that undergoes dynamic reversible exchange reaction.

2.2 Step-growth PUU or PUa Networks

Step-growth networks of PUUs and PUas have been generally fabricated by the polyaddition of polybulkyamines, polyols and/or polyamines with polyisocyanates. Polybulkyamines are generally secondary with various bulkyamino groups, including mainly t-butylamino group as well

as piperazine, isopropylamino, pyrazole, and phenylamino groups. Depending on the number of the bulkyamino groups, they can be classified to be di, tri, tetra functional or polymeric bulkyamines. This section summarizes various strategies to fabricate dynamic step-growth PUU or PUa networks containing HUBs with respect to various polybulkyamines.

2.2.1 Difunctional Bulkyamines Bearing t-Butylamino Group(s)

Figure 2.2 shows the chemical structures of difunctional bulkyamines bearing t-butylamino groups that have been used to synthesize dynamic PUU network materials with reversible HUBs. These t-butylamino-bearing bulkyamines are commercially available or have been synthesized by facile organic reactions. The t-Butylamino group reacts with an NCO group of polyisocyanates to form t-butylamino-based HUB on the backbones of PUU networks.

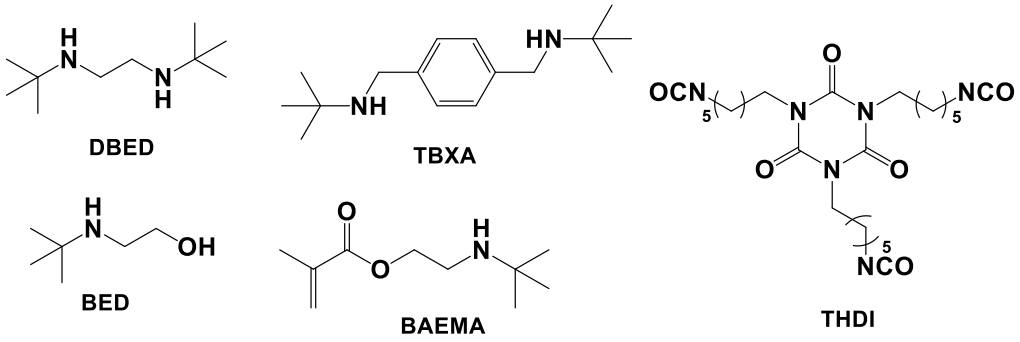

Figure 2.2. Chemical structures of various secondary bulkyamines (DBED, BED, TBXA, and BAEMA) and a trifunctional polyisocyanate (THDI) used for the fabrication of dynamic PUU networks bearing t-butylamino-based HUBs.

N,N-di-(t-butyl)ethylenediamine (DBED) is an aliphatic, secondary amine bearing two t-butylamino bulky groups. DBED is commercially available and has been extensively used for step-growth polymerization through the polyaddition of polyols (or polyamines) with polyisocyanates to fabricate dynamic PUU materials based on t-butylamino-bearing HUBs. Ko and coworkers reported self-healable PUU elastomeric materials synthesized by the polyaddition of DBED with a reactive mixture consisting of 3-isocyanatomethyl-3,5,5-trimethylcyclohexyl isocyanate (IPDI) and polycaprolactone diol (PCL-DOH) in the presence of DBTDL (a tin catalyst). The synthesized PUUs were coated on poly(ethylene naphthalate) and then spin-coated with silver nanowires (AgNWs) to fabricate a transparent, flexible, and self-healable thermoacoustic loudspeaker based on AgNW-PUU conductive electrode. The device generated a sound pressure level of 61 dB at 10

kHz frequency (alternating current 7 V/direct current 1 V). Further, it recovered the original sound after healing the surface damages of electrodes at 95 °C and 80% relative humidity.[100] Zheng and coworkers fabricated an organic-inorganic hybrid PUU elastomer by the incorporation of polyhedral oligomeric silosesquioxane (POSS) diol to the polyaddition of DBED with 4,4′-methylene bis(phenyl isocyanate) (MDI). The formed hybrid PUUs were microphase-separated and the POSS cages were aggregated into the microdomains with the size of 10-20 nm. The POSS microdomains acted as nano-crosslinking sites, rendering the PUUs physically crosslinked and imparting shape memory properties to the PUUs. The formed films displayed the properties of thermoset elastomers with good thermomechanical properties.[101] The synthesized PUU materials turned to be linear thermoplastic elastomers because all reactants used are difunctional (functionality, f = 2). These thermoplastic PUUs are known to be phase-separated with hard domains. Although being physically crosslinked through hydrogen bonding interactions of urethane or urea bonds in the hard domains, they could be mechanically weak and dimensionally unstable when external stress is applied.

Chemical crosslinking can afford to improve such drawbacks of thermoplastic PUU materials as to fabricate chemically crosslinked PUU network materials. An approach to chemical crosslinking is to incorporate multifunctional, particularly trifunctional alcohols (f > 2) as crosslinkers into the polyaddition of DBED with diisocyanates and diols, yielding crosslinked PUU networks containing dynamic t-butylamino-based HUBs. Figure 2.3 shows the general scheme for the approach.

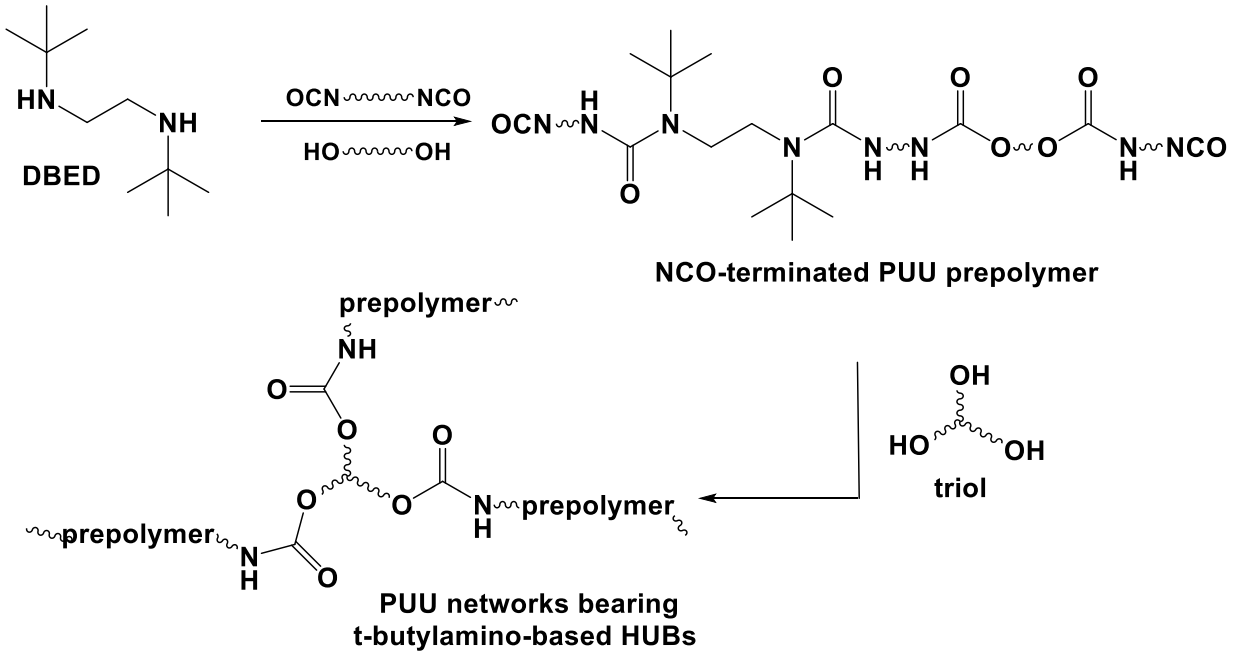

Figure 2.3. An approach exploring the incorporation of a trifunctional alcohol (a triol) as a crosslinker into the polyaddition of DBED with diisocyanates and diols to fabricate crosslinked PUU networks containing dynamic t-butylamino-based HUBs.

Cheng and coworkers used triethanolamine (a triol) for the polyaddition of DBED, poly(tetramethylene ether glycol) (PTMEG), and 1,6-hexanediisocyanate (HDI). The crosslinked PUU networks were capable of catalyst-free dynamic property change and autonomous repairing at low temperatures.[71] Zhang and coworkers introduced renewable castor oil (a triol) in the polyaddition of DBED with IPDI to develop biobased PUU network materials for repairability, reprocessability, and robust mechanical properties. The network materials had extremely low relaxation times (12.3 to 221 s at 100 °C), excellent scratch healing efficiency (88.9 -100% at 100 °C for 10 min) and recyclability. Furthermore, they exhibited high adhesion strength when bonding stainless steel and turned to be re-used at least 5 times without significant deterioration in adhesion strength.[102] Other reports describe the use of 1,1,1-tris(hydroxymethyl)propane (a triol) with 1,3-bis(isocyanatomethyl)cyclohexane, PCL-DOH, and DBED in polyaddition to fabricate reconfigurable PUU thermoset with triple-shape-memory performance[103] as well as glycerin (a triol) with HDI, poly(ethylene glycol) (PEG), and DBED for healable, reconfigurable, reprocessable thermoset shape memory PUU with highly tunable topological rearrangement kinetics.[104]

Another approach is to use multifunctional isocyanates as crosslinkers for the polyaddition of diols with DBED to fabricate crosslinked PUU networks. A trifunctional homopolymer of hexamethylene diisocyanate, i.e. (2,4,6-Trioxotriazine-1,3,5(2H,4H,6H)-triyl) tris(hexamethylene) isocyanate (called THDI) has been typically used and its chemical structure is shown in Figure 2.2. Sun and coworkers fabricated ultra-durable ionic skins with excellent healability and high sensitivity by impregnating ionic liquid (IL) into a mechanically robust PUU network. As illustrated in Figure 2.4, the ionic PUU networks were prepared by crosslinking through the polyaddition of THDI with linear PUU prepolymer consisting of PCL-DOH, PEG, HDI, and DBED, followed by mixing with 1,2-dimethyl-3-ethoxyethyl-imidazolium bis(trifluoromethanesulfonyl)imide. The resulting ionogel-based ionic skins had high mechanical strength, good elasticity, Young's modulus similar to that of natural skin, and excellent healability. Further, they exhibited a high sensitivity to a wide range of strains (0.1–300%) and pressures (0.1–20 kPa) as well as highly reproducible electrical response over 10,000 uninterrupted strain cycles.[2] Cheong and coworkers developed a self-healing automotive clearcoat based on dynamic PUU network which contains N-butyl-substituted diammonium borate as a photothermal dye. The network was crosslinked by the polyaddition of THDI with a polyurea prepolymer formed from DBED and IPDI. Upon optimization of dynamic HUBs and the concentration of the photothermal dye, the transparent automotive clearcoat exhibited excellent and fast scratch-healing performance compared with a commercial automotive clearcoat, when being heated to 70 °C under focused sunlight irradiation.[105] The approach utilizing the polyaddition of DBED with THDI has been further explored for the fabrication of hydrolysable PUU networks[106] and shape memory PUU networks with triple dynamic covalent bonds.[107]

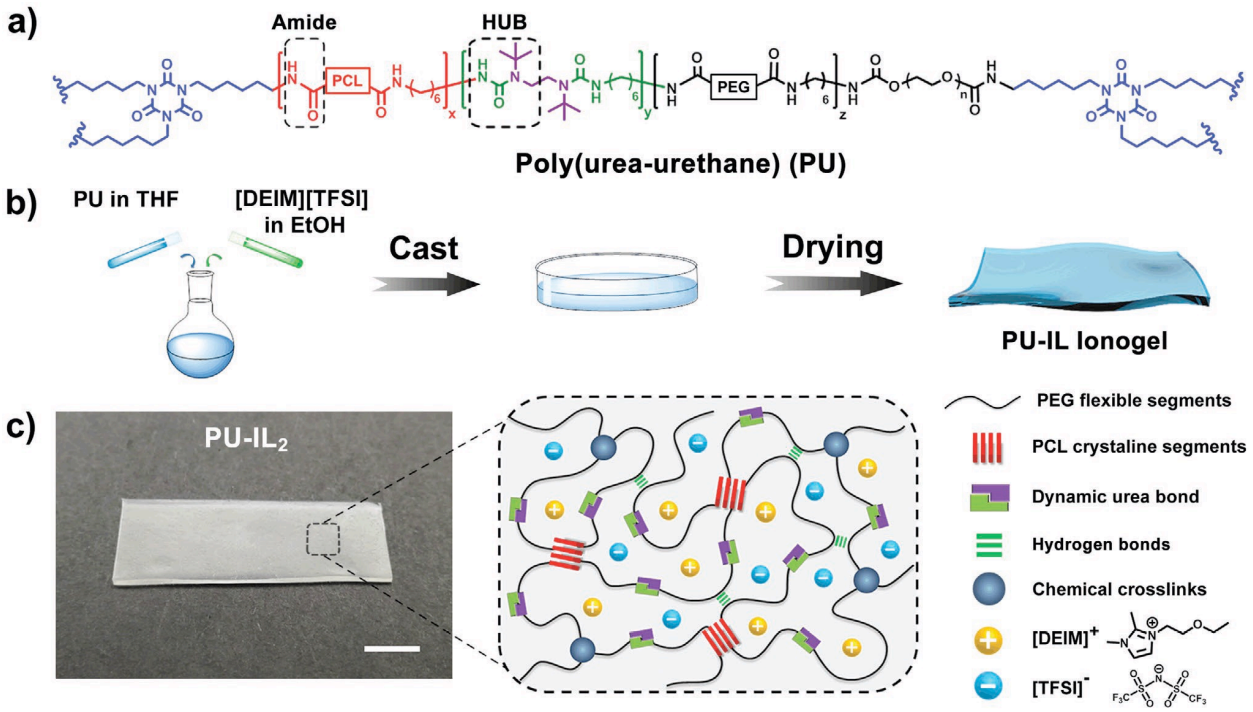

Figure 2.4. As an example to illustrate an approach to fabricate dynamic PUU networks bearing t-butylamino-based HUBs with the use of trifunctional HMDI polyisocyanates: chemical structure of dynamic PUU network bearing t-butylamino-based HUBs (a), schematic illustration to fabricate PUU-IL ionogels (b), digital image of PUU-IL ionogel and its corresponding schematic structure (scale bar = 2 cm) (c).[2] Copyright 2020 WILEY.

1-(*t*-Butyl)-1-ethylurea (BEU) shown in Figure 2.2 consists of both a t-butylamino group that can form t-butylamino-based bulky urea bond and a hydroxyl group that can form a urethane bond by the reaction with NCO group of polyisocyanates. To synthesize dynamic HUB-based PUU networks with BEU, other polyols are not needed. Cheng and coworkers explored the polyaddition of BEU with THDI crosslinker to develop malleable and recyclable PUU thermosets. The new thermoset exhibited malleability under mild heating without the need for a catalyst, while having comparable mechanical properties and solvent resistance to conventional thermosets, as well as efficient recyclability.[108] Rowan and coworkers fabricated a variety of dynamic PUU networks crosslinked through the polyaddition of THDI with four different aminoethanol compounds that contain secondary amine groups of varying bulkiness, e.g. 2,2,6,6-tetramethyl-4-piperidinol, BEU, 2-(isopropylamino)ethanol, and 2-(ethylamino)ethanol. Given the results obtained from thermomechanical properties and FTIR studies, they concluded the impact of steric hindrance of

N-alkyl substituents on reaction conversion, network connectivity, and therefore the relaxation of the dynamic networks.[109]

In addition to aliphatic bulkyamines (DBED and BEU), aromatic moiety-containing N,N'-di-t-butyl-p-xylylenediamine (TBXA) shown in Figure 2.2 was synthesized in an attempt to improve mechanical properties and thermal stability for dynamic PUU networks fabricated with DBED. As illustrated in Figure 2.5, linear PUU prepolymers were synthesized by the polyaddition of the synthesized TBXA with m-xylylenediisocyanate, PEG, and poly(propylene glycol) (PPO), which were further crosslinked with TEA, yielding crosslinked PUU networks. The incorporation of aromatic moiety-containing TBXA greatly improved the thermal and mechanical performance of the resulting PUU networks, while maintaining the desirable recycling, self-healing, and reprocessing properties. The dynamic HUBs significantly reduced the relaxation timescale and allowed the PUU networks to be recycled multiple times. The healed and recycled PUUs regained most of the mechanical strength and integrity of the original material.[3]

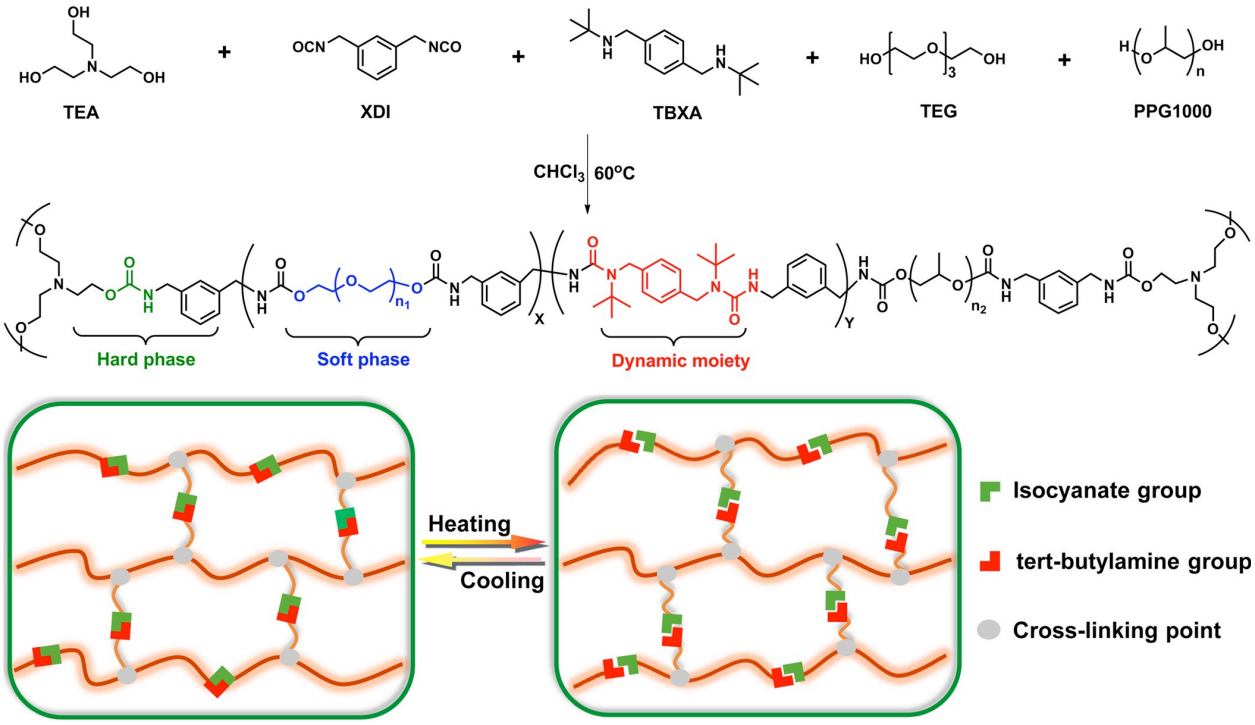

Figure 2.5. Schematic illustration of the polyaddition of aromatic moiety-containing TBXA with m-xylylenediisocyanate, PEG, and (PPO), crosslinked with TEA, to fabricate crosslinked PUU networks bearing t-butylamino-bearing HUBs as well as reversible exchange of HUBs upon the change in temperature.[3] Copyright 2020 American Chemical Society.

2.2.2 Multifunctional Bulkyamines Bearing t-Butylamino Groups

A variety of multifunctional bulkyamines bearing multiple t-butylamino groups have been synthesized and examined as dynamic crosslinkers. This approach is elegant and efficient because no multifunctional alcohols or isocyanate crosslinkers are required to fabricate dynamic crosslinked networks. This approach is unique because as to allow for the fabrication of dynamic networks crosslinked with HUBs where crosslinks are dynamic HUBs.

Small molecule multifunctional bulkyamines have been explored. Oh and coworkers synthesized a four-arm bulkyamine labeled with t-butylamino groups (e.g. a tetrafunctional bulkyamine) by a click type thiol-ene reaction of tetrakis(3-mercaptopropionate) with BAEMA (called T-NH). As illustrated in Figure 2.6, the formed T-NH was used as a dynamic crosslinker for the polyaddition with a polyurea prepolymer formed by the reaction of IPDI and PDMS-DA, yielding dynamic PUa network materials crosslinked with t-butylamino-based HUBs. The networks that formed under a catalyst-free condition had the rapid void filling and self-healing of micron-sized cracks on film surfaces at ambient condition through the reversible exchange of hindered urea linkages upon the change in temperature. Given their feature to be self-healable, transparent, and reprocessable, the developed PU films enabled the fabrication of a robust triboelectric nanogenerator (TENG) device that possesses excellent interfacial polarization-induced triboelectric performance superior to the reported systems as well as rapid recovery through effective self-healing.[4]

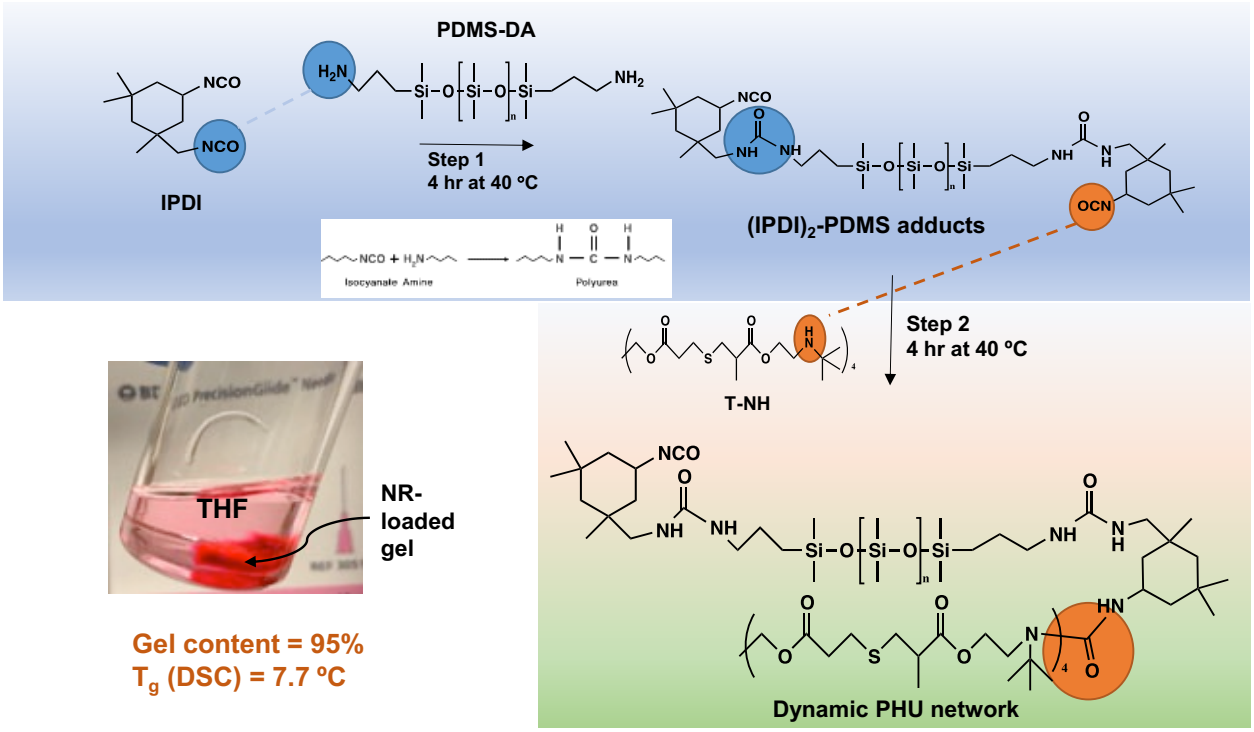

Figure 2.6. Schematic illustration to fabricate dynamic PUa networks by the polyaddition of a four-arm bulkyamine labelled with t-butylamino groups (T-NH) with a polyurea prepolymer synthesized from a reaction mixture of IPDI and PDMS-DA. Copyright 2020 American Chemical Society.[4]

Further, various polymeric crosslinkers, particularly poly(meth)acrylates bearing pendant t-butylamino groups, have been synthesized and explored to fabricate effective network materials crosslinked with HUBs. 2-(t-Butylamino)ethyl methacrylate (BAEMA) is commercially available and has been mainly used to copolymerize with other monomers. Its chemical structure is shown in Figure 2.2.

A reactive random or block copolymer approach has been recently explored to synthesize robust PUa networks crosslinked with t-butylamino-based HUBs. The approach centers on the synthesis of well-controlled copolymers composed of both t-butylamino pendants (for the formation of t-butylamino-based HUB crosslinks) and functional pendants (for the compatibility with end-use properties) by a controlled radical polymerization, particularly reversible addition-fragmentation chain transfer (RAFT) polymerization technique.[110-114] These copolymers have been used as multifunctional polymeric crosslinkers for the polyaddition of polyisocyanates with polyamines to fabricate self-healable, reprocessable, covalent adaptive PUa network materials. As

illustrated in Figure 2.7a, a well-defined block copolymer consisting of poly(2,2,2-trifluoroethyl methacrylate) (PTFEA) block and PBAEMA block (called FBCP) with narrow molecular weight distribution and predetermined molecular weight was synthesized by consequent RAFT polymerization of TFEA and then BAEMA, thus forming PTFEA-block-PBAEMA. The synthesized FBCP is designed with dielectric fluorinated groups for improved triboelectric output and dynamic *t*-butylamino groups for self-healability and reprocessability. Figure 2.7b illustrates that the synthesized block copolymer was used as a multifunctional crosslinker for the polyaddition with a polyurea prepolymer synthesized by the reaction of IPDI with PDMS-DA to fabricate a robust self-healable, reprocessable, and mechanically strong fluorinated PUa networks crosslinked with t-butylamino-based HUBs. An integration of ionic liquid as an efficient dielectric material induced ionic polarization through interactions with pendant fluorinated groups to raise dielectric constant and thus increase triboelectric performance as well as improved self-healing capability simultaneously for the dynamic PU networks. The fabricated materials exhibit excellent self-healability at elevated temperatures as micron-sized surface cracks were recovered up to >95% in 10 min at 90 °C. Furthermore, the materials were effective for negative triboelectric materials for enhanced TENG output. Importantly, TENG output was completely recovered upon the healing of surface cracks.[5] Further, a well-defined random copolymer was synthesized by RAFT polymerization of 2,2,2-trifluoroethyl methacrylate (TFEMA) and BAEMA. The synthesized P(TFEMA-ran-BAEMA) copolymer was used as a reactive crosslinker to fabricate ionic fluorinated PUa networks upon the addition of IL. The developed TENG fabricated with fluorinated PUa networks integrated with ILs exhibited a high TENG output performance as well as high TENG output recovery upon repairing their surface damages.[115]

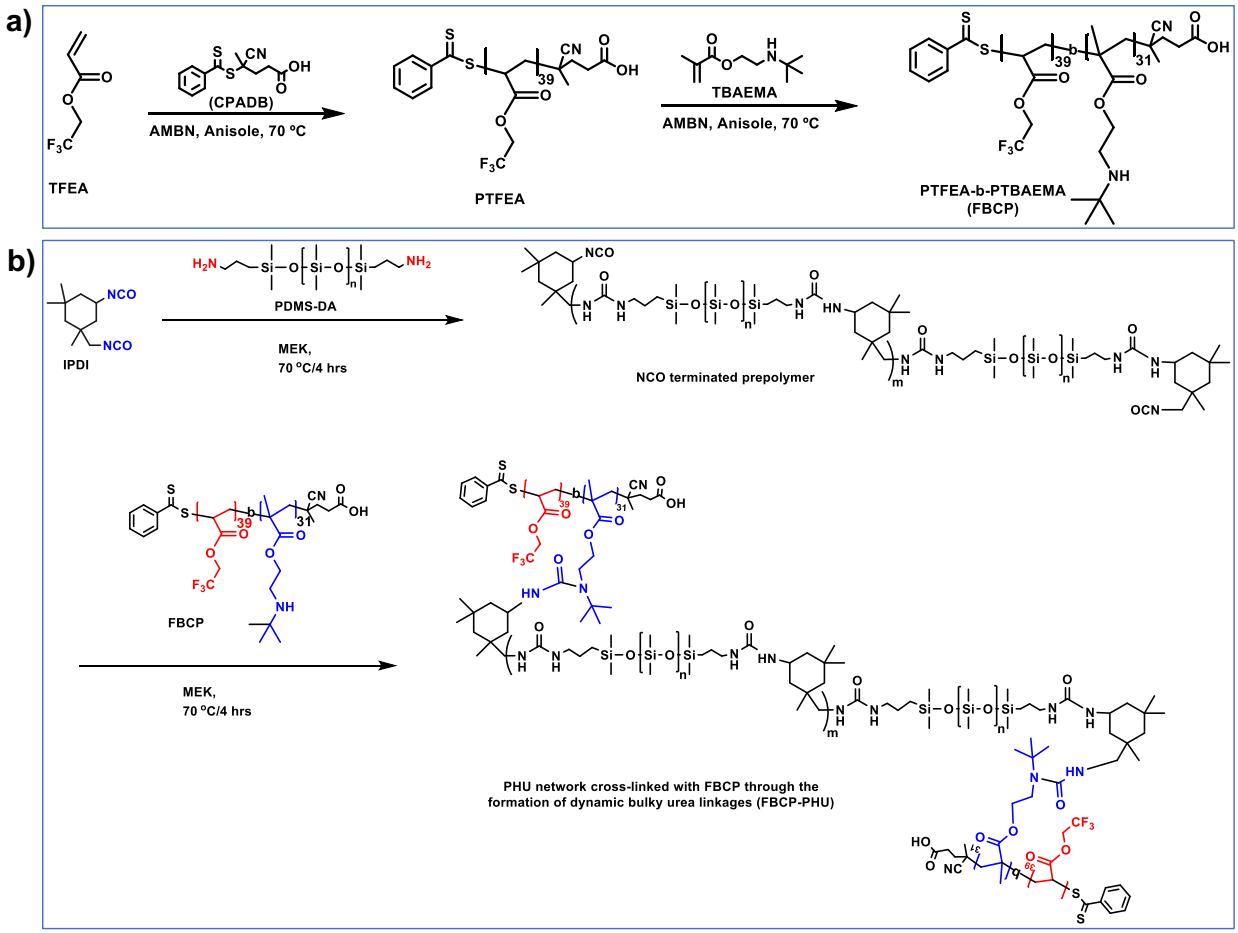

Figure 2.7. Schematic representation of a well-defined block copolymer consisting of PTFEA and PBAEMA blocks (called FBCP) with narrow molecular weight distribution and predetermined molecular weight (a) and two-step polyaddition to fabricate PUa network crosslinked through the formation of dynamic BCPs with well-defined FBCP bearing pendant fluorinated species in a block and bulky t-butylamino groups in the other block (b).[5] Copyright from Royal Society of Chemistry 2022.

Other random copolymers composed of BAEMA units, thus containing multiple t-butylamino pendants, have also been explored to develop dynamic PUU materials crosslinked with HUBs. Cheong and coworkers synthesized a poly(meth)acrylate random copolymer bearing t-butylamino pendant groups by free radical polymerization of BAEMA, methyl methacrylate (MMA), and n-butyl acrylate (BA) at the molar ratio of 1/10/10. The formed P(BAEMA-ran-MMA-ran-BA) had a single glass transition at 2 °C (relatively soft), determined by differential scanning calorimetry, suggesting that it was designed to be soft. The copolymer was used as a multiple crosslinkers for the polyaddition with either HDI or IPDI. The formed networks were dynamic, exhibiting that

self-healing against a single scratch was accelerated and repeated up to a certain number of times even in water.[116] Further, the scope has been expanded to the synthesis of a diblock copolymer consisting of a random copolymer block of P(BAEMA-ran-MMA-ran-BA) and the other block of poly(4-vinyl pyridine) (PVP), thus forming PtB-b-PVP, by RAFT polymerization. The block copolymer formed spherical micelles with PVP cores surrounded with PtB coronas in PtB matrix when being mixed with PtB. The formed hetero-structured mixtures were crosslinked through the formation of dynamic HUBs upon the reaction with HDI. They claimed that the introduction of self-assembled block copolymers improved self-healing efficiency and mechanical properties.[117] A report also describes the fabrication of dynamic PMMA networks bearing t-butylamino HUBs by the synthesis of a random copolymer consisting of BAEMA and MMA, thus dynamic poly(MMA-co-BAEMA) having pendant t-butylamino groups, followed by its crosslinking with HDI.[118]

2.2.3 Piperazine-based Diamines

Piperazine (PAZ) and its derivatives have been explored for the synthesis of dynamic PUU network materials containing PAZ-based HUBs.[119] Figure 2.8 summarizes their chemical structures examined in literature.

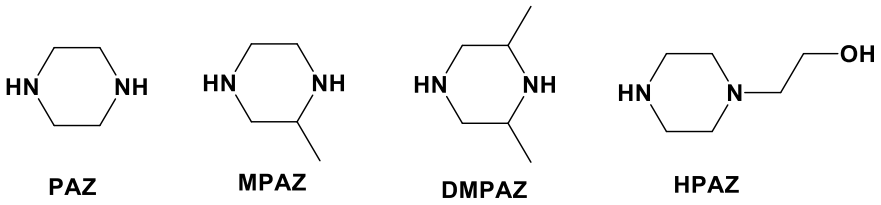

Figure 2.8. The chemical structures of piperazine and its derivatives are examined in the literature.

Cheng and coworkers developed dynamic silicon-based PUU network materials labelled with PAZ-isocyanate HUBs for flexible electronics. As illustrated in Figure 2.9, the polyaddition of PAZ with HMDI and PDMS-DA enabled the synthesis of polyurea prepolymers bearing PAZ-isocyanate HUBs on their backbones, which were subsequently crosslinked with glycerol (a triol), to yield crosslinked PUU networks. Given good healability and recyclability, the synthesized PUU networks exhibit high intrinsic insulation properties, comparable to commercial silicone materials.[120] Upon the addition of graphene, flexible conductive materials were fabricated, which possess admirable flexibility, healing ability and sensitive response to resistance changes that

could be prototyped by a flexible circuit with the light signal.[6] In another report, PAZ was used as a chain extender with a polyurethane prepolymer prepared by the reaction of castor oil (a triol) with IPDI to fabricate biobased dynamic polymer networks derived from castor oil which improves the mechanical properties of castor oil-based polyurethane materials.[121]

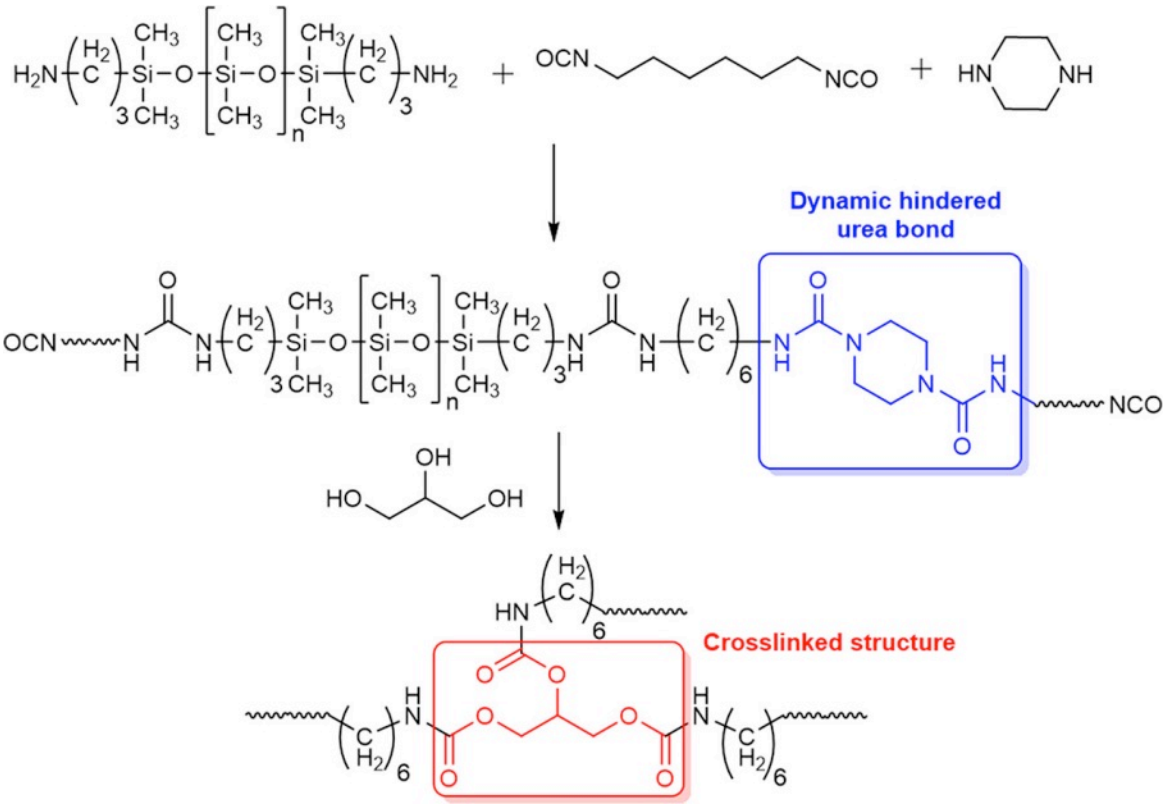

Figure 2.9. A schematic representation of the synthesis of dynamic silicon-based PUU network materials labelled with PAZ-based HUBs for flexible electronics.[6] Copyright from American Chemical Society 2021.

Zhang and coworkers reported the facile preparation of dual functional wearable devices based on HUB-Integrated reprocessable PUU networks and AgNWs. As illustrated in Figure 2.10, 2-methylpiperazine (MPAZ) was mixed with trimethylolpropane tris[poly(propylene glycol), amine-terminated] ether (T-403) and poly(propylene glycol) bis(2-aminopropyl ether) (D-2000). The formed amine mixture reacted with HDI to form crosslinked PUU networks containing PAZ-isocyanate HUBs. The crosslinked PUU networks were then spray-coated with AgNWs to robust dual-functional wearable devices. The fabricated electrodes exhibit both electrical heating capability and strain-sensing functionality.[7]

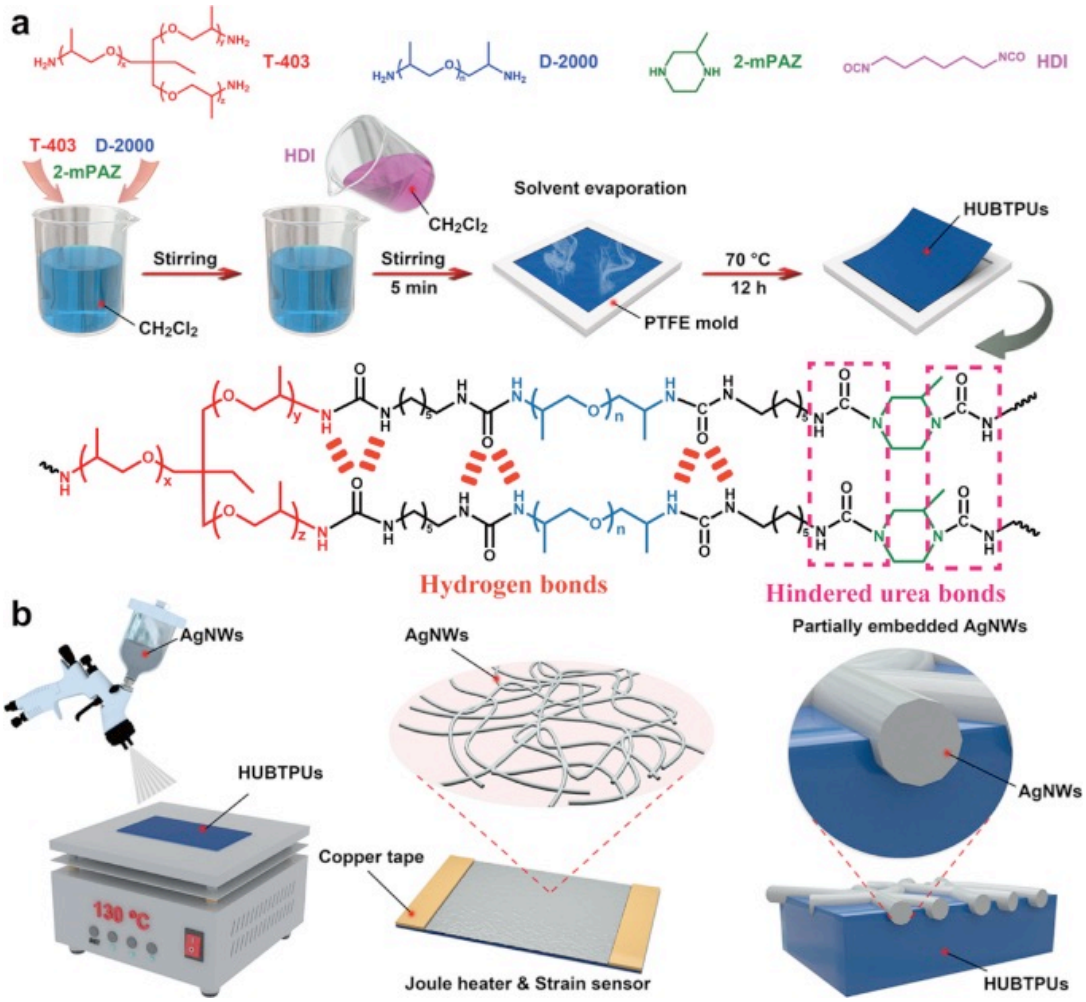

Figure 2.10. A schematic representation of the synthesis of dynamic PUU network materials bearing MPAZ-based HUBs (a) and preparation of dual functional wearable devices by spray-coating AgNWs on the PUU substrates.[7] Copyright from American Chemical Society 2022.

Lei and coworkers developed mechanically robust, recyclable and shape memory PUU network materials for wearable devices. 2,6-Dimethyl piperazine (DMPAZ) containing bulk substituents of two methyl groups was incorporated into the polyaddition with IPDI and PEG to form linear polyurethane prepolymers with PAZ-isocyanate HUBs. These prepolymers were crosslinked by reaction with PHDI (a triisocynate crosslinker). The fabricated PUU networks were dynamic with excellent mechanical properties and exceptional reprocessability. Upon multiple rounds of reprocessing, the breaking strength and elongation at break turned out to be equivalent to those of the original elastomers. Furthermore, the network materials had outstanding 3D permanent shape reconfigurability via topological rearrangements.[122] Zheng and coworkers

developed sustainable, malleable, and recyclable castor oil-derived PUU networks with tunable mechanical properties and shape memory performance. The networks were fabricated by the polyaddition of N-(2-hydroxyethyl) piperazine (HEPAZ) with polyurethane prepolymers made of castor oil (a triol) and 4,4′-methylenedicyclohexyl diisocyanate (HMDI). The crosslinked networks labeled with PAZ-isocyanate HUBs had variable tensile behavior over a wide range from a soft elastomer to tough and hard plastics, excellent malleability, stable reprocessability, and multiple recyclability as well as excellent shape memory performance and reconfigurability, allowing them to be reprocessed into various complex shapes without using a mold.[123]

2.2.4 Polyamines Bearing Other Bulky Groups

In addition to bulkyamines bearing t-butylamino and piperizine groups, other bulky groups through polybulkyamines shown in Figure 2.11 have been explored to fabricate dynamic PUU network materials.

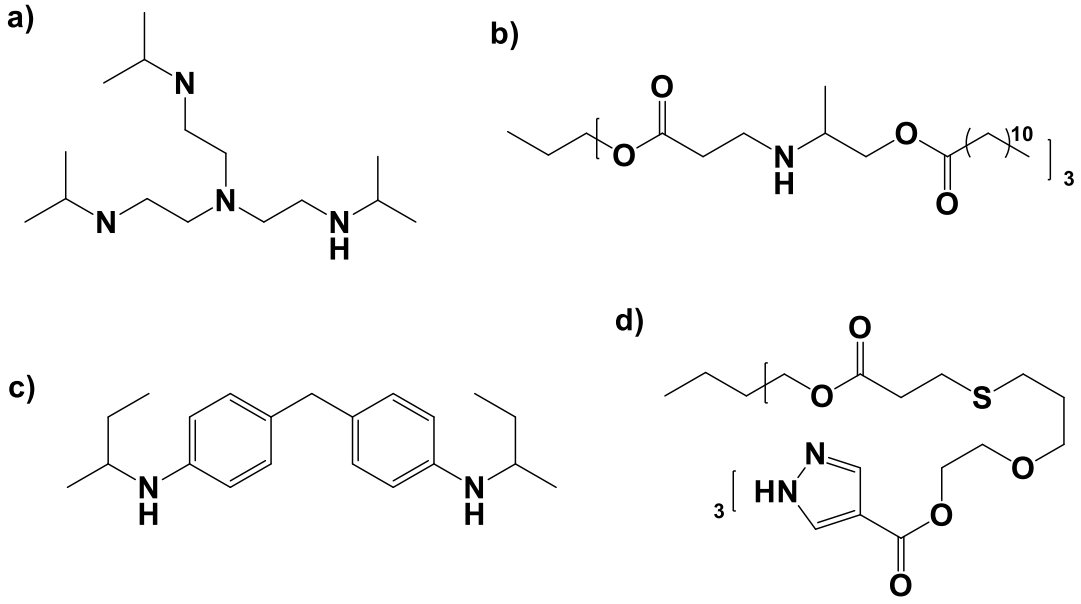

Figure 2.11. Chemical structures of polybulkyamines bearing other bulky groups, including tris[2-(isopropylamino)ethyl]amine (a),[8] HDLA-100 (b),[9] 4,4′-bis(*sec*-butyl)methylenedianiline (c),[10] and a pyrazole-bearing 3-arm bulkyamine crosslinker (d).[11]

Polyamines bearing isopropylamino groups have been explored. Bella and coworkers reported the polyaddition of tris[2-(isopropylamino)ethyl]amine (a trifunctional bulkyamine) with HDI, followed by the reaction with PEG, to fabricate self-healable PEG-based PUU gel electrolyte for lithium batteries. The newly designed gel electrolyte materials possessed self-healable properties

and higher ionic conductivity than the commercially available liquid electrolyte embedded in a porous Celgard® 2500 separator.[8] Lei and coworkers synthesized HDLA-100, a trifunctional dynamic crosslinker bearing substituted isopropyl group, by reaction of trimethylolpropane tris[3-(2-methylaziridin-1-yl)propionate] (HD-100) with lauric acid. Polyaddition of HDLA-100 with IPDI yielded PUU networks crosslinked with dynamic hindered urea bonds, which had great abilities of permanent shape reconfiguration and self-healing.[9]

Polybullyamines including 4,4′-bis(*sec*-butyl)methylenedianiline[10] and a pyrazole-bearing 3-arm bulkyamine crosslinker[11] were synthesized and explored to fabricate dynamic PUU networks bearing HUBs. In addition, the polyaddition of 4,4'-methylenedianiline with a prepolymer synthesized by the reaction of a trifunctional PPG with IPDI allowed for the synthesis of crosslinked PUU networks labeled with phenyl-bearing hindered urea bonds.[124]

2.3 Step-growth/Polyaddition to Other Polymers

Dynamic epoxy networks containing HUBs have been developed. Liang and coworkers synthesized 1,1′-(4-methyl-1,3-phenylene)bis(3-benzyl-3-(4-(4-(benzylamino) benzyl)-phenyl) urea) (MPBU), a dibulkyamine labeled with phenyl and benzyl groups, by the reaction of 4,4'-diaminodiphenylmethane with benzyl bromide. The resulting MPBU reacted with TDI to form a polyurea prepolymer containing HUBs, which reacted with bisphenol A-based diglycidyl ether, yielding dynamic epoxy cross-linked networks. The networks had optional recyclability, good reprocessability under simple hot-pressing procedure and rapid self-healing property.[125]

Dynamic polysulfide networks containing HUBs have been reported. Zhang and coworkers synthesized a dimethacrylate bearing PUU by the reaction of BAEMA with a NCO-terminated PUU prepolymer synthesized by the polyaddition of PTMEG with TDI. Next step was a click-type photo-initiated thiol-ene reaction of the synthesized dimethacrylate with trimethylolpropane tris(3-mercaptopropionate). The dynamic polysufide materials possessed a uniform structure and versatile properties, such as high stretchability, self-recoverability, high self-healing efficiency, high recyclability, and good weldability. Upon rupture, the as-prepared elastomer completely restores its original mechanical properties.[126]

2.4 Chain-growth Poly(meth)acrylate Networks

Chain-growth networks have been fabricated by chain-growth polymerization of vinyl monomers through a radical mechanism. This approach requires the synthesis of a functional dimethacrylate precursor as a dynamic crosslinker bearing HUBs. The synthesized methacrylates are copolymerized with other vinyl monomers including (meth)acrylates for end-user applications. The formed networks are crosslinked through the formation of carbon-carbon bonds (thus poly(meth)acrylate networks) and HUB-bearing PUU or PUa chains are positioned on the bridges between crosslinks. This feature differs from PUa networks fabricated by the polyaddition of polymeric crosslinkers labeled with bulkyamino pendants with polyisocyanates that are crosslinked through the formation of HUBs and carbon-carbon bonds are positioned on their backbones. Several approaches have been explored to synthesize dynamic dimethacrylate crosslinkers bearing t-butylamino-based HUBs.

An approach utilizes BAEMA that reacts with various diisocyanates. The use of small molecular diisocynates such as IPDI and TDI has been reported.[127, 128] As an example, Wu and coworkers developed highly stretchable sensors prepared by crosslinking an enhanced 3D printed UV-curable sacrificial mold. A bifunctional dimethacrylate was synthesized by the reaction of BAEMA with MDI. The formed crosslinker was copolymerized with 4-acryloylmorpholine by photo-initiated free radical polymerization to create crosslinked polymer network, preventing the dissolution of printed parts in the uncured resin. A porous flexible strain sensor (PFSS) fabricated by casting polyurethane/carbon nanotube composites into the sacrificial molds had high stretchability and excellent recoverability.[127] Further, the synthesis and use of NCO-terminated polyurethane prepolymers formed by the polyaddition of diisocyanates with polyols have been reported.[12, 129] Zhang and coworkers developed dynamic crosslinked PUa/polydopamine (PDA) nanocomposites for photo-responsive self-healing and photoactuation. As illustrated in Figure 2.12, a macro-dimethacrylate was synthesized by the reaction of BAEMA with a polyurethane prepolymer formed by the polyaddition of TDI with PTMEG. Photo-initiated polymerization of the crosslinker with N-methylolacrylamide in the presence of PDA nanoparticles enabled to fabricate dynamic chain-growth crosslinked PDA network nanocomposites. They had high toughness and stretchability, exhibit rapid self-healability in response to near-infrared light when damaged, and were malleable and easily recyclable.[12]

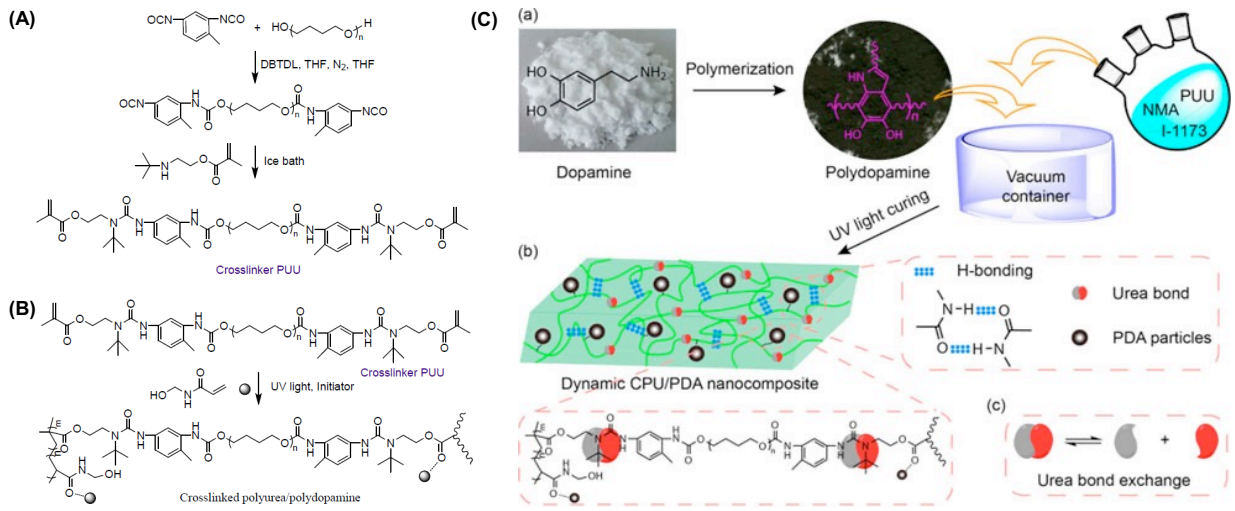

Figure 2.12. (A) Synthetic routes to a macro-dimethacrylate bearing t-butylamino-based HUBs and (B) a dynamic chain-growth crosslinked PDA network as well as (C) schematic illustration to fabricate PDA-containing dynamic nanocomposites by photo-initiated free radial polymerization in the presence of PDA nanoparticles (a), chemical structure of a dynamic chain-growth crosslinked PDA network (b), and dynamic exchange reaction of HUBs (c).[12] Copyright from American Chemical Society 2022.

Another approach involves the use of DBED that reacts with functional (meth)acrylate precursors.[130, 131] Torkelson and coworkers synthesized 5,8-di-tertbutyl-4,9-dioxo-3,5,8,10-tetraazadodecane-1,12-diyl bis(2-methyl acrylate), a dimethacrylate bearing t-butylamino groups, by reacting 2-isocyanatoethyl methacrylate with DBED. The synthesized dynamic crosslinker was copolymerized with hexyl methacrylate by free radical polymerization to fabricate dynamic chain-growth polymethacrylate networks bearing t-butylamino-based HUBs. The dynamic covalent networks could be (re)processed at 80 °C and exhibited full recovery of cross-link density after multiple recycling steps. However, the network showed delayed and extremely slow stress relaxation at the processing temperature.[131]

2.5 Conclusion and Outlook

Effective strategies have been explored to fabricate robust CANs bearing dynamic HUBs exhibiting excellent self-healability and reprocessability. The strategies involve the integration of various HUBs based on mainly t-butylamino group as well as other bulkyamino groups including piperazine, isopropylamino, pirazole, and phenylamino groups in various polymeric thermoset materials. Because of the adaption to form HUBs, HUB-bearing networks of PUU and PUa have

been extensively synthesized by step-growth polyaddition of polyisocynates with polyols and/or polyamines along with polybulkyamines through the formation of HUBs on their backbones or as their dynamic crosslinks. In addition, HUB networks of epoxy resins, polysufides, and polymethacrylates have been prepared by their chemical routes and through the design and synthesis of their reactive precursors bearing HUBs. These precursors include HUB-bearing amines for epoxy networks (utilizing amine-exoxy reaction) as well as HUB-bearing (meth)acrylates for polysulfide networks (utilizing thiol-ene reaction) and polymethacrylate networks (utilizing radical polymerization mechanism). The formed networks turned to be dynamic, undergoing reversible exchange reactions through dissociation/association of the corresponding isocynate and bulkyamino groups, thus attaining self-healing and reprocessing. These developed network materials have found various applications requiring dynamic properties, such as energy harvesting[4, 5, 115] and storage,[8] sensor,[100, 127] flexible and wearable electronics,[2, 126, 129] and surface coatings.[105, 128]

Despite these advances, further efforts should be made with focus on the development of advanced polymeric network materials. Most HUB-based materials have been designed with soft polymeric networks of relatively low glass transition temperatures. These soft materials could facilitate enhanced void-filling and thus self-healing; however, they might scarify their mechanical properties. Effective approaches must be developed to achieve excellent self-healability and mechanical strength simultaneously. An introduction of nanoadditives (or nanofillers) into HUB-based networks could solve the challenge. Further, this approach can allow for the development of heterogeneous dynamic networks possessing the intrinsic properties of those nanoadditives such as fluorescence, light adsorption, magnetic properties, upconversion, etc. Further, the design and fabrication of advanced networks should be explored for value-added applications such as energy harvesting, energy storage, and wearable electronics.

Chapter 3. Self-healable Reprocessable Triboelectric Nanogenerators Fabricated with Vitrimeric Poly(hindered urea) Networks

3.1 Introduction

Collectable environmental mechanical energy has become a significant research concern in the field of energy harvesting.[132-135] Particularly a triboelectric nanogenerator (TENG) has been widely and rapidly developed as a new type of energy harvesting device. TENG converts mechanical stimulus to electrical signals through the combination of triboelectric effect with electrostatic induction.[136-138] This combined effect displays higher output performance compared to the other nanogenerator devices. It possesses tremendous benefits including simple design structure, low cost, high conversion efficiency, good friction energy, and environmental friendliness. Further, TENG can collect different types of mechanical energy, typically mechanical vibration,[139, 140] human motion,[141-144] wind,[145, 146] and water waves.[147, 148] However, the major issue of conventionally-designed TENGs involves the failure of their self-charging power and the suppression of their output performance and lifetime. This is mainly because they are subjected to long-term mechanical impact and thus susceptible to fracture and surface damage. The promising solution to address this issue is the integration of dynamic (or reversible) linkages in the design of triboelectric materials, thus developing self-healable TENGs (SH-TENGs).[27, 149, 150] An early approach utilizes relatively weak supramolecular (physical) associations, particularly hydrogen bonding.[52, 151, 152] The resultant SH-TENGs suffer from poor mechanical properties and low creeping resistance. This output made devices worsen of robustness and durability, once they are damaged under frequent mechanical impact during repeated operation cycles. The promising approach involves the development of vitrimeric polymers crosslinked with reversible covalent bonds through typically disulfide,[58, 153, 154] boronic ester,[155, 156] and imine[56, 157] chemistries. These crosslinked network materials exhibit vitrimeric properties based on elastic-plastic transition through metathesis exchange reaction in polymer network in response to an external stimulus.[76, 78, 82, 158] However, these SH-TENGs still exhibit lower performance to be addressed, compared with the counterpart TENGs.[159]

Hindered urea chemistry employing a bulky urea group, typically t-butylamine group, attached to one of the urea nitrogen atoms has been explored for the development of covalent adaptable network (CAN) materials since the first reports by Cheng's research group.[71, 106] Compared with

other dynamic chemistries that require the introduction of heteroatoms such as sulfur and boron and hetero-bonds such as -C=N- bonds, the bulky urea linkages are the essential building blocks for industrially-important polyurethanes and polyureas.[160] Further, poly(hindered urea) (PHU) networks are less-costly degradable and synthesized by a facile step-growth polymerization of various polyamines including multifunctional bulky amines with polyisocyanates. Several reports have described the development of crosslinked poly(urea-urethane) and PHU vitrimers to achieve thermally malleability and recyclability.[108, 124, 161-164] Further, reports has explored the use of silsesquioxane,[101] bisphenol S,[165] and a three-arm star isocyanate[107, 109] that react with a difunctional hindered amine (*N*,*N*-di-(tert-butyl)ethylenediamine) and the synthesis of a methacrylate bearing t-butylamine pendants.[116] Despite these advances, the development of a robust approach is required for the fabrication of PHU networks with enhanced mechanical properties as well as excellent self-healability and processability. Further, to the best of knowledge, no reports have yet described the application of hindered urea chemistry to the development of self-healable, reprocessable TENGs.

Herein, we report self-healable TENG built with dynamic and reprocessable PHU networks. Our approach to fabricate robust PHU networks centers on the synthesis of a four-arm star hindered amine (T-NH) that was used for a facile step-growth polymerization with a polydimethylsiloxane (PDMS)-based diamine (PDMS-DA) and a polyisocyanate under catalyst-free condition. The formed network films were characterized for void-filling and self-healability, mechanical and viscoelastic properties, and reprocessability. Given the promising results, the vitrimeric PHU film was tested to fabricate robust TENG that displays greater triboelectric outputs through an interfacial polarization technique, compared with the reported healable TENGs. Further, the material exhibits the rapid recovery of scratches and thus TENG performance upon excellent self-healing.

3.2 Experimental

Instrumentation and analyses. ^{1}H-NMR spectra were recorded using a 500 MHz Varian spectrometer with the $CDCl_3$ singlet at 7.26 ppm and DMSO-d_6 quintet at 2.5 ppm selected as the reference standards. Molecular weight and molecular weight distribution were determined by gel permeation chromatography (GPC) with a Viscotek VE1122 pump and a refractive index (RI) detector. Two PolyAnalytik columns (PAS-103L and 105L, designed to determine molecular

weight up to 2 000 000 g/mol) were used with THF at a flow rate of 1 mL/min. Linear poly(methyl methacrylate) standards were used for calibration. Aliquots of the samples were dissolved in THF. The clear solutions were filtered using a 0.25 μm PTFE filter to remove any THF-insoluble species. A drop of anisole was added as a flow rate marker.

Thermogravimetric analysis (TGA) was conducted with a TA Instruments Q50 analyzer. Dried samples (5-10 mg) were placed in a platinum pan inside a programmable furnace and then heated from 25 to 800 °C at a heating rate of 20 °C/min under nitrogen flow. Mass loss was then calculated.

Differential scanning calorimetry (DSC) analysis was carried to determine thermal properties including glass transition temperature (Tg) of crosslinked films with a TA Instruments DSC Q20 differential scanning calorimeter. Samples were dried for 24 h in vacuum oven to remove residual solvents. Temperature ranged from −80 to 200 °C with heating and cooling cycles conducted at a rate of 10 °C/min (cycles: cool to −80 °C, heat up to 200 °C (1st run), cool to −80 °C, heat up to 200 °C (2nd run), and cool to 25 °C). The Tg values were determined from the 2nd heating run.

Materials. Isophorone diisocyanate (IPDI, 98%), bis(3-aminopropyl) terminated polydimethylsiloxane (PDMS-DA, M_n = 2,500 g/mol), 2-(t-butylamino)ethyl methacrylate (TBAEMA, 97%), triethylamine (Et_3N, 99.5%), pentaerythritol tetrakis(3-mercaptopropionate) (T-SH, >95%) were purchased from Sigma-Aldrich and used as received. Oxidized multiwall carbon nanotubes (o-CNTs) were prepared by heat treatment of multiwall carbon nanotubes (>90 wt% on carbon basis, 110-170 nm in diameter, 5-9 μm in length, Sigma-Aldrich) under acidic conditions according to the procedure in the previous literature.[166]

Synthesis of T-NH. T-SH (8 g, 16 mmol) and Et_3N (2 mL, 19 mmol) were mixed with TBAEMA (5 mL, 24 mmol) in DMSO (28 mL) under stirring for 12 hrs at room temperature. The reaction mixture was precipitated from water more than five times to remove excess TBAEMA. The product was dried using rotary evaporation and then dried in vacuum oven set at room temperature for 12 hrs as a white powder with a yield of 98%.

Fabrication of thermoreversible PHU networks and films by three routes. For Route A, IPDI (77 mg, 0.35 mmol), T-NH (105 mg, 86 μmol), and PDMS-DA (432 mg, 0.17 mmol) were mixed in THF (1.6 mL) under stirring at 40 °C for 4 hrs. For Route B, IPDI (77 mg, 0.35 mmol) was mixed with T-NH (105 mg, 86 μmol) in THF (2.0 mL) under stirring at 40 °C for 4 hrs to form $(IPDI)_4$-T-NH adducts. Then, the addition of PDMS-DA (432 mg, 0.17 mmol) was followed at 40

°C. The resulting mixture was stirred at the same temperature for additional 4 hrs. For Route C, IPDI (230 mg, 1.0 mmol) was mixed with PDMS-DA (1.3 g, 0.5 mmol) in THF (5 mL) under stirring at 40 °C for 4 hrs to form IPDI-PDMS adducts. Then, the addition of a solution of T-NH (0.3 g, 0.3 mmol) dissolved in THF (1 mL) was followed at 40 °C. The resulting mixture was stirred at the same temperature for additional 4 hrs. For all three Routes, after being cooled down to room temperature in air, the clear solution was poured on a glass plate or in a polypropylene mold and allowed to dry at room temperature for 24 hrs to cast clear films.

Gel content measurements. Pieces of dried films (approximately 50 mg) were mixed with THF (10 mL) for 48 hrs. THF was carefully decanted and precipitates were dried in fume hood for 3 days. Gel content was calculated as the weight ratio of dried precipitates to initial films. To better visualize the gel, Nile Red (a fluorescent dye) was added into the PHU solution before drying.

Sol-gel transition. Mixtures consisting of pieces of dried PHU films (200 mg) with anisole (2 mL) were sealed and placed at 60 °C for 12 hrs. The formed sol was allowed to cool down to room temperature to form a free-standing gel in a vial.

Optical microscopy. Fresh cuts were made using a sharp blade on surfaces of the crosslinked films and annealed in an oven at given temperatures (25 and 35 °C) for 4 hrs. The occurrence of void-filling was followed by an optical microscope (Olympus BX51) coupled with a digital camera.

Scratch recovery and self-healing using nano-scratch tester (NST)/atomic force microscopy. A nano-scratch tester (NST^3, Anton Paar Tritec SA, Switzerland) was used to observe scratch patterns and mar resistance on the surface of a crosslinked film. A sphero-conical 90° indenter with a 2 μm radius tip horizontally applied the gradual load from 0.1 to 50 mN over a length of 1mm with 2 mm/min of scanning speed on the film surface. Self-healing of scratches generated by NST test was scrutinized using AFM (AFM Wide Scan, Anton Paar Tritec SA, Switzerland) at the location where 30 mN load was applied (that is, near 0.6 mm from the start-up of tip) under various thermal conditions such as healing temperatures and duration times. The AFM images were obtained with 256 scan lines for 256 s in a squared-scan area of 77.1 μm x 77.1 μm. The temporal recovery patterns of scratches through 1D cross-cuts and 3D images were compared at various healing temperatures of room temperature, 35, 60, and 80 °C and duration time up to 8 hrs.

Measurements of mechanical properties. Dynamic mechanical analysis (DMA) was conducted with a TA Instruments Q800 in the strain-controlled mode (0.1%) at a constant frequency of 1 Hz.

The data were recorded by heating the samples at 5 °C/min from −60 to 140 °C. The dimensions of the specimens were 60 mm×10 mm×0.1 mm. Universal tensile measurements were performed to measure tensile strength and elongation of crosslinked samples with an Instron Universal Testing Machine (UTM) 5982 at a constant force (100 mm/min) with a cross-head at room temperature. The dimensions of the specimens were 60 mm×10 mm×0.2 mm.

Measurements of viscoelastic properties. Viscoelastic moduli were measured with a TA Instruments DHT-2 rheometer in amplitude oscillatory shear mode with parallel plate geometry (24 mm diameter). A cyclic change of amplitude oscillatory from 5% strain for 1500 s to 95% strain for 500 s was applied. The gap was set to obtain an axial force of 1.5 N at room temperature and this cycle is repeated three times. The diameter and thickness were maintained to be 1.2 cm and 0.2 cm, respectively.

Recyclability. PHU films were first cast in the polypropylene mold (1.2 cm diameter and 0.2 cm thickness). They were cut into small pieces and then mixed with THF (10 mL). The resulting mixtures were heated to 60 °C for 24 hrs. The formed sol was re-casted in the polypropylene mold and then dried at room temperature for 24 hrs. The fried films were maintained with a similar diameter to be 1.2 cm and a thickness to be 0.2 cm.

Fabrication of triboelectric nano-generators. An organic solution of as-synthesized PHU (0.5 g) dissolved in chloroform was mixed with different amounts of o-CNT and sonicated for 30 min in a sonication bath. The resulting homogeneous solution was poured into a Teflon mold. Solvent was slowly evaporated to form o-CNT/PHU composite films. The prepared films were coated on the surface of Al electrode at 90 °C and then used as negative triboelectric films.

Measurements of triboelectric properties. The performances of the triboelectric device based on the dielectric polymer film (1 × 1 cm^2) were measured using a sourcemeter (S-2400, Keithley) and an oscilloscope (DPO 2022B, Tektronix, US) under loading of 10 N by means of a pushing tester (JIPT-100, Junil Tech). To obtain the dielectric constants of the polymer films, the capacitances were measured by a metal-insulator-metal capacitance method using an impedance analyzer (Agilent) at room temperature. The samples were prepared by sandwiching the polymer films with different concentrations of o-CNT between two Al electrodes. Then, the dielectric constant was calculated as follows: $\varepsilon = (C \times d)/(\varepsilon_o \times A)$, where *C, d, A*, and ε_0 denote the capacitance, film thickness, measured area, and permittivity in a vacuum, respectively. The surface potentials were measured by using a multimode AFM (Veeco) system with Pt/Ir-coated silicon

tips (tip radius 25 nm; force constant 3 N/m; resonance frequency 75 kHz). The samples were prepared by coating each polymer solution on the surface of SiO_2 substrate.

3.3 Results and Discussion

3.3.1 Fabrication of Dynamic PHU Networks

Our experiment began with the synthesis of a new T-NH (shown in Figure 3.1) by a click type thiol-ene through Michael addition reaction, depicted in Figure 3.S1. The synthesis and detailed characterization using ^{1}H-NMR (Figure 3.S2) and GPC (Figure 3.S3) techniques are described in the supporting information.

Given our successful synthesis of T-NH with high purity, the approach to synthesize PHU networks explored a step-growth polymerization through polyaddition of the synthesized T-NH, a poly(dimethylsiloxane) (PDMS)-based diamine (PDMS-DA), and isophorone diisocyanate (IPDI) as a polyisocyanate. The networks were designed with a 1/1 NCO/amine mole equivalent ratio and 1/1 mole equivalent ratio of T-NH/PDMS-DA, thus being equivalent to IPDI/PDMS-DA/T-NH = 12.6/70.9/16.5 wt/wt/wt. Three synthetic routes were examined to optimize the process that enables to synthesize PHU networks: one-step and two-step processes. The formed polymers were cast into dried films for initial assessment of gel content using gravimetry and thermal properties, particularly glass transition temperature (T_g), using DSC. Route A for one-step process involves the polymerization of all three reactants at once at 40 °C. The formed polymer films were clear and flexible with the T_g = -4 °C (Figure 3.S4a). However, their gel content was as low as 56% in THF. In contrast, two-step process involves the sequential reaction of two amine monomers (T-NH and PDMS-NH) with IPDI. To achieve the 1/1 of NCO/amine ratio, each step is designed with 1/0.5 of NCO/amine ratio to synthesize NCO-terminated polyurea. As illustrated in Figure 3.S5, Route B for one of the two-step processes involves the reaction of IPDI with T-NH to yield $(IPDI)_4$-T-NH 4-arm star adducts at 40 °C in the first step. In the next step, the formed adducts reacted with PDMS-DA. The formed crosslinked PHU films were clear and flexible with its T_g = -9 °C (Figure 3.S4b); however, its gel content turned to be as low as 57% in THF.

Next, as illustrated in Figure 3.1, Route C, the other for two-step process, began with the reaction of IPDI with PDMS-DA to form IPDI-PDMS prepolymer at 40 °C. The reaction was followed by their sequential reaction with T-NH to form crosslinked PHU networks that had >95%

gel content in THF. They were clear and flexible with its T_g = -7.7 °C (Figure 3.S4c). Further, the major weight loss occurred at 180 - 550 °C with a residue of <3%, by TGA analysis (Figure 3.S6).

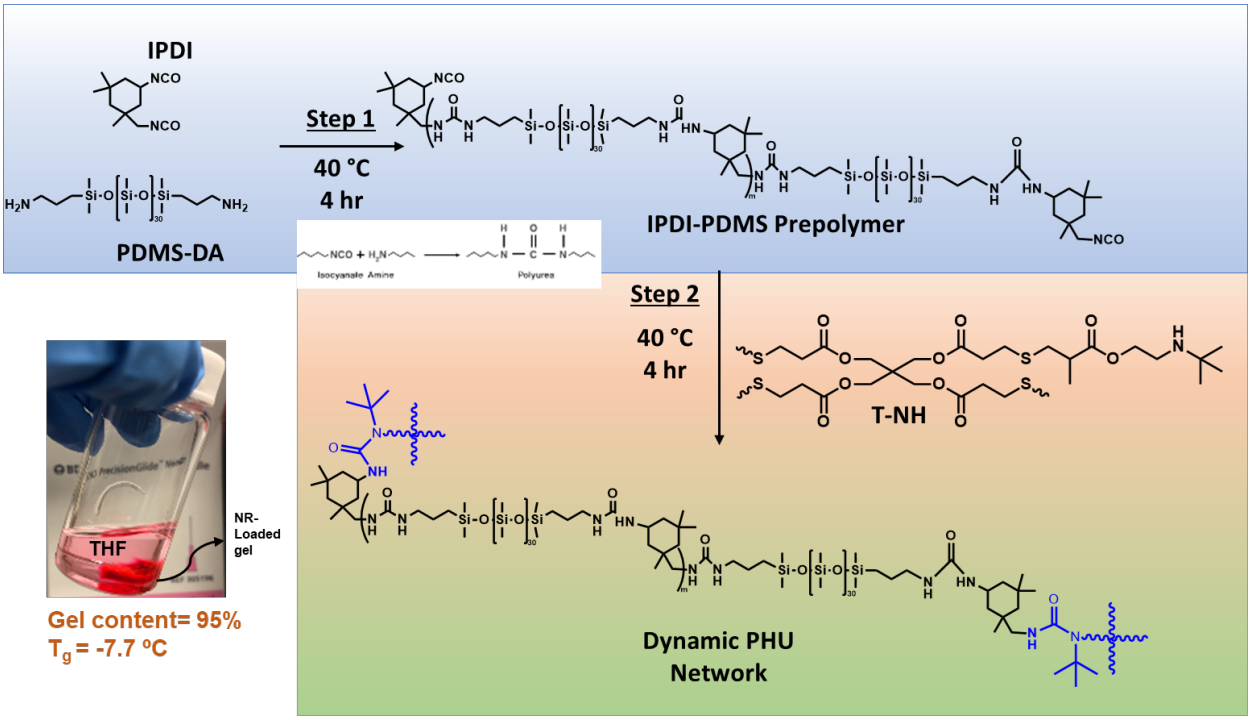

Figure 3.1. Schematic illustration of Route C with a two-step process exploring the reaction of IPDI with PDMS-DA to form IPDI-PDMS prepolymer, followed by their sequential reaction with T-NH to fabricate PHU networks. Digital photo shows the formed gels containing Nile Red in THF for clear visualization.

3.3.2 Temperature-Induced Reversibility and Void Filling

The formed PHU networks are crosslinked with dynamic hindered urea bonds with a bulky tertiary butyl group. As illustrated in Figure 3.2a, the dynamic bonds undergo reversible exchange reaction through associative bond exchange of polymeric chains upon heating. FT-IR was conducted on the films that were annealed at elevated temperatures. As seen in Figure 3.2b, the spectra of PHU network kept unchanged at temperatures ranging at 25 - 120 °C. Similar result of temperature-independent FT-IR spectra is reported for a PHU vitrimer network fabricated from polyaddition of trimethylolpropane tris[3-(2-methylaziridin-1-yl)propionate] to IPDI.[162] Temperature-induced transition was examined to further investigate the dynamic properties of the network films. As shown in Figure 3.2c-3.2e, the dried films cast on a glass plate at room temperature were cut to small pieces which were mixed with anisole (3.2c). When being heated to

60 °C for 12 hrs, the resulting mixture did not turn to a clear solution, but to a turbid swollen gel (3.2d). It then turned to a free-standing gel retaining crosslinked networks when being cooled down to room temperature (3.2e).

Then, the void filling ability was tested as micron-sized cuts on the surfaces of the dried films were made using a blade. They were annealed at ambient temperatures (25 and 35 °C) for 2 hrs. Figure 3.2f shows optical microscope images of the cuts on the films before and after void-filing. Note that cuts were presented as black-colored straight parts in all the images before healing. It is not straightforward to differentiate the kinetics of the disappearance of man-made cuts at two temperatures because it depends on their shapes and sizes (width, depth, and integrity). This result is promising in that the micron-sized cuts rapidly and significantly disappeared at 35 °C and even at room temperature. Given our promising initial results obtained from optical microscopy, more reliable and quantitative results are described in the next section using nano-scratch tester (NST)/atomic force microscopy (AFM) technique.

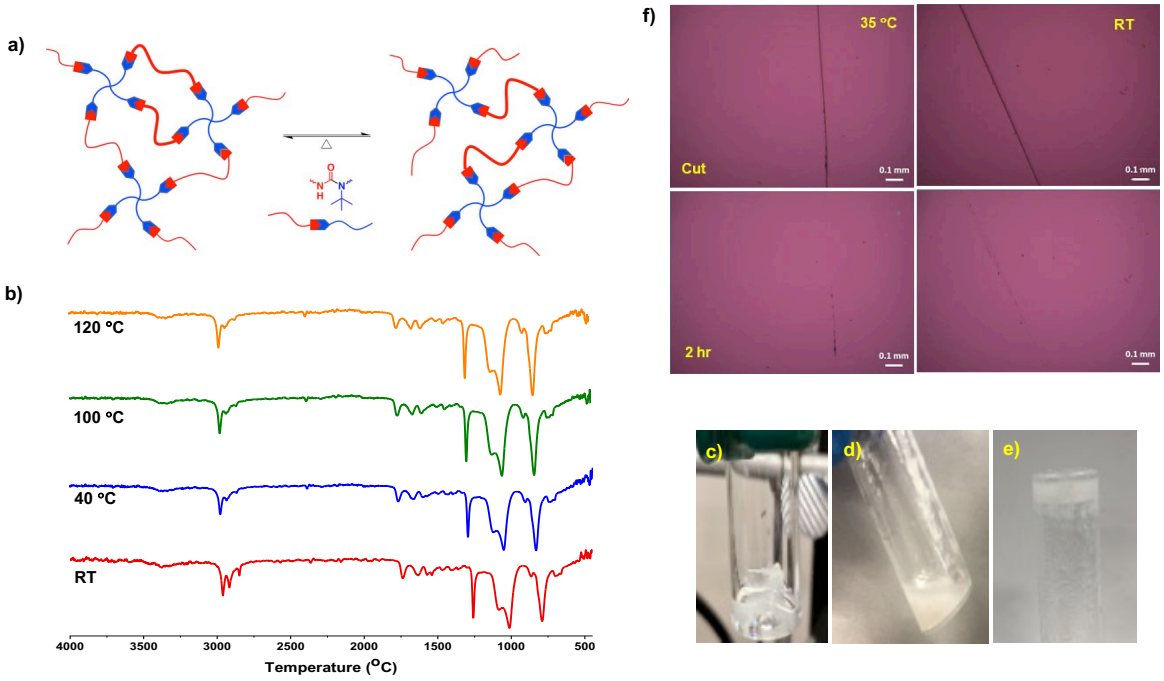

Figure 3.2. Schematic illustration of reversible exchange reaction of dynamic hindered urea bonds if PHU network upon heating (a); FT-IR spectra upon annealing at 25, 40, 100, and 120 °C (b); digital images (c-e) to show sol-gel transition through thermoreversibility: a reactive mixture at 10 wt% consisting of pieces of dried PHU films with anisole at room temperature (c), heated at 60 °C for 12 hrs (d), and gradually cooled down to room temperature to form standing gel (e); and optical microscope images of micron-sized cuts made by a sharp blade on the surfaces of PHU network films before and 2 hrs after annealing (f).

3.3.4 Self-healing Studies Using NST/AFM

Given our qualitative evaluation, void-filling and self-healability of the films were further investigated as the surface changes of scratched films were monitored before and after healing through a scratch recovery test using AFM (see Figure 3.S7). Scratches were made on surfaces of crosslinked films to check the surface resistance from NST tests and then placed under different thermal environments up to 8 hrs duration time. As seen in Figure 3.3a, initial scratches created at room temperature gradually or quickly faded along the duration time, depending on the given temperature. From the temporal scratch patterns realized by AFM in Figures 3.3a and 3.3b, the scratches on the film surfaces have remarkably disappeared with increasing temperature, especially fully recovered after 0.5 hrs at 80 °C. This result implies that PHU crosslinked films play an important role in effectively healing damaged surfaces above moderate temperatures. Further, the scratch recovery changes were quantified in Figure 3.3c. %Recovery is defined as the ratio of transient recovered area with respect to the initial scratch area near the position where 30 mN load was applied from the data shown in Figure 3.3a. At room temperature, ca 50% recovery of the scratch was observed with no external stimuli or catalysts. When the temperature increased, recovery becomes faster; >95% scratches are recovered in 8, 0.5, and 0.5 hrs at 35, 60 and 80 °C, respectively. These results demonstrate the fast recovery of scratches under moderate thermal healing conditions.

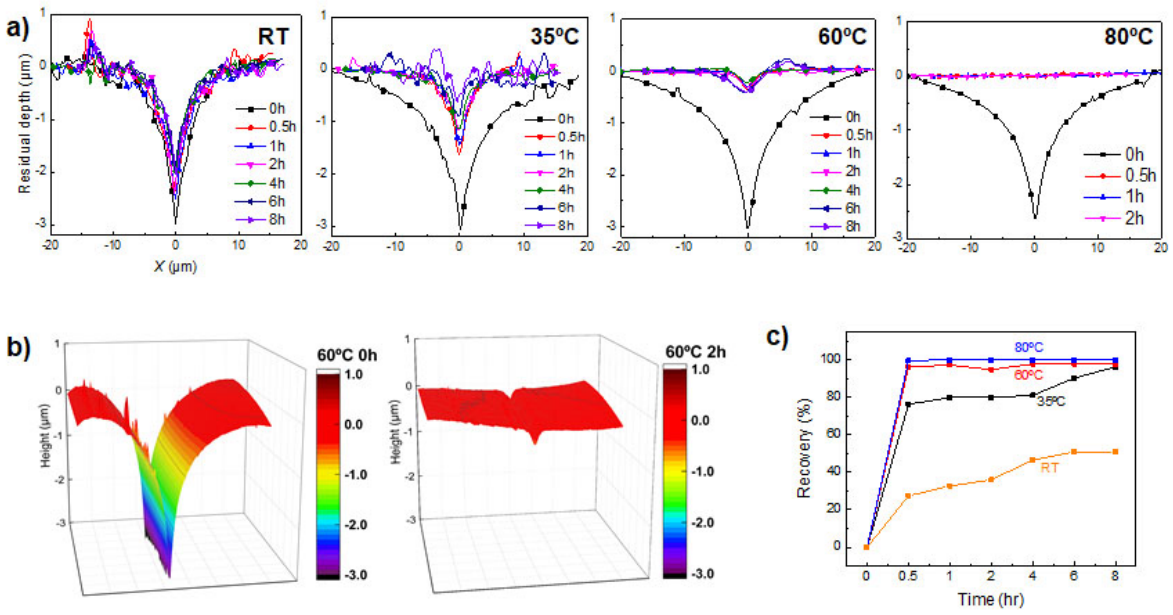

Figure 3.3. Evolution of AFM profiles of scratches made on the surfaces of PHU films annealed at RT, 35, 60 and 80 °C (a), temporal scratch patterns realized by AFM annealed at 60 °C (b), and %recovery of the scratches at the temperatures (c).

3.3.5 Mechanical and Viscoelastic Properties of PHU Network Films

Mechanical properties of the PHU network were measured using dynamic mechanical analysis (DMA) over a temperature range at -60 - 140 °C. Rectangular films with the dimension of 10 x 1 x 0.1 mm were cast at 40 °C for 2 hrs. Figure 3.4a shows their storage and loss moduli upon a temperature scan mode. After the storage modulus underwent a gradual glass transition with an onset point of 50 °C, the modulus kept a plateau in a short range of temperature up to 125 °C, retaining crosslinked networks in the temperature. Different from conventionally-crosslinked networks, the modulus decreased upon further increase in temperature. Similar DMA result is reported for a vitrimer-like poly(alkylurea-urethane) network, where the onset of flow temperature is defined as the initial temperature where the modulus starts to deviate from the plateau.[167] Further to DMA test, tensile measurements using Universal Testing Machine (UTM) were conducted. As seen in Figure 3.4b, the networks had the Young's modulus = 0.57 ± 0.02 MPa and the maximum tensile strength = 1.9 ± 0.4 MPa at break with 156 ± 5% elongation.

Next, to get an insight into self-healability of PHU network, self-healing elasticity was examined so as to measure their viscoelastic properties using a rheometer upon a cyclic change of

oscillation force: 5% strain for 1500 s to 95% strain for 500 s under the constant 10 rad/s frequency. As seen in Figure 3.4c, the initial elastic modulus (G') of the film was 6.5×10^4 Pa when a 5% strain was applied. Upon the change of oscillating force to 95% strain, the G' modulus dropped to 2.1×10^3 Pa. Then, the G' modulus was restored when the oscillation force was recovered back to 5% strain. Such a reversible restoration of G' modulus was able to be repeated several times, exhibiting self-healing elasticity of the crosslinked polymeric networks.

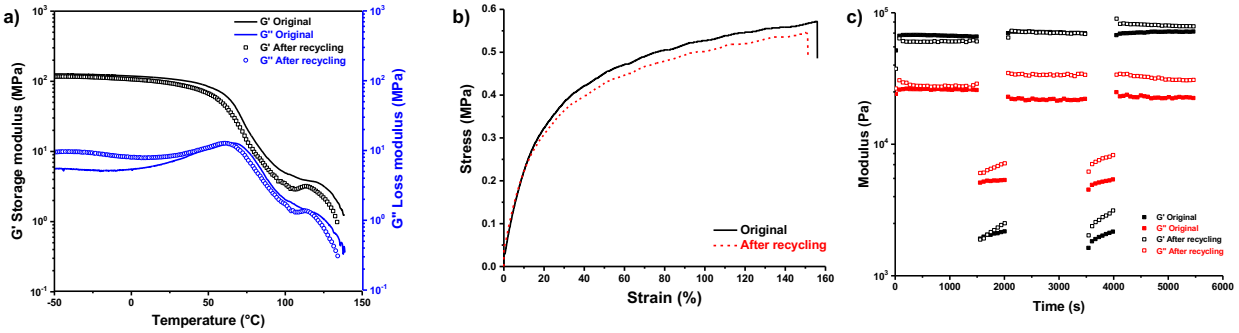

Figure 3.4. Mechanical properties as storage and loss moduli measured using DMA over a temperature range at -60 - 140 °C (a) and tensile measurements using UTM (b) as well as viscoelastic properties using a rheometer upon a cyclic change of oscillation force: 5% strain for 1500 s to 95% strain for 500 s under the constant 10 rad/s frequency (c) for original and recycled PHU network films.

3.3.6 Reprocessability Upon Self-healing

The PHU networks exhibit temperature-induced reversibility and thus their reprocessability was investigated. The dried PHU films were pulverized into small pieces, and then mixed with THF. The resulting mixture was heated at 60 °C and then recast in a Teflon mold to the films. As compared in Figure 3.4, the recycled films had similar mechanical and viscoelastic properties, as compared with those for original counterparts. Young's modulus = 0.55 ±0.01 MPa and the maximum tensile strength = 1.7 ± 0.4 MPa at break with 151 ± 4% elongation imply >97% recovery of those properties. For self-healing elasticity, they gained initial elastic modulus (G') to be 6.0×10^4 Pa in a 5% strain, which corresponds to 93% recovery upon reprocessing of the original PHU films. Such dynamic nature of the networks could be advantageous of polyurea or polyurethane plastics designed with PHU networks as building blocks for reprocessability

3.3.7 Fabrication and Performance of Self-healable Triboelectric Nanogenerator

Here, self-healable PHU was mixed with o-CNT to fabricate o-CNT/PHU composite films as negative triboelectric materials, along with Al electrode used as a positive triboelectric material (Figure 3.5a and 3.5b). Note that o-CNT/PHU composites are more negative triboelectric materials than the Al electrode because of the difference in triboelectric polarity (Figure 3.S8a-c). Additives such as carbon-based materials or metal oxides have been widely used to improve triboelectric performance through increasing dielectric constant (ε_r) in polymer matrix.[168-171] An introduction of o-CNT into polymer matrix increases the work function through the oxygen-containing functional groups in o-CNT.[172, 173] In addition, o-CNT increases the dielectric constant of polymer composites because of the interfacial polarization at the interface between the polymer and o-CNT,[174, 175] leading to the improvement of triboelectric performance. Given these features, o-CNTs were embedded in PHU network composites, which decreased the surface potential of polymer composites (Figure 3.S8b and 3.S8c). The as-prepared o-CNT/PHU composite films show a smooth and clean black color (Figure 3.S9), indicating o-CNTs being well dispersed in the network compared to pristine CNTs showing rough surface with stained black color. After all, the self-healable o-CNT/PHU composite was placed on the surface of Al electrode (Figure 3.5c), leading to the metal-dielectric based triboelectric nanogenerator.

When the polymer composite film and Al top electrode were contacted and separated repeatedly, the triboelectric device underwent contact electrification and electrostatic induction (Figure 3.S10a), producing the periodic electric output signals (Figure 3.S10b). For the triboelectric output performance, the output open-circuit voltage was used to analyze the peak-to-peak values, which refers to the difference between the highest and lowest values of the signal in a period. Figure 3.5d shows the triboelectric peak-to-peak voltage of polymer composites with various concentrations of o-CNTs up to 0.7 wt%. Surface potential decreased with the increase of o-CNT amount in the polymer composite film (Figure 3.S8b and 3.S8c). However, higher output peak-to-peak voltage (125 V) was displayed with 0.2 wt% of o-CNT (Figure 3.S11a-d), which is mainly caused by higher dielectric constant (5.4 at 100 Hz and 10 N) (Figure 3.S11e). It should be noted that dielectric constant is a more critical factor to enhance the triboelectric performance than the surface potential.[176, 177] Moreover, for the polymer composites with 0.2 wt% o-CNT that displays similar surface potentials independent of the film thickness (Figure 3.S12a), the output voltage increased with the decrease of thickness of composite films from 380 to 240 μm (Figure

3.5e and 3.S12b-e). This result is attributed to the increased dielectric constant through interfacial polarization at interface between polymers and o-CNTs (Figure 3.S12f). However, upon further decrease of film thickness, dielectric constant reduced because of the leakage current for thinner film (Figure 3.S12g). This reduced dielectric constant decreased the triboelectric voltage. These results suggest that 0.2 wt% o-CNT/PHU polymer composite with 240 μm thick shows the greatest triboelectric voltage.

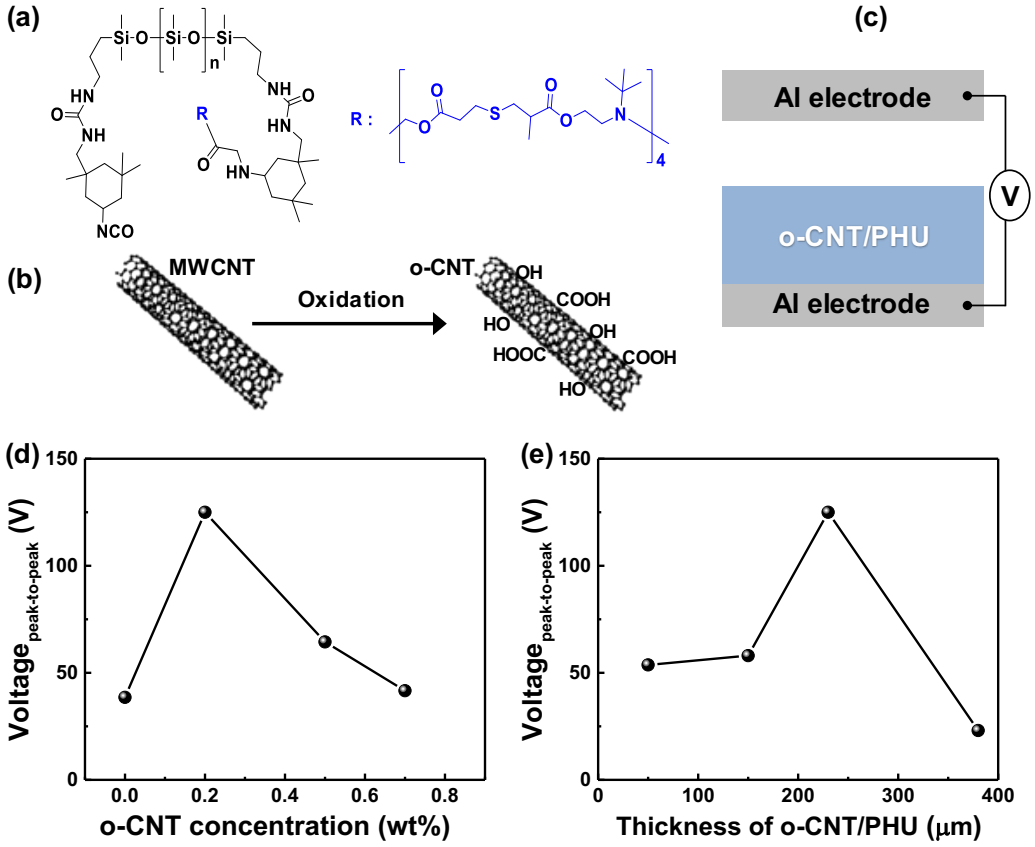

Figure 3.5. Scheme of the self-healable polymer (a) and oxidized MWCNT (b) for the self-healable polymer composite, and the triboelectric devices composed of single-layered polymer composite film (c). Triboelectric peak-to-peak voltages of the device depending on the concentration of oxidized MWCNT in the polymer composite film (d) and thickness of the polymer composite with 0.2 wt% o-CNT (e).

3.3.7 Enhancement and Recovery of Interfacial Polarization-Induced Triboelectric Output Upon Self-healing

It is well-known that multilayered dielectric film with a large contrast of permittivity and electrical conductivity can induce the interfacial polarization between dissimilar layers to greatly

enhance the dielectric constant.[178, 179] In order to further improve the output performance of self-healable triboelectric nanogenerators, we utilized a layer-stacked polymer composite film as a negative triboelectric material. In this work, a bilayered polymer film was prepared with two heterogeneous layers consisting of a bare PHU layer with the thickness of ≈130 μm (ε_r: 3.2−3.8) and a 0.2 wt% o-CNT/PHU composite layer with the thickness of ≈240 μm (ε_r: 5.0−5.4) (Figure 3.6a). It can be anticipated that the difference in permittivity can induce interfacial polarization and increase the dielectric constant. As seen in Figure 3.6b, the bilayered polymer film exhibited an increased output peak-to-peak voltage (169.9 V) compared to the single-layer films. Such increase is attributed to the increased dielectric constant (7.2 at 100 Hz and 10 N, Figure 3.S13) through the interfacial polarization induced at the interface between the dissimilar polymer films. Compared with the reported healable triboelectric devices, our device displays analogous or even-higher output performance (see Figure 3.S14, Table 3.S1 and Table 3.S2).

By comparison, the dielectric constant of bilayered polymer films with the same PHU films (3.5 at 100 Hz and 10 N) is similar to the single layer PHU film (3.8 at 100 Hz and 10 N), implying no induced interfacial polarization because of no difference in permittivity (Figure 3.S13), which leads to the suppression of triboelectric performance (51 V, Figure 3.S15). Therefore, the self-healable PHU with reversible hindered-urea bonding can cause the formation of layered polymer films through the specified interaction between the self-healable polymers, resulting in the increased dielectric constant through the interfacial polarization between dissimilar layers, enhancing the triboelectric performance.

The self-healing property is required to retain the output performance in the triboelectric device when the device surface is damaged.[52, 151, 152, 180] We investigated the behavior of triboelectric voltage before and after self-healing. Micron-sized scratches were made by rubbing the surface of a 0.2 wt% o-CNT/PHU polymer composite film with a sandpaper (800 grits) (Figure 3.6c). As seen in Figure 3.6d, its output voltage decreased from 125 to 88 V, which is caused by the decrease of contact area through the uneven surface (Figure 3.6e).[181] Very promisingly, after self-healing process at 90 °C and 80% humidity condition for 20 min, the film surface was restored to its initial one (Figure 3.6c) through reversible hindered-urea chemistry. This results in the recovery of triboelectric voltage (130 V, Figure 3.6d). Owing to the self-healing property of PHU film, the self-healable triboelectric nanogenerator shows long-term stability over 10000 cycles and also

operates even after healing process over 5 times (Figure 3.S16 and 3.S17), which is comparable to the others in the previous reports.[58, 182]

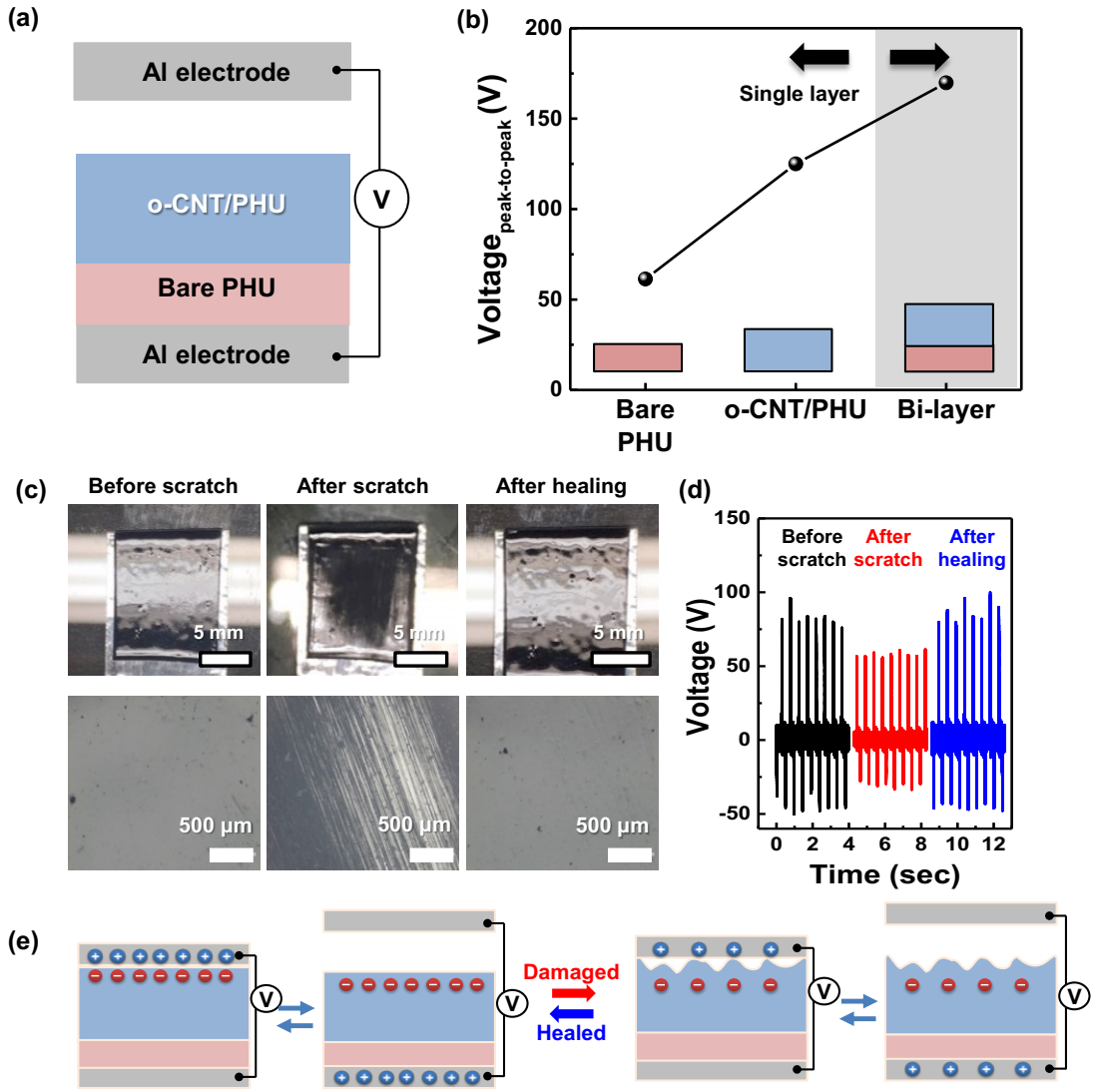

Figure 3.6. Scheme of the triboelectric device composed of bi-layered polymer composite film (a). Triboelectric peak-to-peak voltage of the optimized single- and bi-layer films (b). Digital photographs (top) and optical images (bottom) of polymer composites with 0.2 wt% o-CNT before and after healing at 90 °C and 80 % humidity condition (c). Triboelectric output voltage of the self-healable polymer composite with 0.2 wt% o-CNT before and after healing (d). Scheme of working mechanism before and after healing (e).

3.4 Conclusion

Dynamic PHU networks crosslinked with bulky urea linkages were developed by step-growth polymerization through a two-step polyaddition process from a reactive mixture consisting of a diisocyanate, PDMS diamine, and 4-arm star t-butylamine at ambient temperature. The networks formed under a catalyst-free condition exhibit the reversible dissociation/reformation of hindered urea linkages upon the change in temperature and thus had the ability to rapid void filling and self-healing of micron-sized cracks on film surfaces at ambient conditions. Further, they were flexible but with greater mechanical properties as high as 1.7 MPa of tensile strength at break and reprocessed to cast PHU films with the recovery of their mechanical and viscoelastic properties as high as >95%. Given these promising results being self-healable, transparent, and reprocessable, the developed vitrimeric PHU films enabled the fabrication of robust TENG device that possess excellent interfacial polarization-induced triboelectric performance superior to the reported systems as well as rapid recovery through effective self-healing. These results offer the versatility of the approach toward the development of advanced TENG materials with great triboelectric output as well as excellent self-healability and reprocessability to increase their lifetime and preserve fossil fuels. Promisingly, this approach can be expanded to other energy-harvesting applications including artificial skins, flexible sensors, nanorobotics, and portable/wearable devices.

3.5 Chapter 3 Supporting Figures

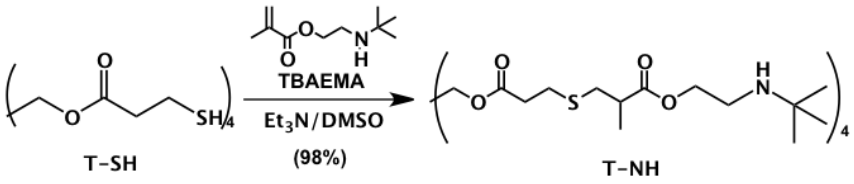

Figure 3.S1. Synthesis of T-NH by a click-type thiol-ene reaction through Michael addition reaction

Figure 3.S1 depicts the synthesis of T-SH with t-BAEMA in the presence of Et_3N, a base catalyst, at room temperature. The formed product was purified with precipitation from water. ^{1}H-NMR spectrum in Figure 3.S2 shows the two peaks at 4.1-4.3 ppm corresponding to two types of methylene protons (a and h) as well as the peak at 1.1 ppm (g) corresponding to t-butyl protons. Their integral ratio was used to estimate the conjugation efficiency as high as >99%. Further, the GPC diagram of the product was clearly shifted to high molecular weight region, with M_n = 1,400 g/mol (Figure 3.S3).

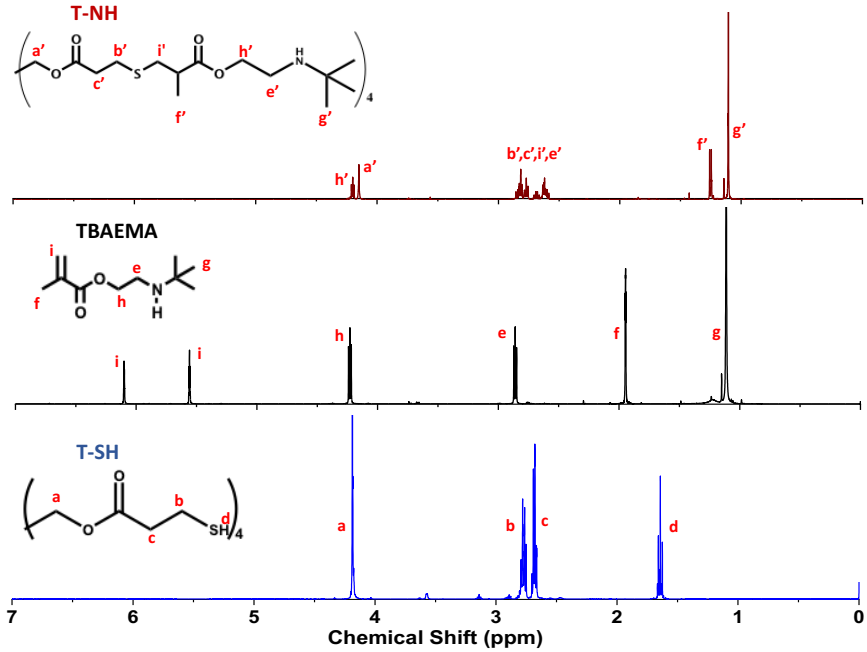

Figure 3.S2. ^{1}H-NMR spectra of T-NH overlaid with its precursors, T-SH and t-BAEMA in $CDCl_3$.

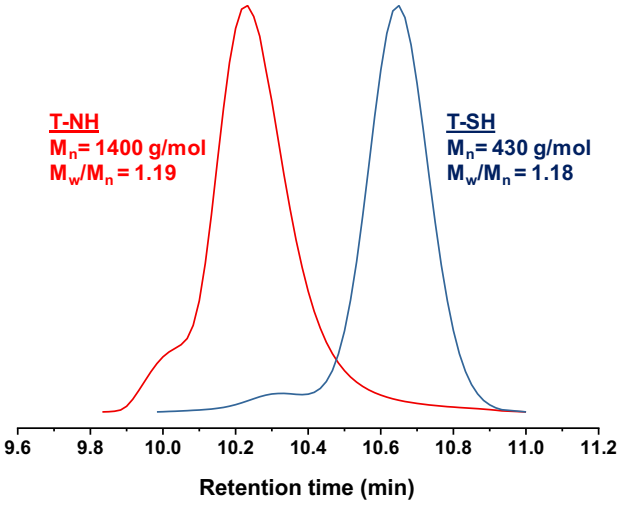

Figure 3.S3. GPC spectrum overlay of T-NH and reagent Tetra-SH.

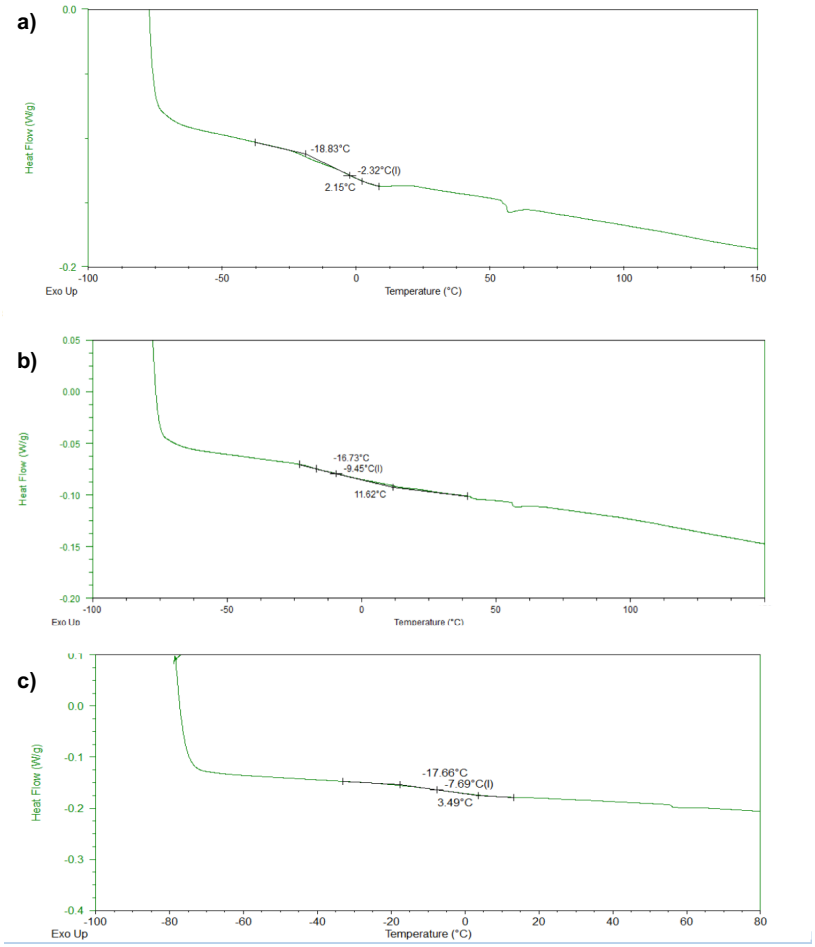

Figure 3.S4. DSC traces of PHU networks fabricated through Route A (a), B (b), and C (c).

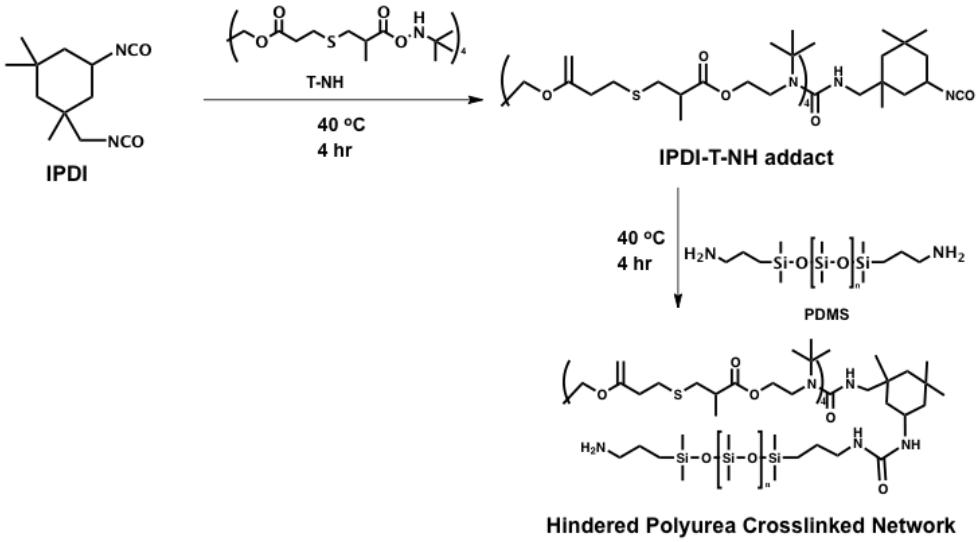

Figure 3.S5. Schematic illustration of Route B.

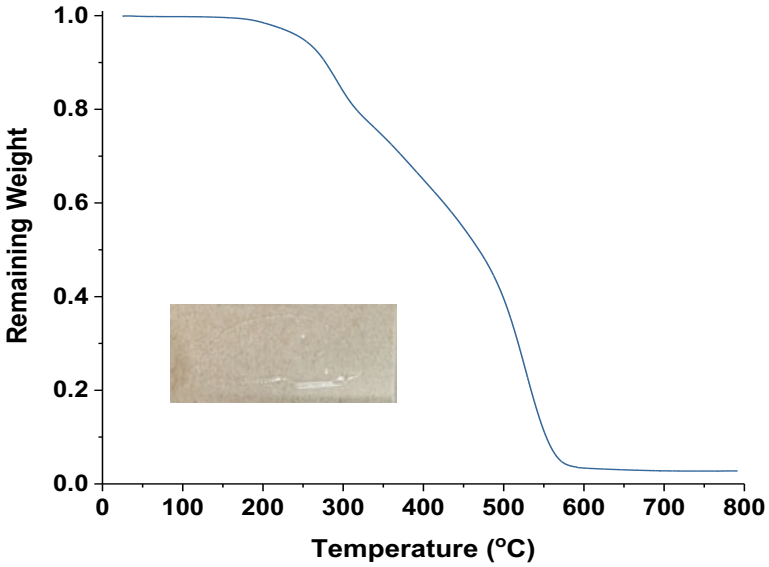

Figure 3.S6. TGA trace of PHU fabricated through Route C. Inset: digital photo of a dried film cast on glass plate.

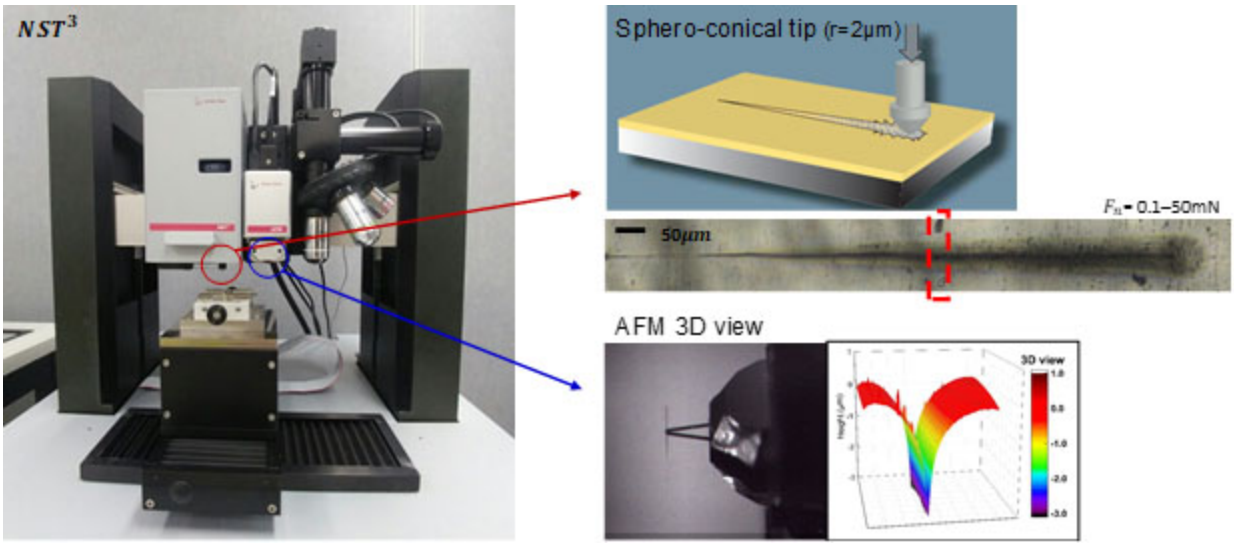

Figure 3.S7. Schematic of nano-scratch tester (NST^3) with optical microscope and AFM.

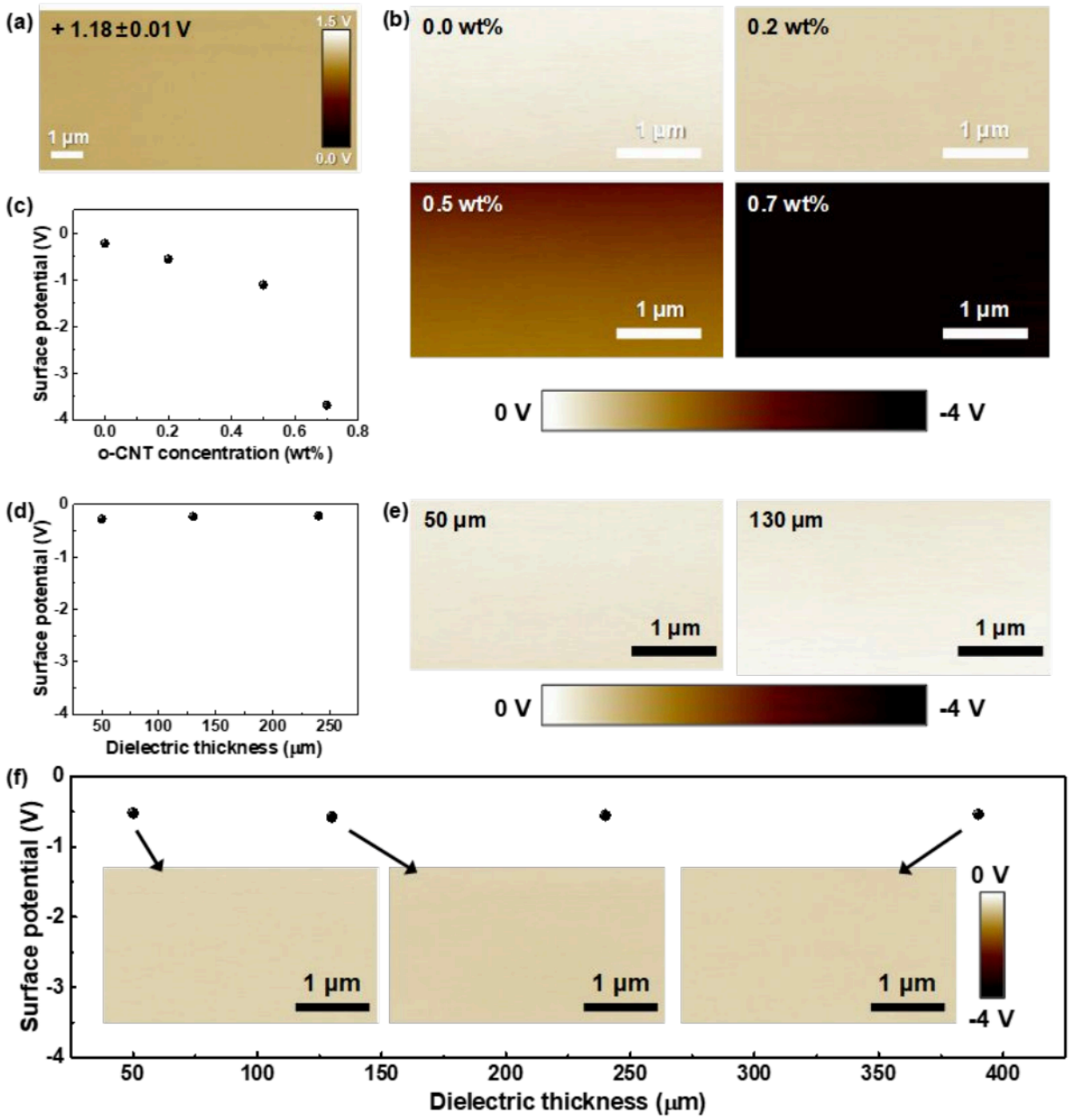

Figure 3.S8. (a) KPFM image of Al electrode. (b) KPFM images and (c) surface potentials of self-healable polymer composite with ~240 μm of thickness at different o-CNT concentration. (d) Surface potentials and (e) KPFM images of self-healable polymer composites with 0.0 wt% of o-CNT at different thickness. (f) Surface potentials of self-healable polymer composites with 0.2 wt% of o-CNT at different thickness; The insets are the KPFM images corresponding to the surface potentials at different film thickness.

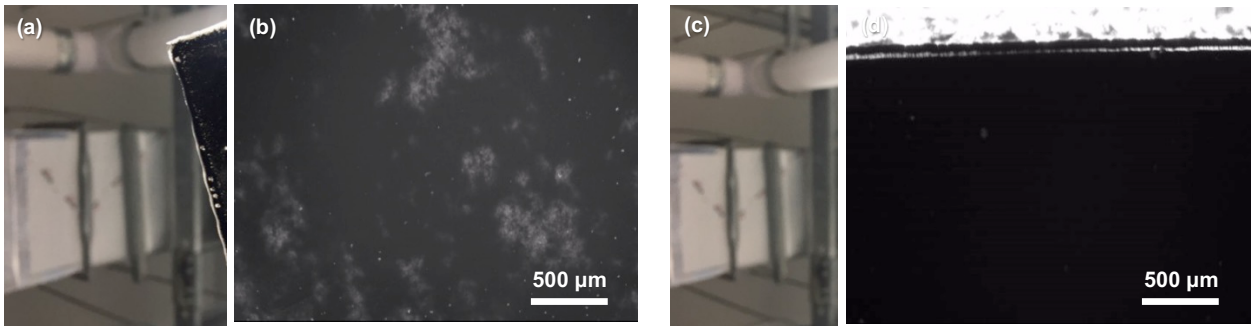

Figure 3.S9. Digital photographs and optical images of self-healable polymer composites with untreated MWCNT (a and b) and oxidized MWCNT (c and d).

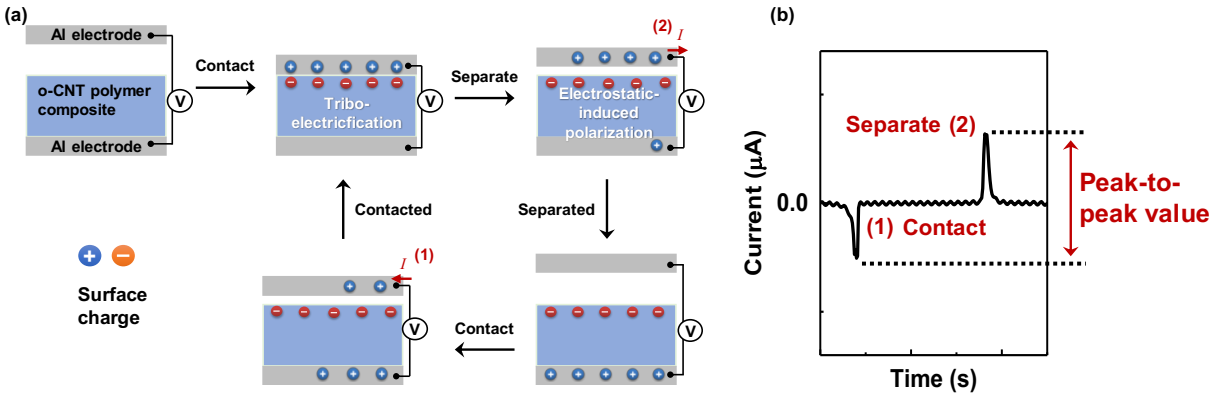

Figure 3.S10. (a) Triboelectric working mechanism of o-CNT-polymer composites *via* contact electrification and electrostatic induction. (b) Triboelectric output signals corresponding to contact (1) and separation (2) processes in (a).

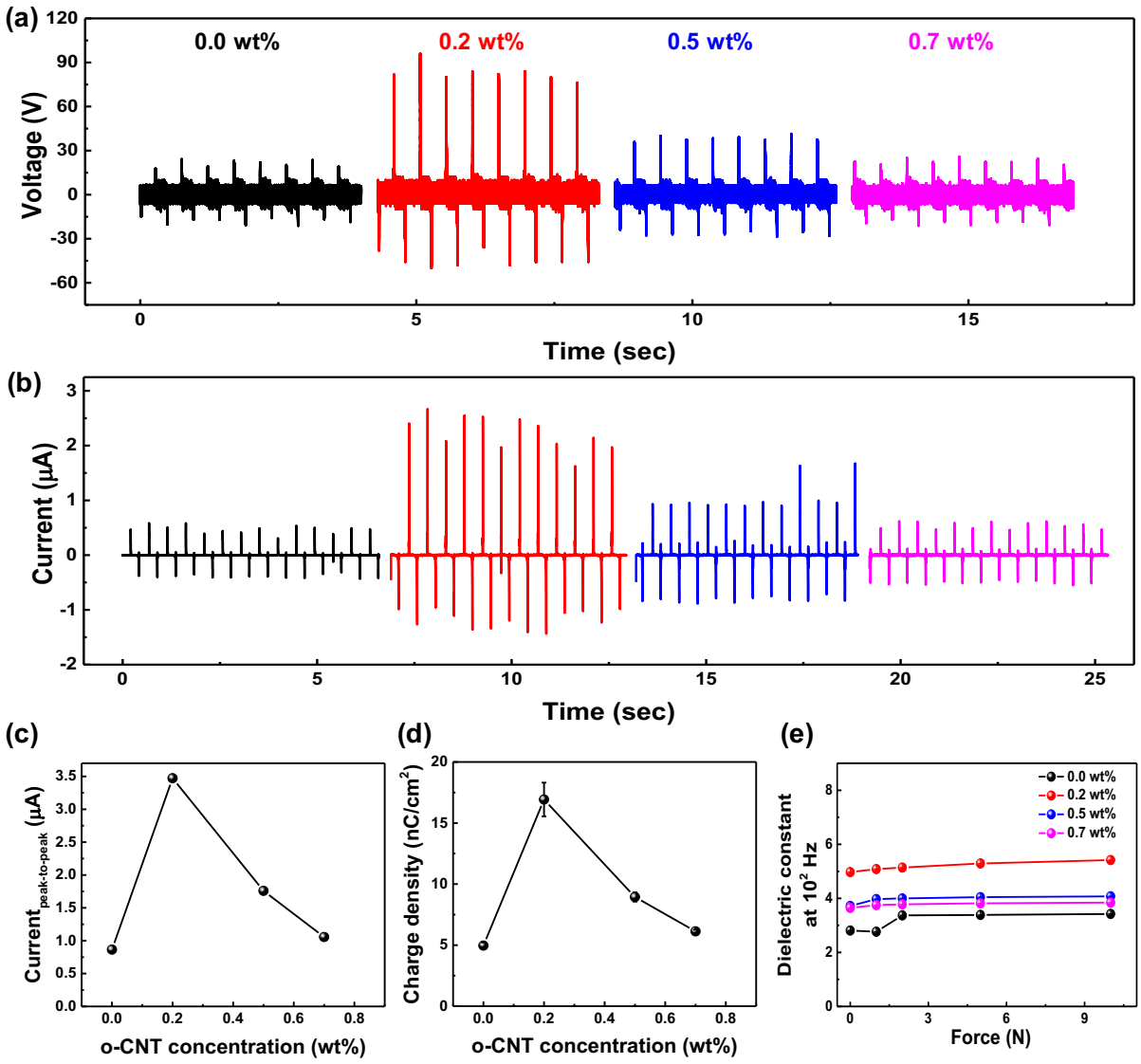

Figure 3.S11. Triboelectric output performances (a-d) and dielectric constant at 100 Hz (e) under different loading force of PHU polymer composites with different concentration of o-CNT at 240 μm; Triboelectric voltage (a), current (b) signals, and plots of (c) the peak-to-peak current values and (d) the transferred charge density

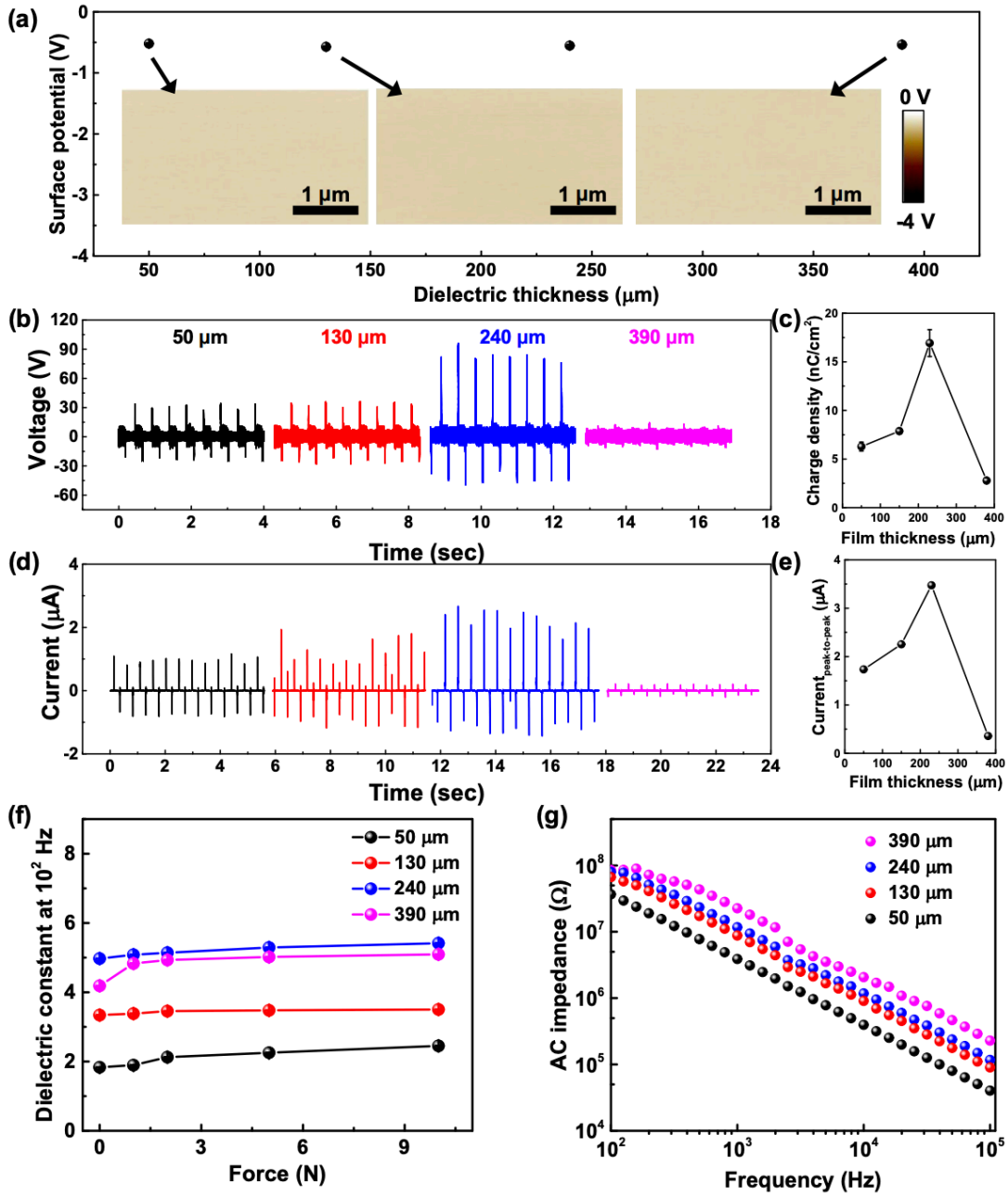

Figure 3.S12. Surface potentials (a), triboelectric output performances (b-e) and dielectric properties (f and g) of self-healable polymer composite with 0.2 wt% of o-CNT at different thickness; The inset in (a) are the KPFM images corresponding to the potentials at different film thickness. Triboelectric voltage signals (b), plot of the transferred charge density (c), triboelectric current signals (d), and plot of the peak-to-peak current values (e). Dielectric constant (f) at 100 Hz under different loading force, and AC impedance (g) of polymer composites with 0.2 wt% of o-CNT at different thickness.

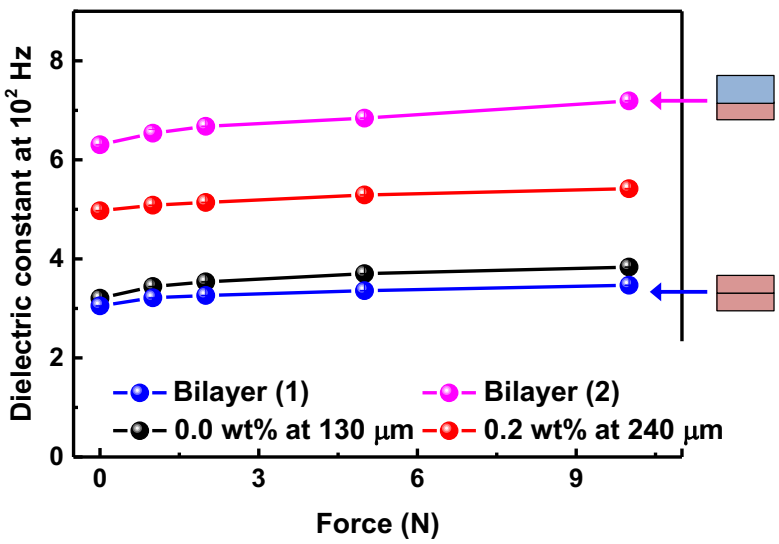

Figure 3.S13. Dielectric constant of single- and bi-layered polymer composite film; Bilayer (1) and (2) indicate homogeneous bilayered polymer film without o-CNT and heterogeneous bilayered film with 0.2 wt% o-CNT coated on 0.0 wt% o-CNT polymer composites.

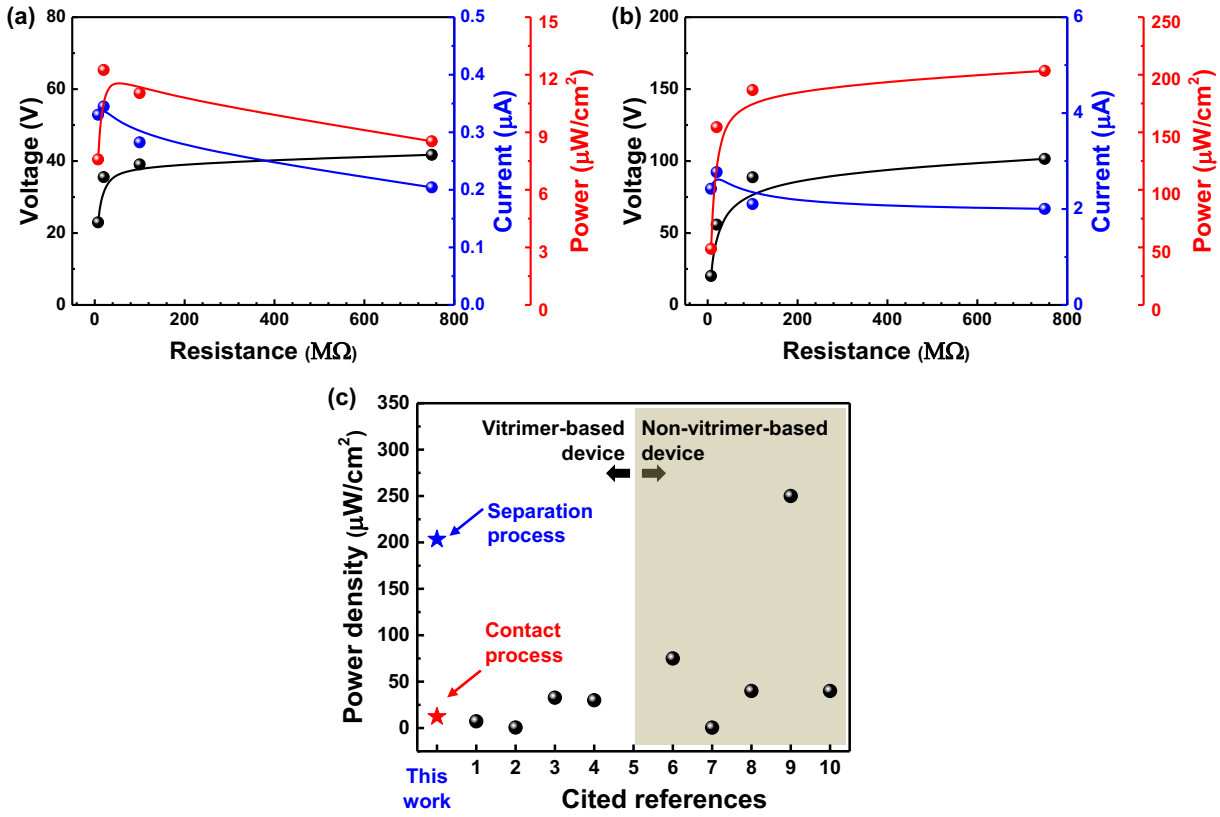

Figure 3.S14. Triboelectric voltage, current, and power density as a function of load resistance of the triboelectric device consisting of optimized bi-layer polymer film during (a) contact and (b) separation process, respectively. (c) Comparison of the power density of self-healable triboelectric devices.

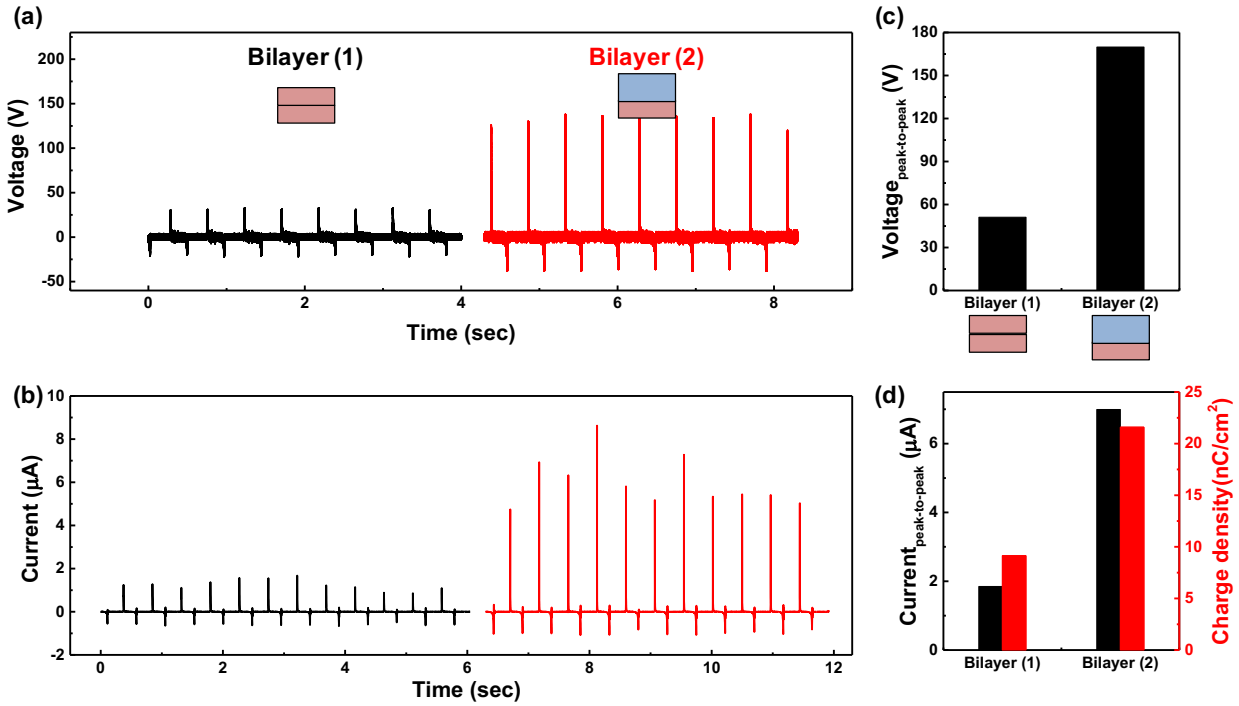

Figure 3.S15. Triboelectric voltage (a) and current (b) signals and the corresponding peak-to-peak values (c and d) of bilayered polymer films: Bilayer (1) and (2) indicate homogeneous bilayered polymer film without o-CNT and heterogeneous bilayered film with 0.2 wt% o-CNT coated on 0.0 wt% o-CNT polymer composites, respectively.

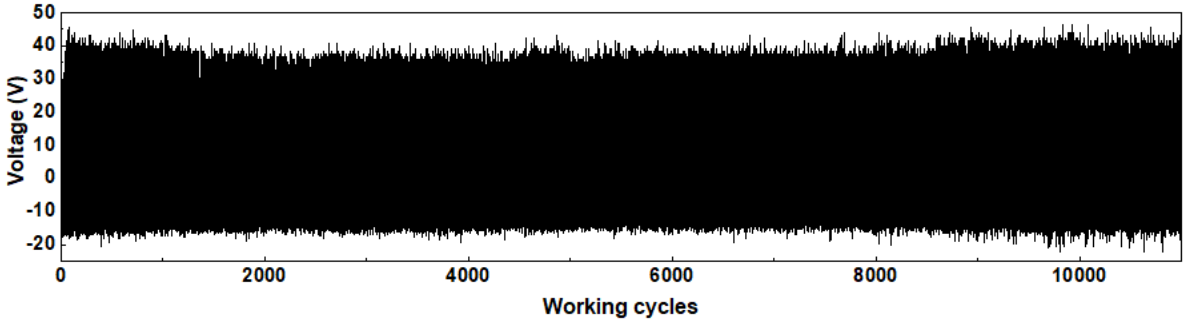

Figure 3.S16. A repeated cycle test of 0.2 wt% o-CNT/PHU film over 10000 cycles at 3 N and 2 Hz.

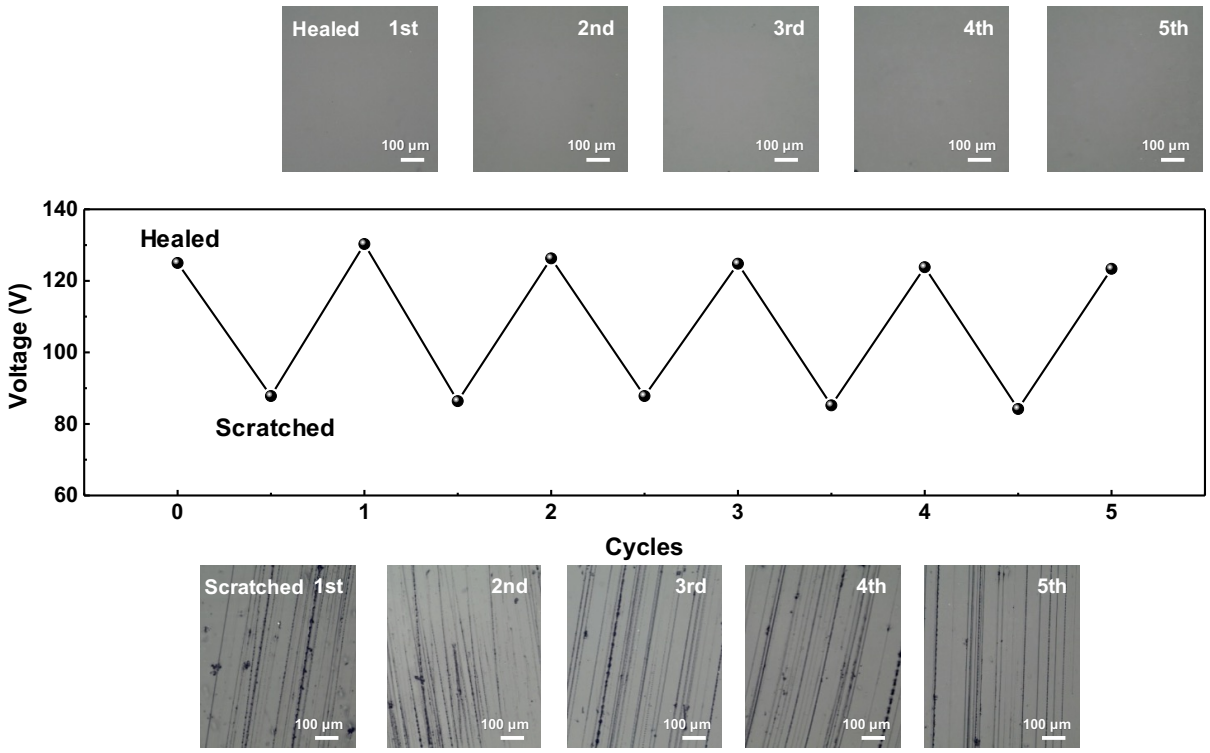

Figure 3.S17. Triboelectric output voltage of 0.2 wt% o-CNT/PHU film during repetitive scratch and healing processes. The surface is scratched by a sandpaper (800 grits) at 1 N and healed at 90 ºC and 80% humidity condition for 20 min. The inset optical images correspond to each surface after scratch and healing process.

Table 3.S1. Comparison of the output performances of vitrimer-based triboelectric devices.

Materials	Driving mode	Triboelectric performance	Self-healing mechanism	Ref.
Epoxy resin-based polysulfide elastomoer embedding Ag NWs	Single electrode mode	V_{OC}~6.5 V/cm^2 J_{SC}~0.09 μA/cm^2 Q_{SC}~2.5 nC/cm^2	Reversible disulfide reaction	58
PDMS-PU assisted by magnetic healable electrode	Contact-separation	V_{OC}~0.9 V/cm^2 J_{SC}~0.08 μA/cm^2	Reversible reaction of disulfide and hydrogen bond links	180
PDMS/Ag-PEDOT	Single electrode mode	V_{OC}~15.7 V/cm^2 J_{SC}~0.17 μA/cm^2 Q_{SC}~5.7 nC/cm^2	Reversible imine bonds	56
Amine-terminated PDMS/PEA with MWCNT	Single electrode mode	V_{OC}~6.0 V/cm^2 J_{SC}~0.6 μA/cm^2 Q_{SC}~2.7 nC/cm^2	Reversible imine bonds and quadruple hydrogen bonding	157
Epoxy resin-based polysulfide elastomoer embedding MWCNT	Single electrode mode	V_{OC}~5.6 V/cm^2 J_{SC}~0.07 μA/cm^2 Q_{SC}~1.8 nC/cm^2	Aromatic disulfide metathesis	153
0.2 wt% oxidized CNT/PHU	**Contact-separation**	**For bi-layer film** **$V_{OC,peak\text{-}to\text{-}peak}$~169.9 V/cm^2** **$J_{SC,peak\text{-}to\text{-}peak}$~7.0 μA/cm^2** **$Q_{SC,peak\text{-}to\text{-}peak}$~21.6 nC/cm^2**	**Reversible hindered urea**	**This work**

Table 3.S2. Comparison of the output performances of self-healable, but non-vitrimer-based triboelectric devices.

Materials	Driving mode	Triboelectric performance	Self-healing mechanism	Ref.
Poly(vinyl alcohol) Polydopamine particle MWCNT	Single electrode mode	V_{OC}~10.6 V/cm^2 J_{SC}~0.11 μA/cm^2 Q_{SC}~3.6 nC/cm^2	Hydrogel	155
Amine-terminated PDMS with Zn catalyst and tetrahydroborate ions	Single electrode mode	V_{OC}~2 V/cm^2 J_{SC}~0.8-2.4 nA/cm^2 Q_{SC}~0.7 nC/cm^2	Hydrogel and metal-ligand interaction	152
Polyurethan acrylate with Ag flakes and liquid metal	Single electrode mode	V_{OC}~11.1 V/cm^2 J_{SC}~4 μA/cm^2 Q_{SC}~12 nA/cm^2	Reversible reaction of hydrogen bond links	151
PDMS/TPU semi-embedding Ag NWs and graphite powder	Contact-separation	V_{OC}~30 V/cm^2 J_{SC}~2.9 μA/cm^2 Q_{SC}~10 nC/cm^2	Hot mething of TPU and reversible hydrogen bonding of PDMS under IR irradiation	183
Slime hydrogel (PVA/tetraborohydrate)	Single electrode mode	V_{OC}~12.5 V/cm^2 J_{SC}~6.5 μA/ cm^2 Q_{SC}~17 nC/ cm^2	Hydrogel	52

Chapter 4. Self-healable Triboelectric Nanogenerators Based on Ionic Poly(hindered urea) Network Materials Cross-linked with Fluorinated Block Copolymers

4.1 Introduction

Energy harvesting is the process of extracting sustainable electrical energy from waste mechanical energy in the environment.[132-134] Triboelectric nanogenerator (TENG) uses triboelectric effect and electrostatic induction to convert mechanical motions from environments into electrical energy. Because of tremendous features including high instantaneous output power, wide range of available materials, eco-friendly and low-cost fabrication process, and various working modes tailored to specific applications, the TENG has been considered as the most effective energy harvester.[34, 184-193] However, the TENG is constantly subjected to external mechanical inputs (bending, twisting, pressing, sliding, etc.), which can cause mechanical damage and lead to malfunction. In order to improve its lifetime and intrinsic functions for mechanical energy harvesting and advanced wearable devices, the development of TENG capable of self-repairing on mechanical damages is highly desired (hereby SH-TENG).[27, 55, 149, 150] A promising approach is to integrate dynamic covalent chemistries in covalent adaptive networks (CANs) as effective triboelectric materials. A few reports describe the exploration of disulfide,[154, 194-197] boronic ester,[155, 156, 198] imine,[56, 199-201] and recently hindered urea[4] chemistries in the development of high-performance SH-TENGs. Despite these advances, the design and synthesis of advanced CANs with their structural variation are highly demanded to understand design principles for the improvement of SH-TENG performance.

Naturally occurring and synthetic polymers have been the choice of triboelectric materials in the construction of TENG devices.[159, 202] These polymers exhibit consistent charge transfer patterns related to their chemical natures and thus can be used as either triboelectric negative or positive material depending on their affinity to electrons. The design principle involves the selection of the pair of triboelectric negative and positive materials retaining as large as electron affinity to increase triboelectric charge, thus, improving TENG performance.[177, 203] Benefiting the strong electron-attractive force of fluorine element, fluorine-containing polymers such as polytetrafluoroethylene,[204-206] fluorinated ethylene propylene copolymer,[21, 207, 208] and poly(vinylidene fluoride)[21, 209, 210] have been extensively used as electron-accepting layers in

TENG devices. Because of their lack of functional groups for further modifications, however, these fluorinated polymers have been physically blended with film-forming polymers. Such a physical blending approach could present a limitation in the development of dynamic CANs covalently conjugated with fluorinated polymers as self-healable triboelectric negative materials for advanced SH-TENGs. Further to the focus on the choice of materials, ionic liquids induce ionic polarization, enhancing dielectric constant and thus triboelectric performance and ionic conductivity.[2, 211-214] Recent reports describe the introduction of ionic liquid to fluorinated networks to improve TENG output through enhanced ionic polarization induced by ion-dipole interactions of pendant fluorinated groups with ionic liquids.[5]

In this work, we have explored a reactive block copolymer approach to fabricate dynamic fluorinated poly(hindered urea) (PHU) network materials containing ionic liquids as effective self-healable negative triboelectric materials. Well-controlled fluorinated block copolymer (FBCP) was designed with a reactive block having pendant bulky t-butylamino groups (self-healability) and the other block containing fluorinated pendants (triboelectric properties), and synthesized by a controlled radical polymerization. The formed FBCP was integrated as a multi-crosslinker in two-step step-growth polymerization to fabricate dynamic PHU network crosslinked through the formation of hindered urea bonds and formulated with dangling fluorinated species. Followed by the addition of an ionic liquid, the formed ionic iFBCP-PHU materials were characterized with thermal, mechanical, and self-healing properties as well as TENG outputs in the construction of robust SH-TENGs. Promisingly, the iFBCP-PHU materials exhibit rapid and high recovery of triboelectric performance upon self-repair of surface damages.

4.2 Experimental

Materials. Isophorone diisocyanate (IPDI, 98%), bis(3-aminopropyl) terminated polydimethylsiloxane (PDMS-DA, MW = 2500 g mol−1), 2-(t-butylamino)ethyl methacrylate (TBAEMA, 97%), 4-cyanopentanoic acid dithiobenzoate (CPADB), 2,2′-azobis(2-methylpropionitrile) (AMBN, 98%) from Sigma-Aldrich as well as 2,2,2-trifluoroethyl acrylate (TFEA, 98%) and 1-ethyl-3-methylimidazolium bis(trifluoromethanesulfonyl)imide (EMIM-TFSI, 98%) from TCI chemicals were purchased and used as received.

Synthesis of FBCP by RAFT polymerization. In the first step to synthesize PTFEA macro-RAFT agent, TFEA (4.0 g, 26.0 mmol), CPADB (145.0 mg, 0.51 mmol), and AMBN (28.0 mg,

0.17 mmol) were dissolved in anisole (5.0 mL) in a 25 mL Schlenk flask. The mixture was deoxygenated by purging under nitrogen for 45 min and then placed in an oil bath pre-heated at 70 °C for 16 h. The polymerization was stopped by cooling to room temperature in an ice bath. In the second step to synthesize PTFEA-b-PTBAEMA block copolymer, TBAEMA (4.0 g, 21.6 mmol), the purified, dried PTFEA macro-RAFT mediator (3.39 g, 0.54 mmol), and AMBN (30.0 mg, 0.18 mmol) were dissolved in anisole (12.0 mL) in a 50 mL Schlenk flask. The mixture was purged with nitrogen for 45 min and then placed in an oil bath pre-heated at 70 °C for 15 h. The polymerization was stopped by cooling to room temperature in an ice bath.

As-synthesized (co)polymers were purified by precipitation from cold hexane (excess) three times. The precipitates were dried in a vacuum oven set at 40 °C for 24 h.

Fabrication of FBCP-PHU crosslinked networks by two-step polyaddition. A mixture of IPDI (0.71 g, 3.2 mmol) with PDMS-DA (4.0 g, 1.6 mmol) dissolved in MEK (60 mL) was stirred at 70 °C for 4 h. After an addition of FBCP (1.24 g, 0.1 mmol), the resulting mixture was stirred at 70 °C for an additional 4 h, yielding a transparent solution of FBCP-crosslinked PHU in MEK. To prepare ionic FBCP-PHU containing 1 wt% EMIM-TFSI, the as-prepared solution of FBCP-PHU was mixed with EMIM-TFSI (60 mg, 0.15 mmol) under stirring at room temperature for 12 h. Optically transparent PHU films were drop-casted on glass plates, pre-dried at room temperature overnight, and further dried at 90 °C for 30 min.

Instrumentation and analyses. 1H NMR spectroscopy using a 500 MHz Varian spectrometer for structure determination and conversion analysis and gel permeation chromatography (GPC) with a Viscotek VE1122 pump and a refractive index (RI) detector for molecular weight analysis calibrated with poly(methyl methacrylate) standards were conducted as described in our previous publications.[215, 216].

Thermal properties were measured by differential scanning calorimetry (DSC) analysis with a TA Instruments DSC Q20 and thermogravimetric analysis (TGA) with a TA Instruments Q50 analyzer.[97, 217] Optically-transparent PHU films drop-casted on glass plates as above were tested for the thermal analysis.

Tensile properties were measured using a Z5 Tensile machine from Hoskin Scientific equipped with a 1 kN load cell. The samples were loaded until failure with a strain rate of 10 mm min−1.

To prepare the type VI (ASTM D638) dumb-bell-shaped specimens for tensile testing, the dried films prepared above were cut into small pieces, placed in rectangular molds (7.5 cm × 1.5 cm), and compressed using a hot press at 130 °C for 3 min at 70 kPa pressure. The resulting films with 2 mm thick were cut to render dumb-bell-shaped samples.

Scratch recovery and self-healing of crosslinked films using nano-scratch tester (NST) with atomic force microscopy (AFM). A nano-scratch tester (NST, Anton Paar Tritec SA, Switzerland) was used to quantitatively compare scratch patterns and recovery features on the surfaces of crosslinked films. A sphero-conical 90° indenter with a 2 μm radius tip applied the progressive load from 0.1 to 50 mN on the film surface by horizontally moving at a 2 mm min−1 scan speed along a 1 mm length. Recovery and self-healing of scratches made on the surfaces of crosslinked films at 30 mN load (i.e., equivalent to nearly 0.6 mm position from the loading start-up) were compared from 2D cross-section cuts using the atomic force microscopy (AFM Wide Scan, Anton Paar Tritec SA, Switzerland) implemented in the NST under annealing times of 30 min at healing temperature of 90 °C and 1 day at 50 °C. The AFM images were acquired in a squared-scan area of 77.1 μm × 77.1 μm with 256 scan lines for 256 s.

Fabrication of triboelectric nanogenerators. An organic solution of as-synthesized FBCP-PHU (0.5 g) dissolved in MEK was mixed with different amounts of ionic liquid. The resulting homogeneous solution was poured into a Teflon mold. Solvent was slowly evaporated to form FBCP-PHU/ionic liquid composite films. The prepared films were coated on the surface of Al electrode at 120 °C and then used as negative triboelectric films.

Measurements of triboelectric properties. The performances of the triboelectric device based on the dielectric polymer film (1 × 1 cm2) were measured using a sourcemeter (S-2400, Keithley) and an oscilloscope (DPO 2022B, Tektronix, US) under a loading of 10 N by means of a pushing tester (JIPT-100, Junil Tech) at 2 Hz.

4.3 Results and Discussion

A well-defined PTFEA-b-PTBAEMA block copolymer (FBCP) with narrow molecular weight distribution was synthesized by a consecutive RAFT polymerization, as depicted in Figure 4.1a.

In the first step, the RAFT polymerization was initiated with AMBN and TFEA in the presence of CPADB, a RAFT mediator, at 70 °C in anisole. The polymerization was designed with the target degree of polymerization (DP) as an initial mole ratio of $[TFEA]_0/[CPADB]_0$ = 50/1. After being purified by precipitation from hexane at 80% monomer conversion, the formed PTFEA was characterized by ^{1}H NMR for its chemical structure and GPC for its molecular weight. 1H NMR spectrum in Figure 4.1b shows a typical peak at 4.4 ppm (b) for TFEA units and 7.4–7.9 ppm (a) for aromatic protons in CPADB RAFT species. Using their integral ratio, the DP of PTFEA was determined to be 39, thus yielding $PTFEA_{39}$ homopolymer. It had a molecular weight as the number average molecular weight of (M_n) = 8.5 kg mol^{-}1 with dispersity (Đ) = 1.30 by GPC analysis (Figure 4.1c).

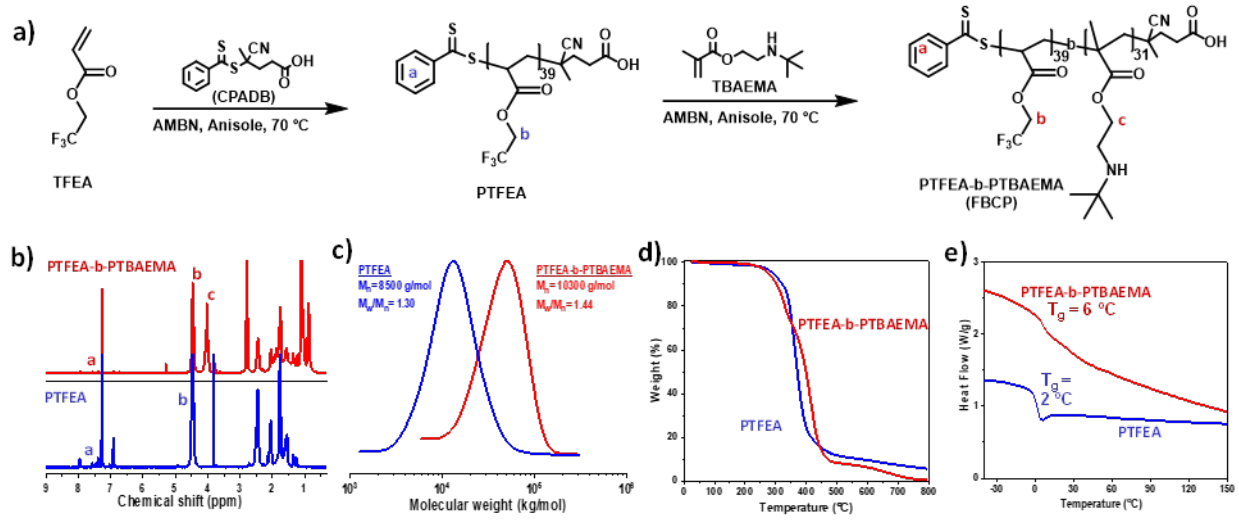

Figure 4.1. Synthesis and characterization of well-defined FBCP block copolymer. Synthetic scheme of FBCP (a); overlaid ^{1}H NMR spectra in CDCl3 (b); GPC traces (c); TGA diagrams (d); and DSC diagrams (e) of FBCP, compared with PTFEA RAFT-macro mediator.

In the second step, the purified, dried PTFEA was used as a macro-RAFT mediator for the RAFT polymerization of TBAEMA with $[TBAEMA]_0/[TFEA]_0$ = 40/1. At 75% monomer conversion, the synthesized polymer was purified by precipitation from hexane. The GPC trace of the formed copolymer shows a clear shift to high molecular weight region with M_n = 10.3 kg mol^{-}1 and Đ = 1.44 and no significant trace of PTFEA macro-RAFT agent (Figure 4.1c). This GPC result confirms the successful chain extension of PTFEA block with PTBAEMA block. ^{1}H NMR shows the typical peaks at 4.0 (c) for TBAEMA units and 4.4 ppm (b) for TFEA (Figure 4.1b). Given the DP of PTFEA block = 39, their integral ratio allowed us to determine the DP of PTBAEMA block

to be 31, thus yielding $PTFEA_{39}$-b-$PTBAEMA_{31}$ block copolymer and the mole ratio of TFEMA/TBAEMA = 0.55/0.45.

Further to the structural analysis, the thermal properties of both PTFEA and FBCP block copolymer were examined. The TGA diagram shows a single-step weight loss with a residue of <5% for PTFEA, whereas a stepwise weight loss with no significant residue for FBCP (Figure 4.1d). DSC analysis confirms a single glass transition (Tg) at 2 °C for PTFEA and 6 °C for FBCP (Figure 4.1e).

The synthesized FBCP is well-controlled with narrow molecular weight distribution and consists of a reactive block having pendant t-butylamino groups for dynamic crosslinking and a dielectric block having fluorinated pendants. The copolymer was used to react with a prepolyurea terminated with NCO as a multi-crosslinker to fabricate fluorinated PHU network materials crosslinked with FBCP through the formation of bulky t-butylamino urea linkages (called FBCP-PHU). Figure 4.2 illustrates our approach of two-step step-growth polymerization via polyaddition. IPDI first reacted with PDMS-DA in MEK at 70 °C with the mole ratio of NCO/amine designed to be 1/0.5 (0.5 equivalent excess NCO) to synthesize IPDI-PDMS prepolymers terminated with reactive NCO groups. In the second step, the formed polyurea prepolymers reacted with FBCP at the same temperature with the mole ratio of NCO/amine (t-butylamino groups) = 0.5/0.5, yielding a clear solution of FBCP-PHU network materials crosslinked with dynamic hindered urea linkages. The materials are characteristic with IPDI/PDMS-DA/FBCP = 11.9/67.2/20.9 wt/wt/wt and PTFEA = 10.4 wt%.

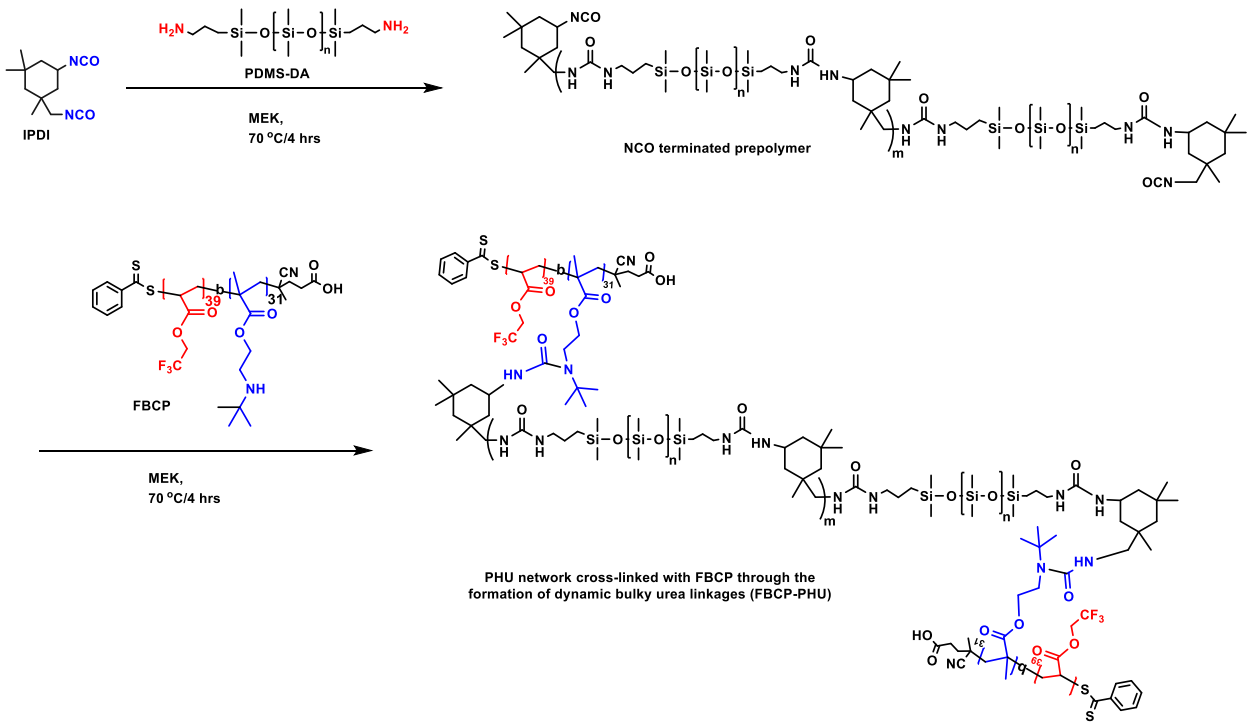

Figure 4.2 A schematic representation of two-step step-growth polycondensation to fabricate FBCP-PHU network crosslinked through the formation of dynamic bulky urea linkages with well-defined FBCP bearing pendant fluorinated species in a block and bulky t-butylamino groups in the other block.

Next, the formed FBCP-PHU network was mixed with 1 wt% EMIM-TFSI in MEK to fabricate iFBCP-PHU materials. Their optical, thermal, viscoelastic, and mechanical properties were characterized and compared with those of bare FBCP-PHU materials (with no EMIM-TFSI). The as-synthesized solutions were drop-casted on glass plates and then dried at 90 °C for 30 min. Both formed films were transparent. TGA and DSC techniques were used to examine their thermal properties. Both networks degraded at 200–660 °C, with <2% residues, from TGA analysis (Figure 4.3a and 4.3b). Interestingly, both films had single glass transition, which occurred at −1 °C, based on DSC analysis (Figure 4.3c and 4.3d). These results suggest that the thermal properties of FBCP-PHU networks were not affected with the presence of 1 wt% EMIM-TFSI.

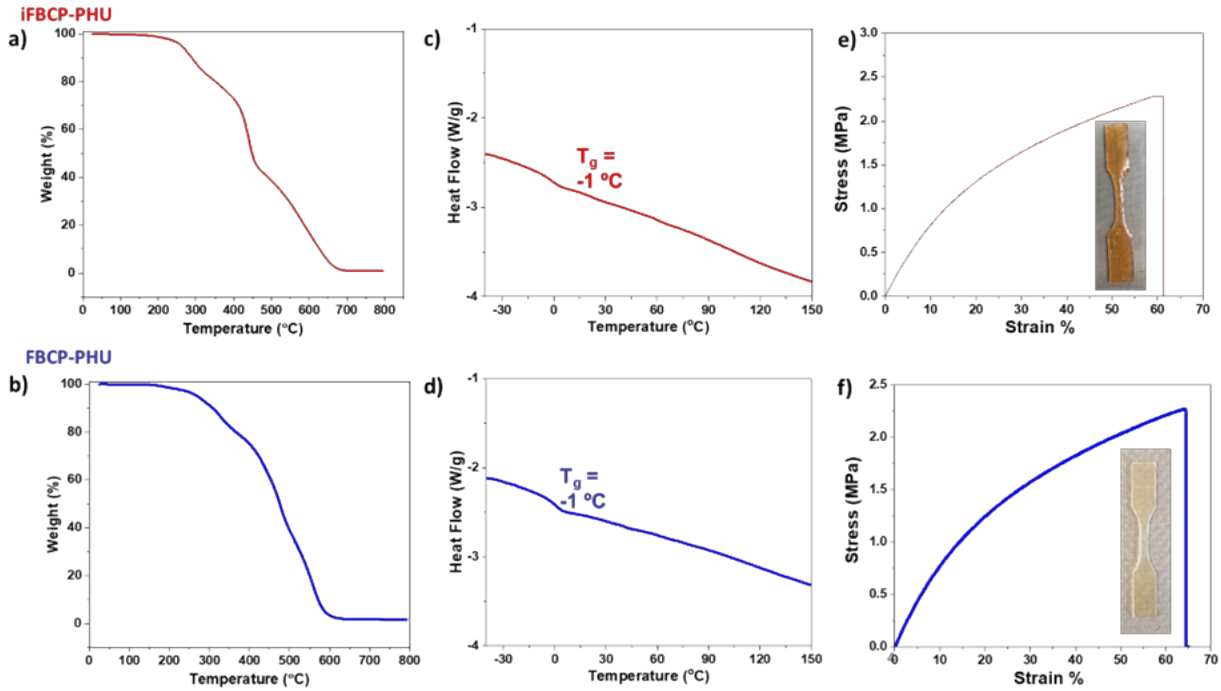

Figure 4.3 Characterization of iFBCP-PHU materials containing 1 wt% EMIM-TFSI, compared with bare FBCP-PHU materials. TGA diagrams (a and b), DSC diagrams (c and d), and stress–strain curves from tensile measurements using UTM (insets: digital images of tested films) (e and f).

Given these optical and thermal properties, mechanical properties of the network materials were measured by a tensile tester. Another network was designed with 5% EMIM-TFSI to determine the effect of IL on the film's mechanical properties. The films cast on glass plates at 100 °C were cut into small pieces, compression-molded to a rectangular-shaped specimens using a hot press, which was cut to a dumb-bell-shaped specimen (insets of Figure 4.3e and 4.3f). iFBCP-PHU network had the maximum tensile strength = 2.3 MPa, elongation at the break = 63%, and Young's modulus = 9.6 MPa, while FBCP-PHU had the maximum tensile strength = 2.0 MPa, elongation at the break = 69%, and Young's modulus = 7.1 MPa (Figure 4.3e and 4.3f). Another network was designed with 5% EMIM-TFSI 5% which had the maximum tensile strength = 3.2 MPa, elongation at the break = 21%, and Young's modulus = 14 MPa, (Figure 4.4a, 4.4b, 4.4c). These results implicate that the incorporation of EMIM-TFSI in the FBCP-PHU network designs mechanically stronger films than bare FBCP-PHU. The reason is not clear; however, it would be associated with the possibility of the blocks of pendant CF_3 species, interacting with ionic liquid in phase-separated microstructures of PHU networks. Similar results have been reported for

different polymeric systems; particularly, polyacrylonitrile films containing 1 wt% 1-butyl-3-methylimidazolium chloride.[218, 219]

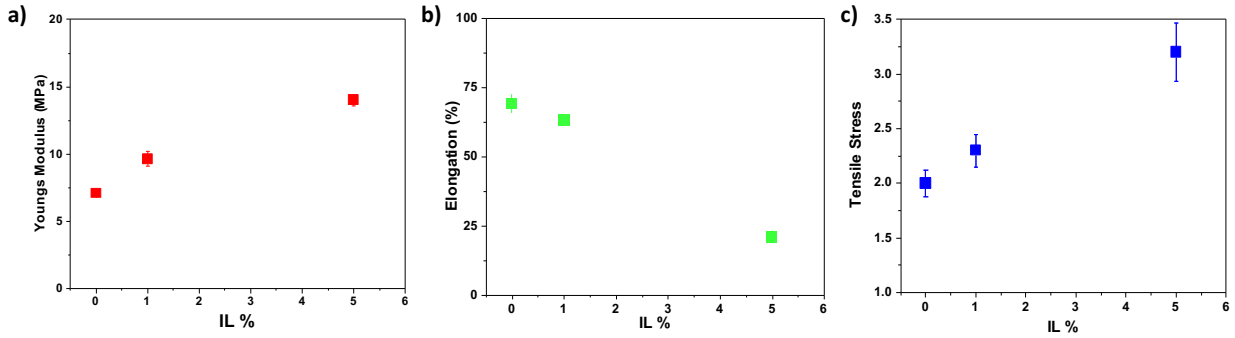

Figure 4.4 Comparing mechanical properties of FBCP-PHU with 1% and 5% EMIM-TFSI Young's modulus (a), elongation at break (b), tensile stress at break (c).

Self-healing and recovery of crosslinked iFBCP-PHU films were investigated with scratches made on their surfaces, employing NST equipped with AFM. Films with uniform surfaces were cast on steel plates at 30 °C for 1 h and annealed at 90 °C for 30 min. Micron-sized scratches (<25 μm) were generated on the surfaces using an indenter under a progressive load ranging from 0.1 to 50 mN. Their healing profiles at 30 mN were examined using AFM at elevated temperatures of 50 °C and 90 °C. Figure 4.5 shows the changes in the scratch patterns for iFBCP-PHU film over 30 min at 50 and 90 °C. By evaluating the area recovered from initial scratched area in 2D AFM crosscut images, the percent recovery was determined. Recovery was enhanced over the annealing time, especially after 10 min, and obviously it turned to be greater at higher temperature (90 vs. 50 °C), as clarified from residual depth profiles scanned by AFM (Figure 4.5d–4.5f). Promisingly, the percent recovery reached >88% within 10 min at 90 °C. Given the promising NST/AFM results, self-healing and recovery of iFBCP-PHU films were further examined with the recovery of mechanical properties by tensile test. Compression-molded dumb-bell-shaped specimens were prepared with micron-sized scratches (100–150 μm wide) on their surfaces by a razor and annealed at 120 °C for 1 h. The scratches appeared to be completely healed with naked eyes (Figure 4.S1a). %Recovery of their mechanical properties as their tensile strengths at break turned to be 163% (Figure 4.S1b and c). In addition to excellent self-healability of surface cracks, the improvement of film integrity upon annealing at elevated temperature could lead to the greater % recovery of tensile strength (>100%). Overall, the results from both NST/AFM and tensile studies suggest excellent surface self-healability of iFBCP-PHU film at high temperatures.

Self-healing features for FBCP-PHU and iFBCP-PHU films are mainly compared during the annealing time of 1 day at 50 °C. Note that the percent recovery data for both films with high recovery performance at 90 °C healing temperature were very similar to each other due to the strong thermal effect that could not distinguish the role of a small amount of the ionic liquid. As expected with their mechanical properties, the percent recovery was somewhat higher on iFBCP-PHU film in a long-term annealing time, compared to FBCP-PHU (Figure 4.S2). In the case of iFBCP-PHU film, the recovery rate was initially lower than that for FBCP-PHU film, and then gradually increased, eventually showing a percent recovery of about 70% (65.6% for FBCP-PHU). This is mainly attributed to the iFBCP-PHU film tougher than its bare precursor.

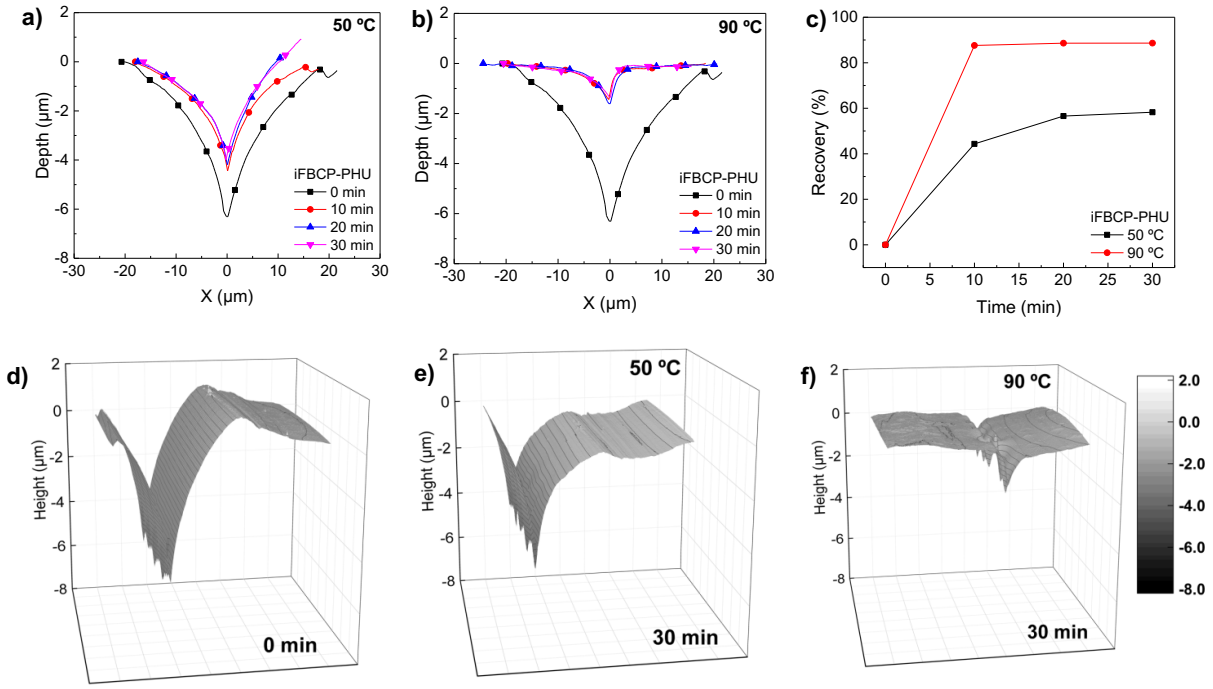

Figure 4.5 Recovery of scratch profile on the surface of iFBCP-PHU crosslinked film at 50 °C (a) and 90 °C (b); the percent recovery data up to annealing time of 30 min (c); 3D AFM scratch images at annealing times of 0 min (d), 30 min for 50 °C (e) and for 90 °C (f).

To evaluate triboelectric performance of iFBCP-PHU networks as negative triboelectric materials, a metal-dielectric-based triboelectric nanogenerator was constructed with Al electrode as positive triboelectric materials (Figure 4.S3 and 4.6a). When PHU film and Al top electrode are periodically contacted, contact electrification and electrostatic induction generate alternating electric output signals. The films were drop-cast in the Teflon mold and annealed at 150 °C on the

surface of Al electrode. The annealing temperature is an important parameter to optimize TENG output since the annealing process causes the rearrangement of polymer chains. It has been reported that the triboelectric output performance of the materials can be enhanced by tuning the surface potential and dielectric constant through the control of free volume in the polymer matrix.[177]In our experiment, the TENG output was dependent on the annealing time at 150 °C. The FBCP-PHU film annealed for 10 min displays higher output current (0.11 ± 0.02 μA) during the contact process than the others (Figure 4.S4a). This is plausibly due to the improved polarization through the polymer chain packing structure, leading to the enhancement of triboelectric performance.[177, 220]

Given the annealing condition, the iFBCP-PHU film containing 1.0 wt% EMIM-TFSI shows the triboelectric output current of 0.21±0.02 μA and 0.56±0.03 μA during contact and separation process, respectively (Figure 4.6b), which is much greater than those for the bare FBCP-PHU film (0.11±0.02 μA and 0.08±0.01 μA during contact and separation, respectively, Figure 4.S4b). This is attributed to the fact that the CF_3 groups in the side chains interact with EMIM-TFSI through ion-dipole interactions,[211] leading to the improved polarization and thus triboelectric performance.

The triboelectric performance is affected by the contact area under different mechanical force.[221] As shown in Figure 4.S5, when the mechanical force increases from 2 N to 10 N, the output performances increase because of the increase in contact area with higher mechanical force. Moreover, the performances during the separation process (Figure 4.S5a-c) are higher than those during the contact process (Figure 4.S5d-f), which is caused by higher separation velocity than the contact velocity.[4, 222] After all, the iFBCP-PHU shows the highest triboelectric power at 40 MΩ (0.37 μW/cm^2 and 3.78 μW/cm^2 during contact and separation process under 10 N, respectively). Moreover, the iFBCP-PHU shows long-term stability over 2000 cycles (Figure 4.S6).

Finally, the TENG performance of iFBCP-PHU materials was examined upon self-healing (recovery) of surface scratches. The iFBCP-PHU film scratched by the sandpaper (2000 grits) at 1 N force displays the void-filling of scratches (Figure 4.6c). However, after healed at 150 °C within 5 min, the scratches are disappeared (Figure 4.6d), indicating the surface recovery to the initial state. As seen in Figure 4.6e, the scratched film exhibits the decrease of triboelectric peak-

to-peak current (0.43 μA), which is 85% to the original film, whereas the healed film shows the full-recovery of output current.

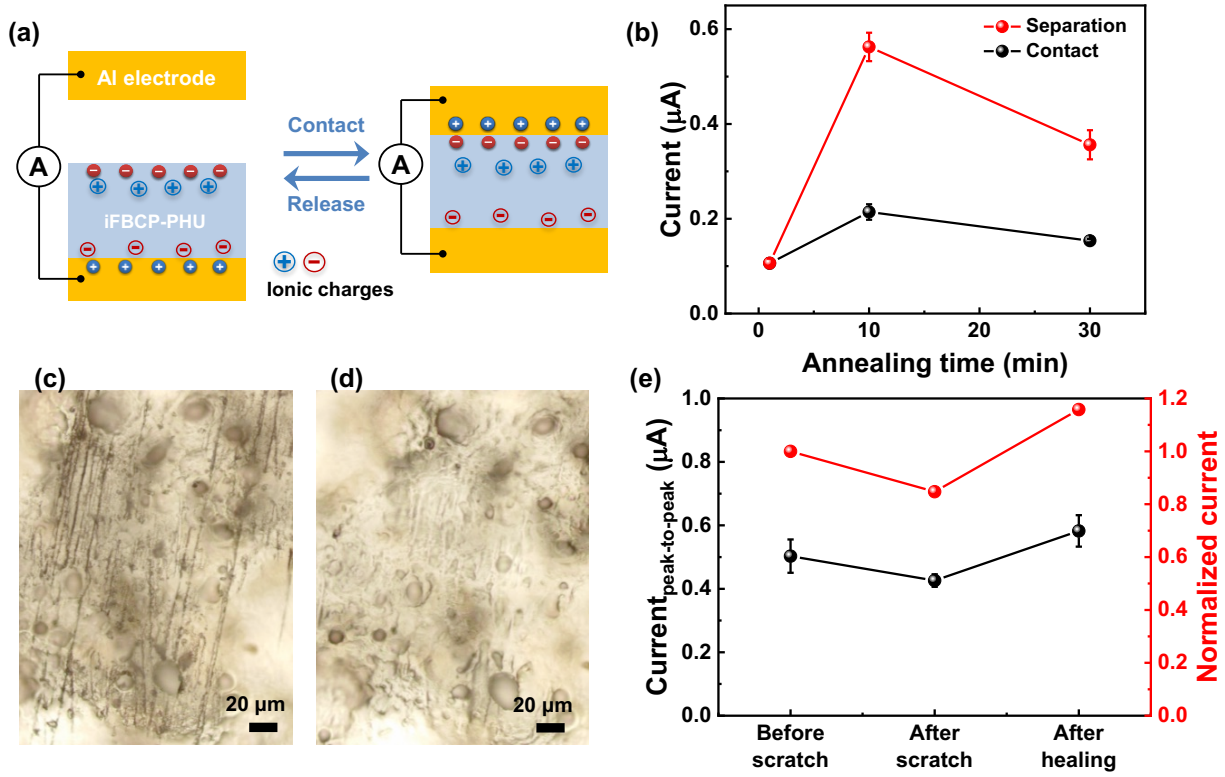

Figure 4.6 Scheme of a triboelectric device composed of iFBCP-PHU as a negative material and Al as a positive material (a); triboelectric output of iFBCP-PHU after annealed at 150 °C for given times (b); optical microscope images of iFBCP-PHU films after being scratched (c) and healed (d) at 150 °C for 5 min; triboelectric peak-to-peak current of iFBCP-PHU film after scratched by sandpaper (2000 grits) and healed at 150 °C for 5 min (e).

4.4 Conclusion

A new approach was developed to fabricate self-healable TENG based on ionic PHU network materials crosslinked through bulky urea groups with reactive FBCP. A well-established RAFT polymerization was employed to synthesize well-controlled FBCP with narrow molecular weight distribution and pre-determined molecular weight, which consist of a reactive block having pendant t-butylamino group covalently attached to a TENG block with fluorinated pendants. The copolymer was used as a reactive crosslinker in two-step step-growth polymerization under mild condition, resulting in the fabrication of ionic iFBCP-PHU network materials upon the addition of ionic liquid. The fabricated materials were highly transparent and flexible, but tough with Young's

modulus as high as 17.4 MPa. They exhibit excellent self-healability at elevated temperatures as micron-sized surface cracks were recovered up to >95% in 10 min at 90 °C, by NST-SFM measurements. Furthermore, the materials were demonstrated to be effective negative triboelectric materials as to show enhanced TENG output. Promisingly, TENG output was completely recovered upon healing of surface cracks.

4.5 Supporting information and figures for chapter 4

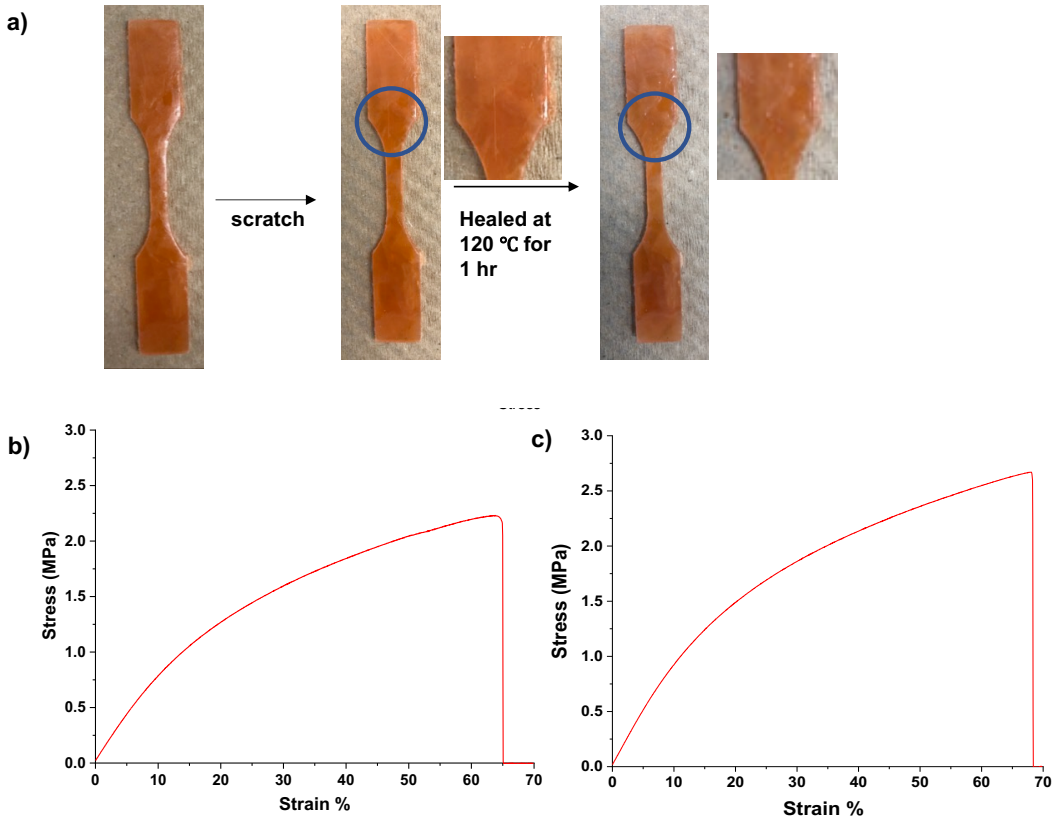

Figure 4.S1. Digital images of tensile specimens (a) as well as stress-strain curves before (b) and after (c) healing at 120 °C for 1 hr. Note that the blue-colored circles show the scratch made with a razor before and after annealing.

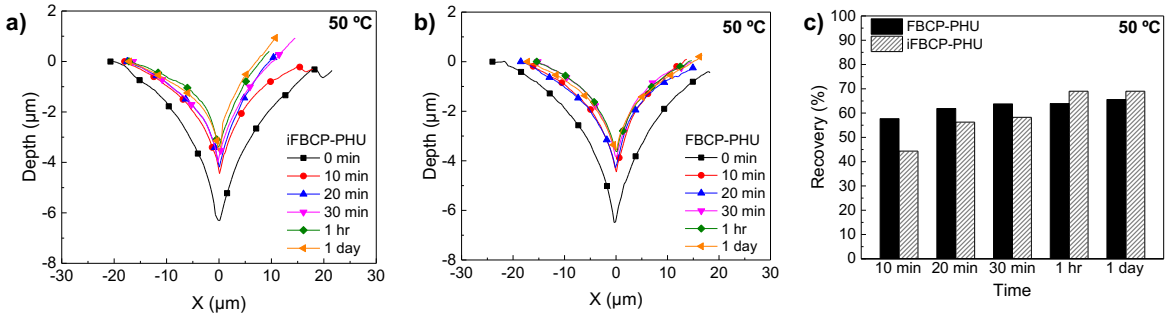

Figure 4.S2. Comparison of temporal scratch profiles for iFBCP-PHU (a) and FBCP-PHU (b) films at 50 °C during annealing time of 1 day; Percent recovery data for two films (c).

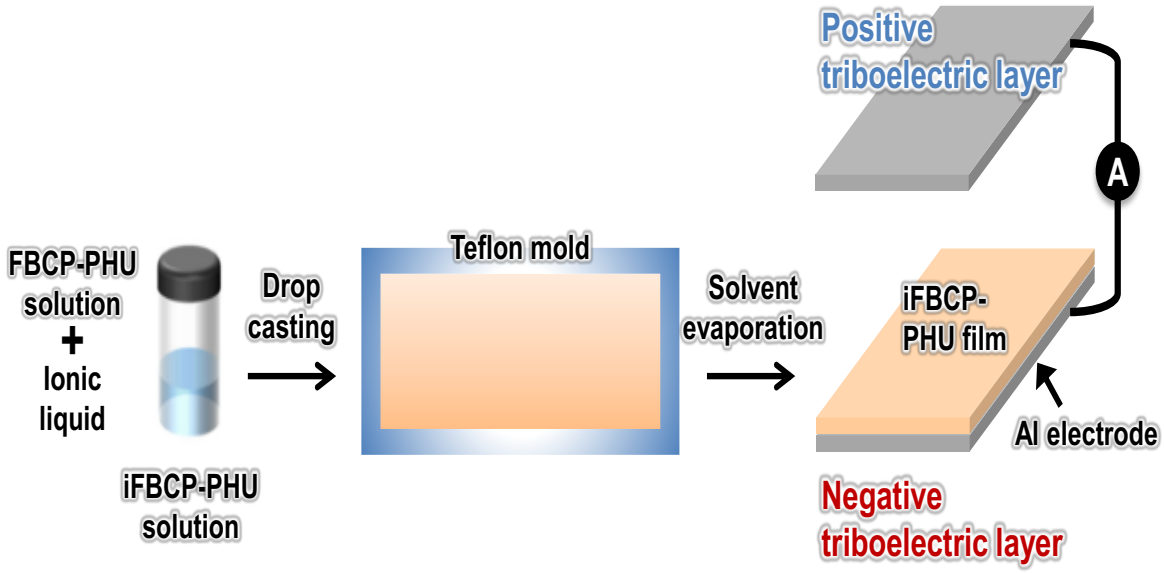

Figure 4.S3. Scheme of the preparation process of a triboelectric device consisting of the FBCPPHU and Al as negative and positive triboelectric layers, respectively.

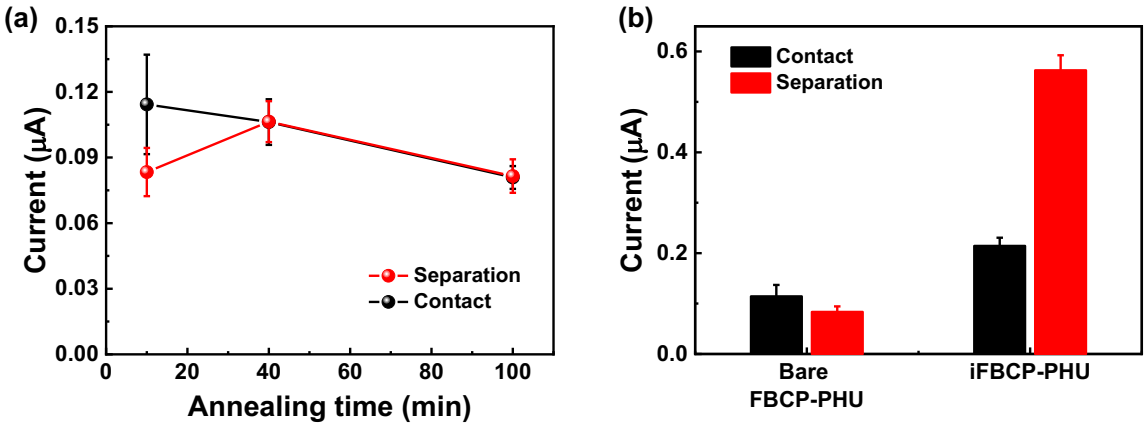

Figure 4.S4. Triboelectric output current of FBCP-PHU without EMIM-TFSI after annealed at 150 ℃ for different time (a). Triboelectric output current of FBCP-PHU without and with EMIM-TFSI after annealed at 150℃ for 10 min (b).

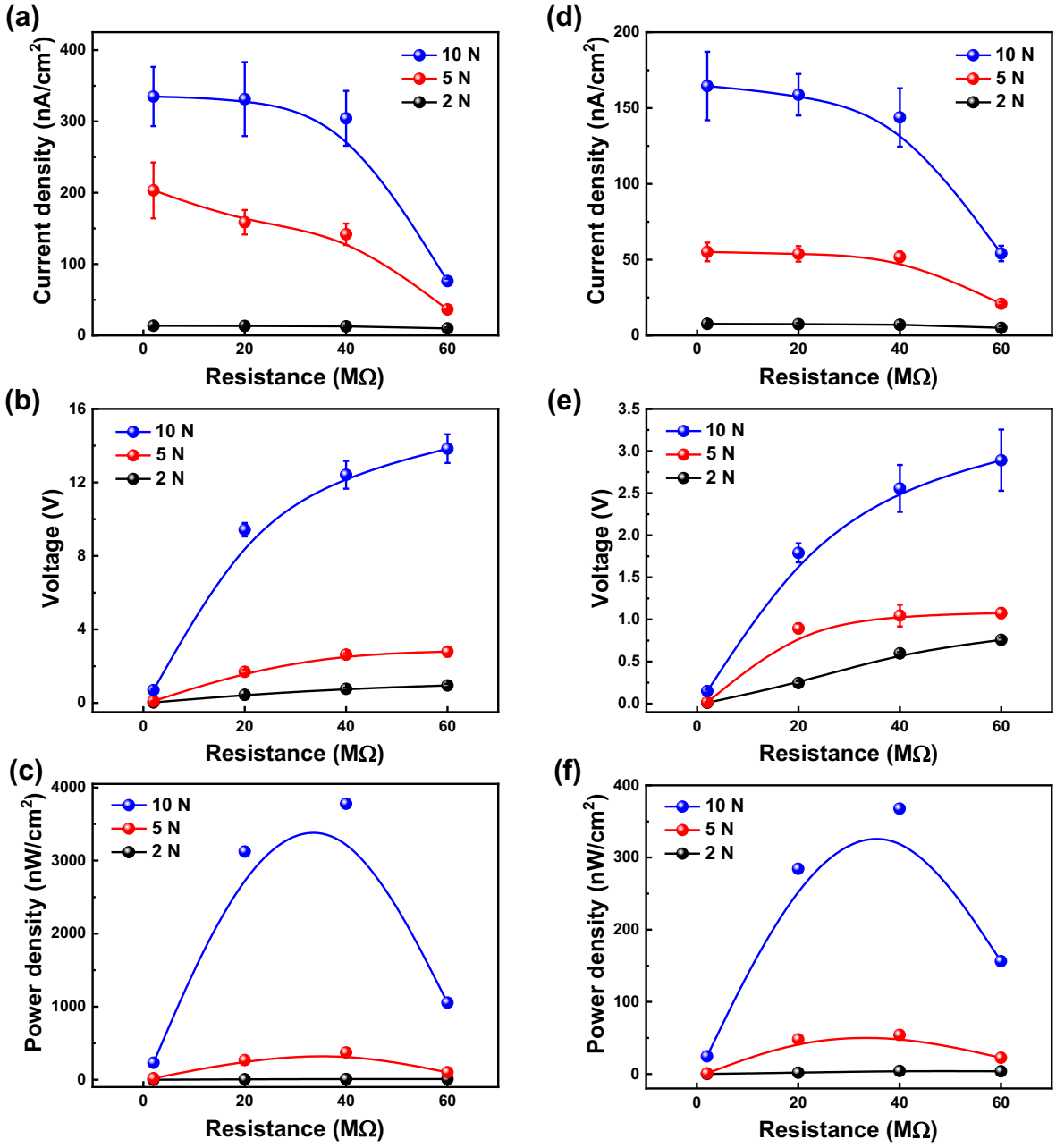

Figure 4.S5. Triboelectric output current (a and d), voltage (b and e), and power density (c and f) of iFBCP-PHU under different mechanical force during separation (a-c) and contact (d-f)) process, respectively.

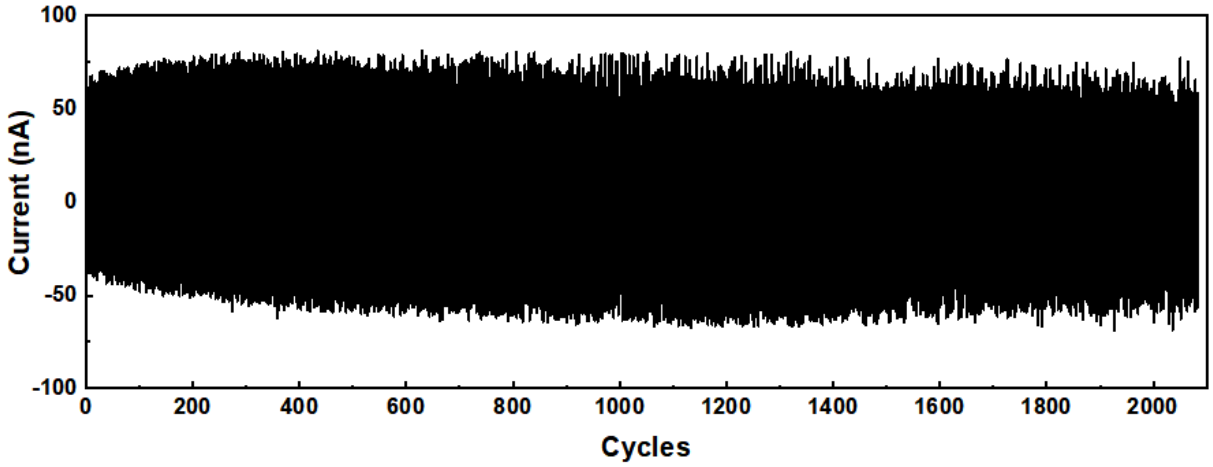

Figure 4.S6. A repeated cycle test of iFBCP-PHU over 2000 cycles at 5 N and 2 Hz.

Chapter 5. Heterogeneous Dynamic Poly(Hindered Urea) Network Materials Crosslinked with Methacrylate Polymer Crosslinker

5.1 Introduction

Polymers with a cross-linked network structure are commonly formed by strong covalent bonds between chains. These traditional cross-linked polymers, which are commonly used in commercial thermosets, cannot be easily disassembled after curing.[61, 223] As a result, they have limited recyclability and cannot be efficiently transformed into high-value products at the end of their life cycle. The inability to recycle these materials is primarily due to the presence of permanent cross-links, which restrict the movement of polymer chains within the network, even at elevated temperatures. To address this challenge, the concept of reprocessable polymer networks has emerged, and extensive research has been conducted in this field for the past two decades. Reprocessable polymer networks, also known as covalent adaptable networks (CANs) are networks that incorporate a significant number of dynamic covalent bonds. These bonds have the ability to dissociate or exchange in response to external stimuli such as heat (high temperature), making the networks malleable and allowing for potential recycling and reprocessing.[59, 60] A few examples of dynamic linkages utilized in CANs include disulfide,[224-226] alkoxyamine,[227] diarylbibenzofuranone,[228] and boronic ester.[229, 230] These discoveries have demonstrated significant promise in areas including energy storage materials, sustainable materials, and electronic devices.

Polyureas, along with polyurethanes, are widely used in various applications such as coatings, elastomers, and foams due to their robustness, affordability, flexibility, durability, and excellent chemical resistance. However, one drawback of conventional polyureas is their inability to be recycled because of the high stability of the amide bonds in urea bonds. Such drawback could be attributed to the conjugation effects between the lone electron pair on the nitrogen atom and the π-electrons on the carbonyl orbital. To address this limitation, researchers have explored the incorporation of bulky substituents on the amide nitrogen atom. This approach weakens the amide bond by disrupting its orbital coplanarity, thereby reducing the conjugation effect and weakening the carbonyl-amine interaction. Consequently, under mild conditions, the amide bonds can undergo reversible amidolysis. Cheng and colleagues investigated the impact of steric hindrance on hindered urea bonds (HUBs) and found that urea bonds with bulky side groups on the nitrogen atom can reversibly dissociate into isocyanates and amines at relatively low temperatures.[231]

Our group has previously studied t-butylamino group as a bulky substituent for amide and showed PHU networks formed under catalyst-free condition.[4] This network exhibited promising results, not only being flexible but having greater mechanical properties and being self-healable, transparent, and reprocessable. Other bulky groups including pyrazole,[232] piperazine,[233] and phenyl[124] groups have also been investigated as crosslinkers for the fabrication of dynamic PHUs. Dynamic covalent PHU was created by polyaddition of 1,6-hexane diioscyanate with pyrazoles at room temperature without the need of a catalyst. The resulting network demonstrated outstanding mechanical characteristics, distinctive crystallization, and successful recycling at a heating temperature of about 130 °C.[232]

HUBs have also been utilized in the synthesis of chain-growth polymer networks. Zechel et al. synthesized poly(butyl methacrylate) networks incorporated with dynamic HUBs.[234] The self-healing behavior of these networks was investigated through scratch-healing and bulk-healing tests. Subsequently, they examined the impact of different healing conditions on the healing efficiency. There have only been a few additional studies have reported on chain-growth networks based on HUBs utilizing methacrylate.[235, 236]

Here we present the synthesis of a catalyst-free polymethacrylate homopolymer bearing t-butylaminoethyl pendants (PM) as a multifunctional bulkyamine crosslinker to fabricate dynamic PHU hybrid network materials. A well-defined PM with narrow molecular weight distribution as dispersity ($Đ < 1.2$) synthesized by a controlled radical polymerization was incorporated into polyaddition with a prepolymer of polyurea. The approach demonstrates a synergistic effect, which encompasses several factors. Firstly, hindered urea bonds enable the network to possess self-healing and recycling capabilities. Secondly, the asymmetric alicyclic structure, specifically isophorone diisocyanate (IPDI), contributes to the desired transparency of the elastomer and provides adequate mobility to facilitate urea bond exchange reactions. Lastly, the inclusion of a flexible segment containing polymethacrylate enhances the mobility of the polymer chains, resulting in improved room temperature self-healing. A series of dynamic PHU-PM hybrid networks with different amounts of PM were prepared to understand their structure-property relationship. The formed networks were characterized for optical, thermal, mechanical properties as well as evaluated for their self-healability and reprocessability. We further studied the networks rheology, including stress relaxation behavior, at elevated temperatures.

5.2 Experimental

Materials. Isophorone diisocyanate (IPDI, 98%), bis(3-aminopropyl) terminated polydimethylsiloxane (PDMS-DA, M_n = 2,500 g/mol), 2-(t-butylamino)ethyl methacrylate (TBAEMA, 97%), tris(2-pyridylmethyl)amine (TPMA, 96%), tin(II) 2-ethylhexanoate ($Sn(EH)_2$, >92%), and methylethylketone (MEK) were purchased from Sigma-Aldrich and used as received. 3-Phenylpropyl 2-bromo-2-methylpropanoate (PP-Br) was synthesized as described in our previous publication.[237]

Synthesis of PM crosslinker by ATRP. TBAEMA (3 g, 16 mmol), PP-Br (92 mg, 0.3 mmol), TPMA (14.1 mg, 0.049 mmol), and [Cu(II)TPMA-Br]Br complex (8.3 mg, 0.016 mmol) were mixed with acetone (4 mL) in a 10 mL Schleck flask. The mixture was deoxygenated by purging under nitrogen for 30 mins. The polymerization was started by the addition of nitrogen-prepurged $Sn(II)(EH)_2$ (52.4 mg, 0. 129 mmol) in acetone at 40 °C. The polymerization was stopped after 5 hrs by exposing to air and allowing to cool to room temperature.

For purification, the as-synthesized polymers were precipitated from hexane three times to remove unreacted monomers. The precipitates were dissolved in a minimal amount of chloroform and then passed through a column filled with basic alumina to remove residual copper species. The solvents were removed by rotary evaporation and the residues were dried in a vacuum oven set at 40 °C for 12 hrs.

Fabrication of PM-PHU network films. In the first step, IPDI (0.54 g, 2.56 mmol) was mixed with PDMS (3.2 g, 1.28 mmol) in MEK (40 mL) under stirring at 70 °C for 4 hrs to form prepolymers of IPDI-PDMS. In the second step, the purified, dried PM dissolved in MEK (2 mL) was added at 70 °C and the resulting mixture was stirred at the same temperature for an additional 4 hrs. After being cooled down to room temperature in air, the clear solution was drop casted onto a glass plate and allowed to dry at room temperature for 24 hrs followed by drying in the oven at 70 °C for 30 min, yielding PM-PHU network films.

A similar procedure was used with PM (0.45 g, 0.067 mmol) for PM-PHU-A and PM (0.90 g, 0.135 mmol) for PM-PHU-B.

Gel content measurements. Pieces of the dried PM-PHU films (approximately 1 g) were mixed with MEK (8 mL) for 24 hrs. MEK was carefully decanted, and residues were dried at room

temperature for 13 hrs and further dried in oven at 70 °C for 13 hrs. Gel content was determined as the weight ratio of dried residues to initial films.

Instrumentation and analyses. ^{1}H NMR spectra were recorded using a 500 MHz Varian spectrometer with CH_3CN singlet at 2.00 ppm.

Differential scanning calorimetry (DSC) analysis was carried to determine thermal properties including glass transition temperature (T_g) of crosslinked films with a TA Instruments DSC Q20 differential scanning calorimeter. Samples were dried for 24 h in vacuum oven to remove residual solvents. Temperature ranged from −80 to 200 °C with heating and cooling cycles conducted at a rate of 10 °C/min (cycles: cool to −80 °C, heat up to 200 °C (1st run), cool to −80 °C, heat up to 200 °C (2nd run), and cool to 25 °C). T_g values were determined from the 2nd heating run.

Thermogravimetric analysis (TGA) was conducted with a TA Instruments Q50 analyzer. Dried samples (5-10 mg) were placed in a platinum pan inside a programmable furnace and then heated from 25 to 800 °C at a 20 °C/min heating rate under nitrogen flow. Mass loss was then calculated.

Universal tensile measurements were performed to measure tensile strength, elongation, and Young's modulus of crosslinked materials using Z5 Tensile Machine (Hoskin Scientific) equipped with 1 kN load cell. The specimens were loaded until failure with a strain rate of 10 mm/min. The dried films prepared above were cut into small pieces, placed in rectangular molds (7.5 cm x 1.5 cm), and compressed using a hot press at 130 °C for 3 min at 70 kPa pressure. The resulting compression-molded films with 2 mm thick were cut to render the type VI (ASTM D638) dumb-bell-shaped specimens for tensile testing.

Stress-relaxation curves were measured with a TA Instruments DHT-2 Rheometer. The specimens were equilibrated between machine grips for 120 s at a predetermined temperature and then loaded with 1 % strain steps. The evolution of the storage modulus with time was recorded for stress relaxation analysis. The specimens were prepared similarly to compression-molded films which were cut to circular specimens. Their diameter and thickness were maintained to be 1.2 cm and 0.2 cm, respectively.

Sol-gel experiment. A piece of dried PM-PHU-A film prepared above (0.78 g) was mixed with MEK (8 mL) at room temperature. After the addition of TBAEMA (0.24 g), the resulting

mixture was heated at 70 °C for 4 hrs, forming a sol. Then, IPDI (0.27 g) was added and the resulting pale-yellow mixture was kept at 70 °C for 4 hrs and then cooled down to room temperature, forming a standing gel.

Scratch recovery and self-healing using nano-scratch tester (NST)/atomic force microscopy (AFM). A nano-scratch tester (NST, Anton Paar Tritec SA, Switzerland) was utilized to quantitatively evaluate scratch patterns and mar resistance on the surface of a crosslinked film. A sphero-conical 90° indenter with a 2 μm radius tip was used to apply progressive load from 0.1 to 50 mN on the film surface. The tip moved horizontally at a scan speed of 2 mm/min along a 1mm length. To examine the self-healing behavior of the scratch damage generated by the scratch test, atomic force microscopy (AFM Wide Scan, Anton Paar Tritec SA, Switzerland) was employed. The scratch depth at the location where 30 mN load was mainly focused (i.e., equivalent to nearly 0.6 mm position from the starting point of loading) under thermal conditions such as healing temperature and duration time. Images from the AFM test were combined from 256 scan lines captured during a duration of 256 s on a squared-scan area of 77.1 μm x 77.1 μm. The temporal recovery patterns of scratches were compared through 2D cross-section cuts and 3D images at healing temperature of 60 °C and duration time up to 3 hour.

5.3 Results and Discussion

5.3.1 Synthesis of t-Butylamino-bearing PM Crosslinker by ATRP

Figure 5.1a depicts our approach via atom transfer radical polymerization (ATRP) to synthesize well-defined PTBAEMA homopolymer, called PM crosslinker bearing t-butylamino pendants. Activators ReGenerated Electron Transfer (ARGET) process for ATRP was employed because it requires the use of a minimal amount of Cu species (<10 ppm) due to the continuous regeneration of active Cu(I) complex by reducing agent and is easy to operation.[238-241] ARGET ATRP was conducted for TBAEMA in the presence of Cu(II)/TPMA complexes, initiated with PP-Br initiator at 40 °C in acetone. $Sn(II)(EH)_2$ was used as a reducing agent to convert Cu(II) species to active Cu(I) species. Under the conditions of $[PP\text{-}Br]_o/[Cu(II)Br_2]_o/[TPMA]_o/[Sn(II)(EH)_2]_o$ = 1/0.05/0.15/0.4, the target degree of polymerization (DP) at the complete monomer conversion was set to be 50 as the initial mole ratios of $[TBAEMA]_o/[PP\text{-}Br]_o$ = 50/1. The formed polymer was purified by precipitation from hexane. ^1H NMR in Figure 5.1b

shows the typical peaks (a, b, c, d) for PTBAEMA and the peak 7.4 ppm (e) for phenyl initiating species. Their integral ratio allowed for the determination of the DP of 33.

The synthesized PM was further analyzed for their thermal properties. TGA diagram shows the stepwise weight loss with a residue of <3% (Figure 5.1c). DSC analysis exhibits a single glass transition temperature (T_g) at 34 °C (Figure 5.1d), which is larger than that 22 °C reported according to BASF technical data sheet.

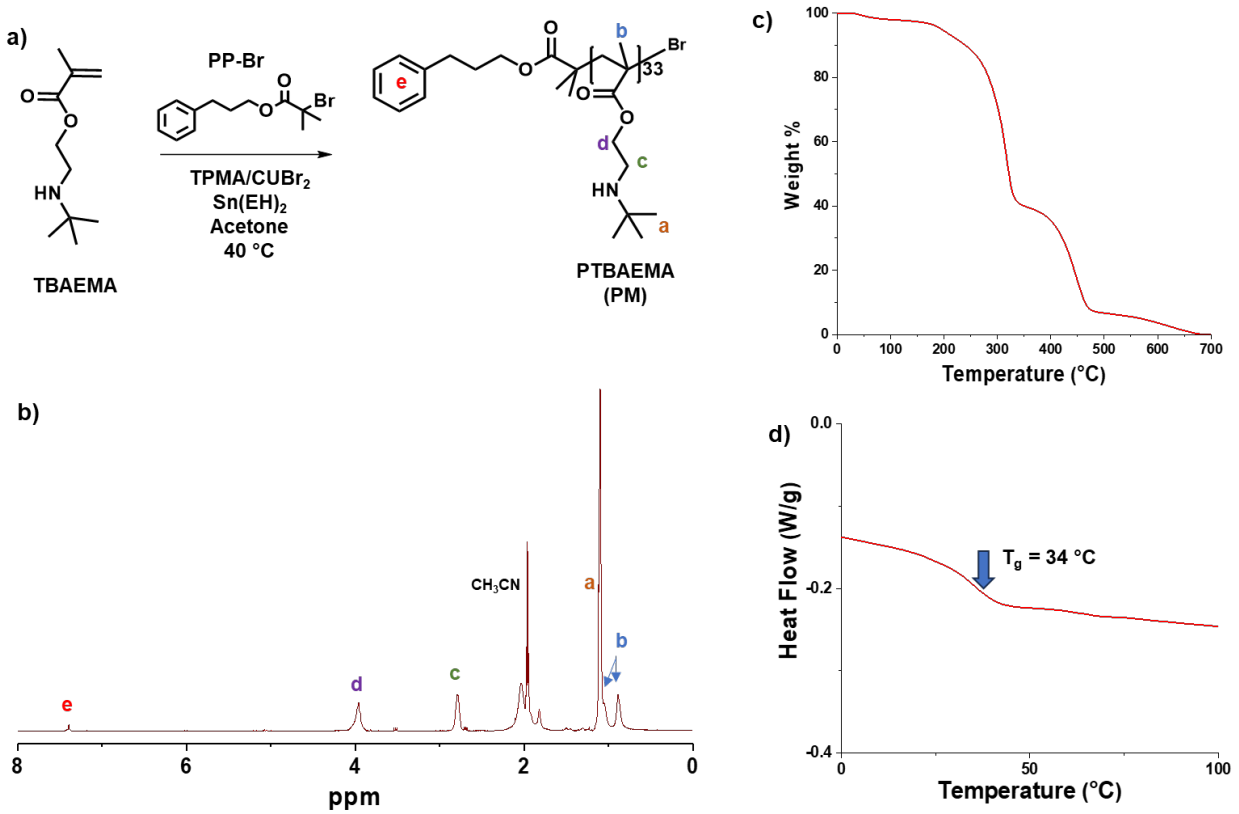

Figure 5.1. Synthesis of PM by ARGET ATRP of TBAEMA in the presence of Cu(II)/TPMA complex, initiated with PP-Br at 40 °C in acetone. Conditions: $[TBAEMA]_o/[PP\text{-}Br]_o/[Cu(II)Br_2]_o/[TPMA]_o/[Sn(II)(EH)_2]_o$ = 50/1/0.05/0.15/0.4, TBAEMA/anisole = 0.8/1 wt/wt (a); ^1H NMR spectrum in $CDCl_3$ (b); TGA diagram (c); and DSC diagram exhibiting a single glass transition at 34 °C (d).

5.3.2 Fabrication of PM-PHU Networks Crosslinked with PM

The synthesized PM was used as multifunctional crosslinker in the fabrication of dynamic PM-PHU networks crosslinked through the formation of t-butylamino-based bulky urea bonds between NCO and t-butylamino groups. As illustrated in Figure 5.2, two-step synthetic approach

for step-growth polymerization was adopted from our previous publications.[4] In the first step, IPDI reacted with PDMS-DA (MW = 2500 g/mol) at a mole ratio of NCO/amine = 1/0.5 (NCO excess) in MEK to yield an IPDI-PDMS prepolymer terminated with reactive NCO groups at both ends. In the next step, PM was added to induce the reaction of excess NCO with t-butylamino groups, yielding PM-PHU networks. Reaction mixtures were kept at 10 wt% of PM-PHU in MEK, which allows for the fabrication of homogeneous PM-PHU solutions. At greater contents of PM-PHU, mixtures became too viscous to be handled or even turned to be standing gels in a reaction flask.

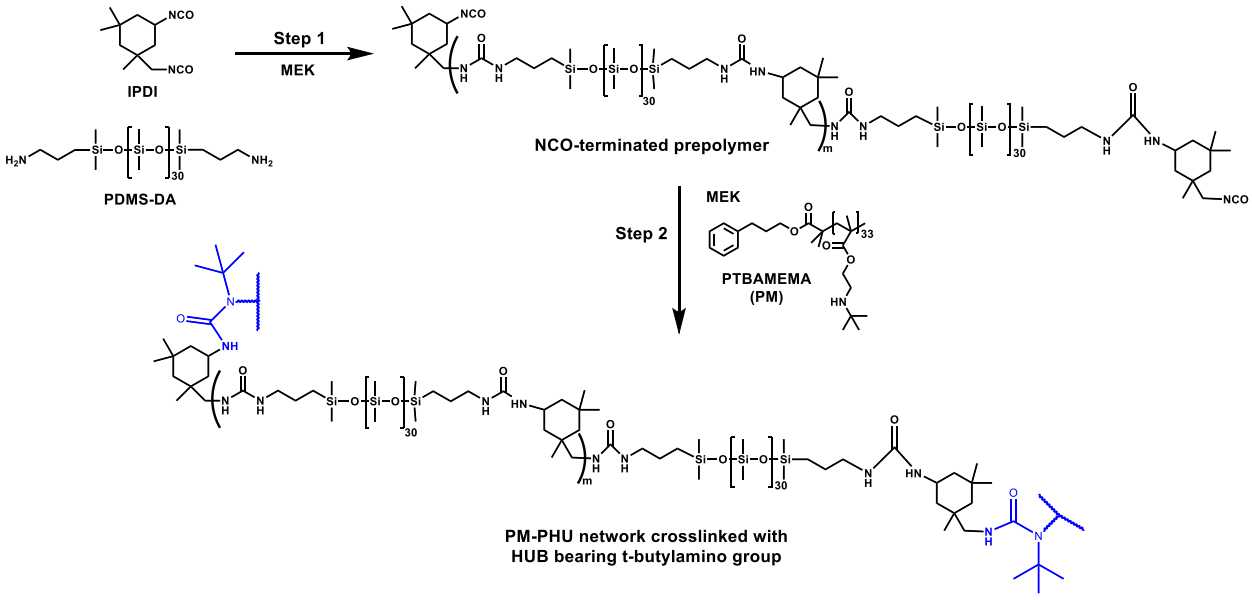

Figure 5.2. Schematic illustration of the approach to fabricate dynamic PM-PHU networks crosslinked with PM crosslinker having multiple t-butylamino pendants.

The amounts of PM were varied at 10.4 and 19.3 wt% corresponding to the mole equivalent ratio of NCO/t-butylamino (t-NH) groups to be 1/1 and 1/2 (excess t-NH) to fabricate PM-PHU networks with different crosslinking densities, named as PM-PHU-A and B. Their characteristics and properties are presented in Table 5.1.

Table 5.1. Characteristics and properties of PM-PHU network materials fabricated by two-step polyaddition consisting of IPDI, PDMS-DA, and PM crosslinker.

Items		**PM-PHU-A**	**PM-PHU-B**
Composition	IPDI	13.4	12.2
(wt%)	PDMS-DA	75.7	68.4
	PM	10.7	19.3
t-NH/NCO		1/1	2/1
Gel Content (%)		83.3 ± 2.9	73.6 ± 2.1
T_g (°C)		32	30
$D_{1/2}$ (°C)		497	477
Young's Modulus (MPa)		10.9 ± 0.2	19.7 ± 1.2
Tensile Stress (MPa)		2.1 ± 0.07	2.2 ± 0.04
Elongation (%)		27 ± 1.4	21 ± 0.7

5.3.3 Optical, Thermal, and Mechanical Properties of PM-PHU Networks

The as-synthesized solutions were drop-casted on glass plates, dried at room temperature, and then annealed at 90 °C for 30 min. Both films were transparent with their UV/Vis %transmittance at 600 – 700 nm to be >85% (Figure 5.3a). They were analyzed for gel contents using gravimetry in MEK based on their mass of insoluble species. The gel content was as high as 83.3% for PM-PHU-A and decreased to 73.6% for PM-PHU-B. Such a decrease could be attributed to the fabrication of less crosslinked networks composed of more soluble species with more PM crosslinker.

Their thermal properties were analyzed using a DSC technique (Figure 5.S1). Both PM-PHU-A and B films exhibited single thermal transitions with their T_g values ranging at 30-32 °C, which turned to be close to that of the PM homopolymer. Their thermal stability was characterized by TGA. Both films degraded at 200-660 °C, with <2% residues (Figure 5.3b). $D_{1/2}$ which defines the temperature where the half weight of the film was lost can be used as a measure of the thermal stability of the films. It was 497 °C for PM-PHU-A and decreased to 475 °C for PM-PHU-B, which is probably attributed to the decrease in the amount of thermally stable PDMS in PM-PHU.

Furthermore, the mechanical properties of PM-PHU materials were measured by a tensile tester. Their films cast on glass plates at 90 °C were cut into small pieces, compression-molded at 130 °C, and cut to dumb-bell-shaped specimens. Figure 5.3c shows their stress-strain curves representative for their networks and their tensile stress at break, elongation, and Young's modulus

were determined. As presented in Table 5.1, tensile strength was 2.1 MPa for PM-PHU-A and slightly increased to 2.2 MPa for PM-PHU-B, while their elongations appeared to range at 21-27%. Young's modulus steadily increased from 11 for PM-PHU-A (10.7 wt% PM) to 20 MPa for PM-PHU-B (19.5 wt% PM). These results suggest that PM-PHU-B has greater mechanical strength than PM-PHU-A.

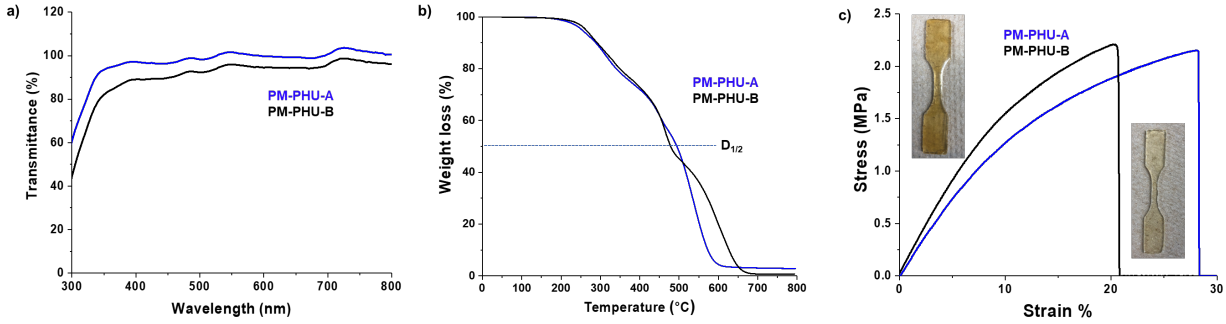

Figure 5.3. UV/Vis spectra by %transmittance (a), TGA thermograms (b), and stress-strain curves with digital images of dumb-bell shaped specimens (c) for PM-PHU-A (10.7% PM) and PM-PHU-B (19.3% PM).

5.3.4 Void-filling and Self-healing Studies using NST/AFM

Given the analysis of the mechanical characterization of the PM-PHU-films, their surface hardness and self-healing properties were examined using a NST equipped with AFM. The PM-PHU-films were uniformly coated on steel plates and held at 30 °C for 1 hr to remove solvents. Subsequently, the coated films were thermally cured at 90 °C for 30 min. Micron-sized scratches were created on the surfaces by an indenter that progressively increased its force from 0.1 to 50 mN. AFM was employed at elevated temperatures to assess the healing profiles of scratches at the site subjected to a 30 mN load.

The scratch depth profiles for PM-PHU films, including the penetration depth and residual depth, were compared (Figure 5.4a). The penetration depth provides an indication of the surface hardness during the progressive scratching process, while the residual depth reflects the elastic recovery of the films immediately after scratching. Based on the results (Figure 5.4a), the hardness was observed as PM-PHU-B>A, which is consistent with the result from tensile measurement. The momentary recovery to residual depth exhibited a comparable higher level between PM-PHU-B, while PM-PHU-A demonstrated a relatively lower level.

The recovery rate of scratched films was evaluated from the area change of scratch depth during healing of 3 hrs at 60 °C (Figure 5.4b). The real-time scratch depth healing behavior over 3 hrs was observed with 2D cross-section cut (Figure 5.4c-5.4d). PM-PHU-A exhibited the lowest recovery rate, with only approximately 40% healing performance observed after 30 min. PM-PHU-B showed continuous healing even after 3 hrs, with over 80% healing efficiency. It is worth noting that the 0 hr depth of each film was measured immediately after scratching, which closely corresponds to the residual scratch depth in micrometers (e.g., depth profile of PM-PHU-A >B scale). In the case of PM-PHU-B, the depth of the scratches decreased consistently over time, indicating a sustained healing process. In contrast, PM-PHU-A exhibited limited healing capability, with only marginal improvements observed over time. Furthermore, 3D images of each film were captured at 0 h and 3 h healing time at 60 °C (Figure 5.S2), providing visual evidence of the healing properties.

Our results imply that void-filling is faster for PM-PHU-B than PM-PHU-A, even though PM-PHU-B is tougher. The plausible reason could be attributed to the presence of excess t-NH groups in PM-PHU-B network that can facilitate their reversible exchanges with HUBs, promoting its network rearrangement.

These results highlight the varying degrees of self-healing efficiency among the tested films. PM-PHU-B exhibited persistent healing behavior, while PM-PHU-A demonstrated relatively poor healing performance. Overall, the findings suggest that PM-PHU-B possesses the most effective and long-lasting self-healing properties among the tested films, making it a promising candidate for applications requiring scratch resistance and self-repairing capabilities.

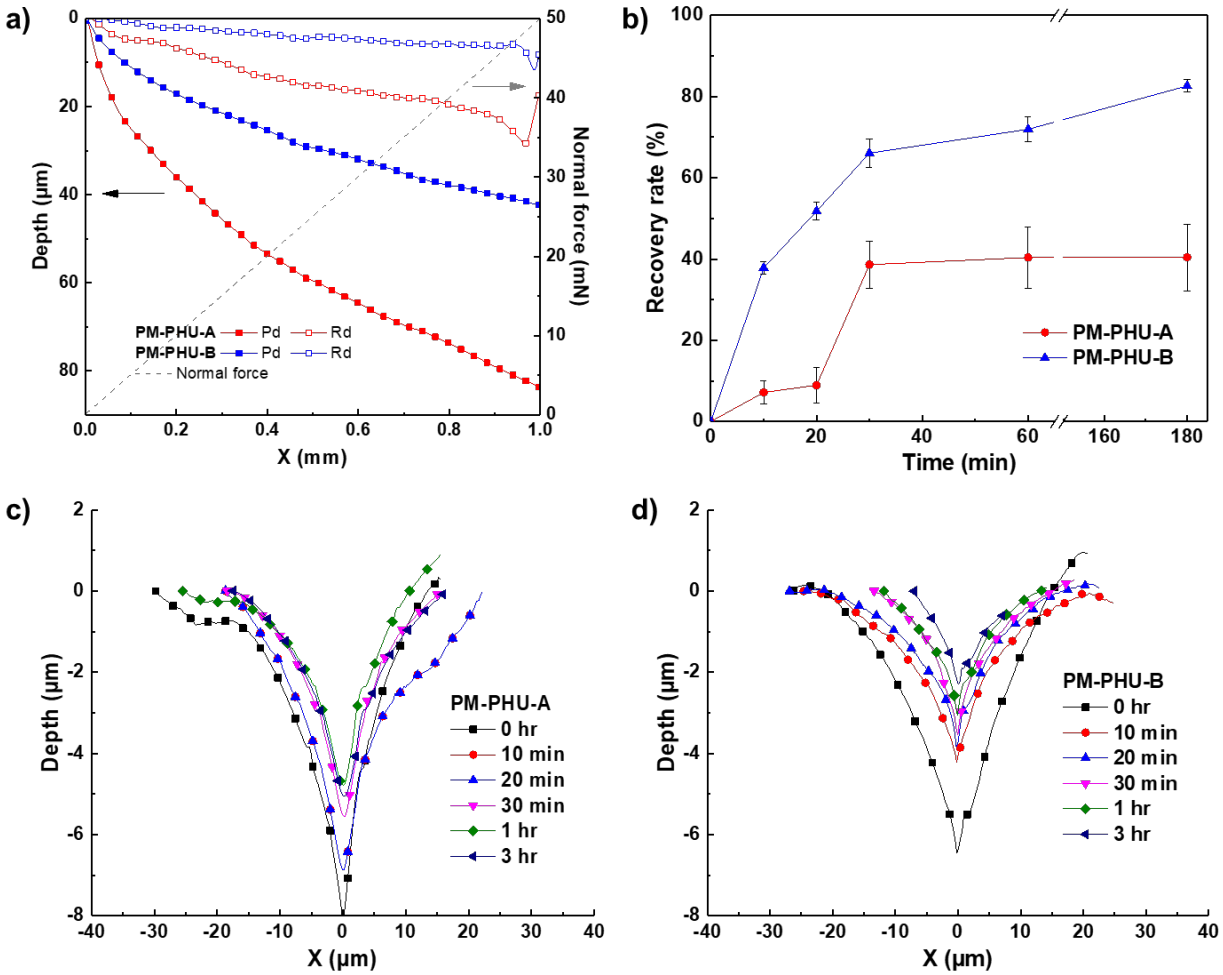

Figure 5.4. Evaluation of scratch profiles on the surfaces of PM-PHU-films (a), recovery rate of films up to 3 hrs at 60 °C (b), real-time healing properties in AFM scratch profiles at the position of 30 mN load with 2D cross-section cut; PM-PHU-A (c) and PM-PHU-B (d).

5.3.5 Dynamic Properties of PM-PHU Networks

Stress-relaxation properties of PM-PHU materials were analyzed using a rheometer with 1% strain. Compression-molded specimens were prepared to measure their viscoelastic properties as elastic modulus in the range of temperatures at 80-150 °C for PM-PHU-A and 50-90 °C for PM-PHU-B. Their stress-relaxation curves of normalized elastic modulus (G/G_o) are constructed in Figures 5.5a and 5.5b. The characteristic relaxation time (τ^*) corresponds to the time of 1/e of the normalized stress relaxation at different temperatures. PM-PHU networks underwent rapid stress relaxation at elevated temperatures. For example, the τ^* of PM-PHU-A network ranged from 20 min at 120 °C to 3 min at 150 °C. Such rapid stress relaxation of PM-PHU network in the absence

of a catalyst could be attributed to the rapid exchange reactions of dynamic HUBs and thus network rearrangement.

Temperature-dependent relaxation follows Arrhenius' equation as $\ln\tau* = E_a/RT - \ln A$, where E_a is the activation energy, A is the pre-exponential factor, T is the experimental temperature in Kelvin, and R is the universal gas constant.[102] The E_a was determined to be 88.3 kJ/mol for PM-PHU-A (with t-NH/NCO = 1/1) and 75.2 kJ/mol for PM-PHU-B (with t-NH/NCO = 2/1, excess t-NH groups). These values appear to be much smaller than that (138 kJ/mol) reported for a dynamic, linear PUU elastomeric vitrimer composed of IPDI, trifunctional poly(propylene glycol) (PPG), and 4,4′-methylenedianiline, measured by rheometer with 2.5% strain in the temperature range at 130-200 °C (Table 5.S1).[124] Interestingly, PM-PHU-B has lower E_a compared with PMA-PHU-A, even though their thermal transition and mechanical strength are slightly greater. This is presumably attributed to the presence of excess t-NH groups in the PM-PHU-B network which promote the reversible exchange of HUBs.

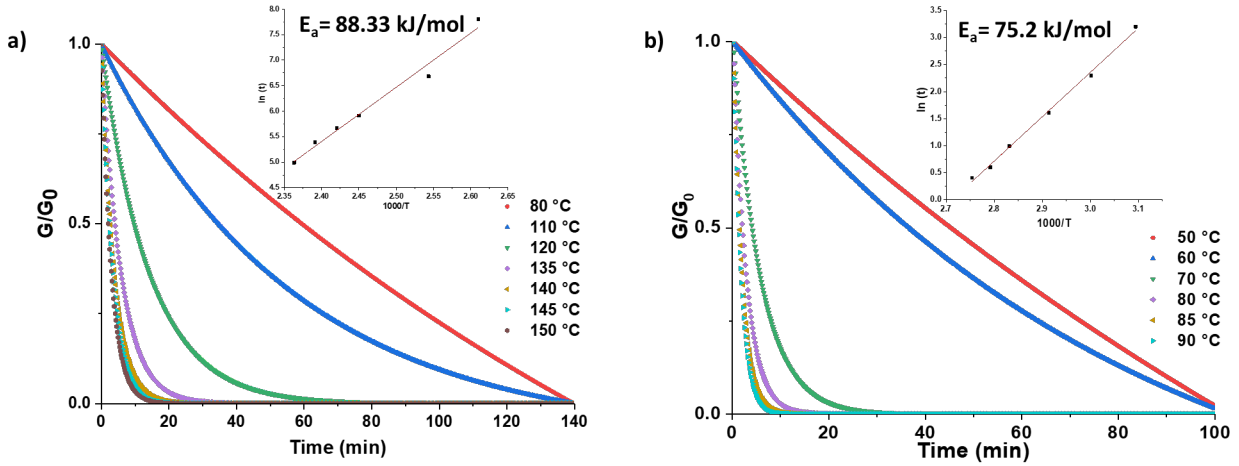

Figure 5.5. Stress relaxation curves of PM-PHU-A (a) and PM-PHU-B (b) with inert plots to fit relaxation time–temperature to Arrhenius equation to determine their activation energies for network relaxation and rearrangement.

Sol-gel experiment was conducted with PM-PHU-A further to study the dynamic properties of HUB-bearing PM-PHU networks. When immersed in MEK at room temperature, a small piece of PM-PHU-A became swollen. The mixture was then heated at 70 °C for 4 hrs, the swollen piece remains insoluble in MEK (Figure 5.6a). Upon an addition of small molecule TBAEMA bearing t-butylamino group (3 equivalent to t-NH groups in PM-PHU-A), the mixture became a homogeneous solution (called a sol) (Figure 5.6b). This is attributed to the reversible exchange of

HUBs bearing bulky t-butylamino groups with TBAEMA and PM-PHU network, resulting in decrease in crosslinking density of PM-PHU network. When IPDI (3 equivalent to NCO), which is the same as that of TBAEMA, was added, the mixture turned to a standing gel at room temperature (Figure 5.6c) as PHU network was reformed with increasing crosslinking density.

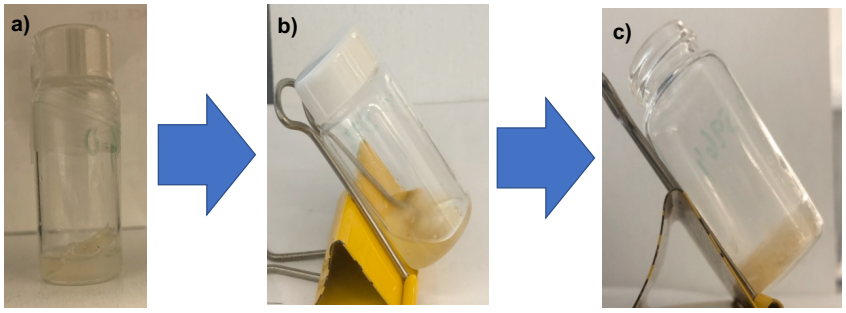

Figure 5.6. Digital images for sol-gel experiment of PM-PHU-A. A mixture of a small piece in MEK at 70 °C before (a) and after the addition of TBAEMA, forming a sol, and followed by the addition of IPDI at 70 °C, forming a standing gel at room temperature (c).

5.3.6 Reprocessability

Given our promising results of void-filing and dynamic nature, the reprocessability of PM-PHU materials was examined with tensile measurements. This method involves the recovery of tensile properties of materials after being reprocessed via hot-melt compression. PM-PHU-B was chosen due to its excellent self-healability at elevated temperatures. Half-cut tensile specimens of PM-PHU-B after their tensile measurements were cut into small pieces and then compression-molded under a pressure of 4 MPa at 130 °C for 5 min (Figure 5.S3). This process was repeated up to three times. The resulting tensile specimens appeared to be transparent and homogeneous. Figure 5.7a compares stress-strain curves of original and reprocessed PM-PHU-B films. The film after being recycled 3rd time had a tensile strength of 2.2 MPa, elongation of 27%, and Young's module of 17.8 MPa. This result indicates that the recovery of tensile properties turned to be >94%. Gel contents of the reprocessed films were kept unchanged and retained at >70% (Figure 5.7b). Furthermore, the reprocessed films had single glass transition at similar temperatures (27-30 °C) which is an acceptable error range (Figure 5.7c). These results confirm that PM-PHU networks had excellent reprocessability and recovery of thermal and mechanical properties, which is mainly attributed to the reversible exchange of dynamic HUBs to maintain crosslinking density of the networks.

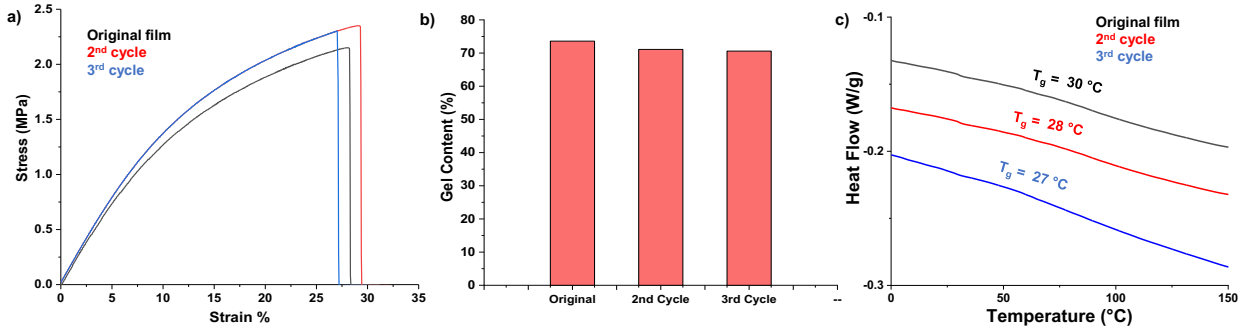

Figure 5.7. Stress−strain curves (a), gel contents (b), and DSC thermograms (c) of original and recycled PM-PHU-B materials.

5.4 Conclusion

A new approach was developed to fabricate self-healable PHU-polymethacrylate hybrid networks that can be effective for TENG applications. A well-controlled PM having t-butylamino pendants was synthesized by ATRP and used as a reactive crosslinker in a two-step polyaddition to fabricate a dynamic PM-PHU hybrid network. PHU networks with varying amounts of PM were designed and the subsequent films are shown to be transparent and flexible, as well as showed strong mechanical strength. Excess t-NH groups (PM-PHU-B) had great mechanical strength and exhibited excellent self-healability and reprocessability at elevated temperatures. This strategy is novel to offer a fresh approach for flexible devices, advancing wearable electronics and sustainable energy in the future.

5.5 Supporting Information and Figures

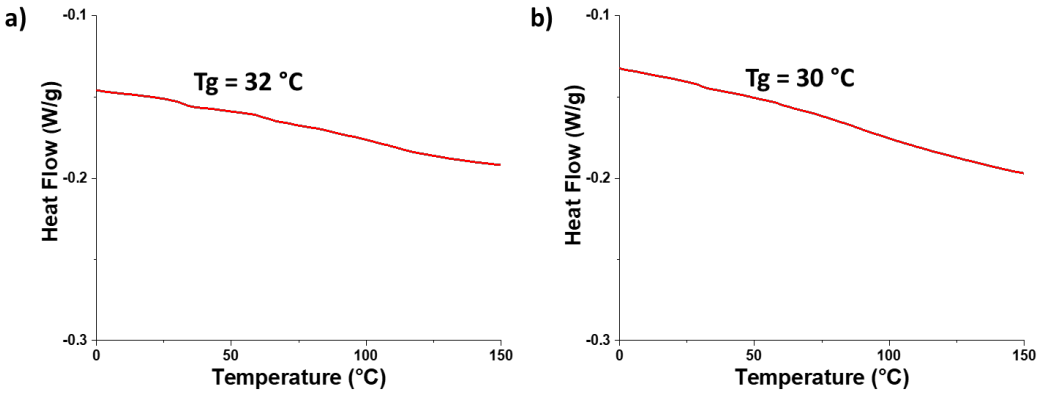

Figure 5.S1. DSC spectra of PM-PHU-A (a); PM-PHU-B (b).

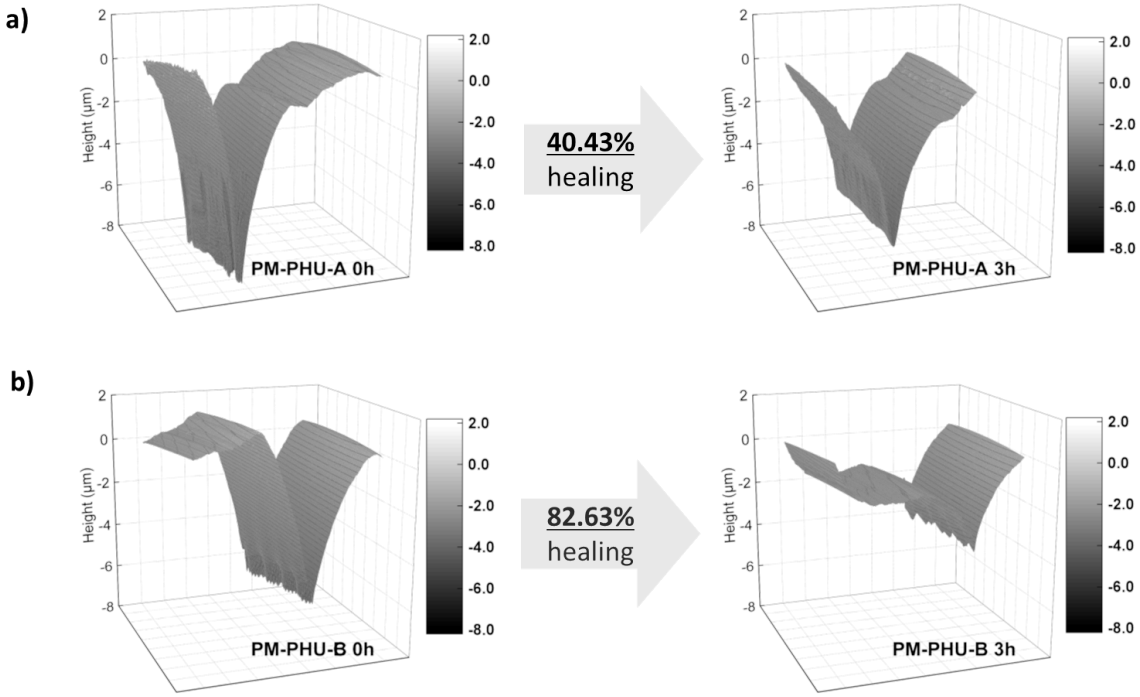

Figure 5.S2. Evaluation of AFM scratch profiles with 3D images; PM-PHU-A (a) and PM-PHU-B (b)

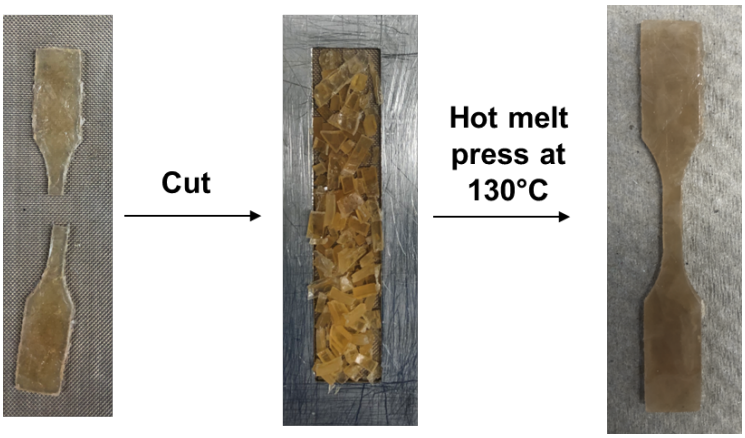

Figure 5.S3. Digital images of reprocessing with hot melt press.

Table 5.S1. Comparison of the activation energy of polyurea-urethane networks.

Network	Type of Crosslinker	Ea (kJ/mol)	Temperature Range (°C)	Instrument	Ref.
PUU	TBXA	59	70-120	DMA	[242]
PUU	MDA	138	160-200	Rheometer	[124]
PUU	TBAE	59	60-120	DMA	[108]
PUU	IPAE (iPr)	130	110-190	DMA	[108]
PUU	EAE (ethyl)	132	110-190	DMA	[108]
PUrethane	Aromatic pinacol	103	70-120	DMA	[243]
PUU	DTBEA	101	120-150	DMA	[244]
PUU	Piperazine	117	100-170	Rheometer	[245]
PUrea	Pyrazole	25	90-130	DMA	[246]
PUrea	4,4'-Diaminodiphenylmethane	34	60-180	DMA	[247]
PUU	TBEMA	48	70-110	DMA	[248]
PUrea	TBAEMA	92	90-130	DMA	[202]
PUU	tris[2-(isopropylamino)ethyl]amine	82	80-160	Rheometer	[8]
PUrea	Multifunctional aziridines	120	100-130	DMA	[249]
PUrea	4,4′-bis(*sec*-butyl)methylenedianiline	85	90-110	DMA	[10]

Chapter 6: Conclusion and future works

6.1 Summary of my Ph.D. thesis

My Ph.D. research brings out the tremendous efforts that have been made to explore dynamic hindered urea chemistry and to study its self-healing and reprocessing abilities, which paves the way for the development of effective self-healable TENGs. Hindered urea chemistry is sought out due to its distinguishing features such as its dynamic and reversible nature which are desired for self-healability, recyclability, and reprocessability. These designed systems were characterized by their self-healing, thermal and mechanical properties as well as their TENG properties to determine their efficiency.

In **Chapter 2,** efficient strategies were investigated for the fabrication of robust covalent adaptive networks containing dynamic hindered urea bonds that demonstrate exceptional self-healing and reprocessability properties. These strategies involve the incorporation of diverse HUBs, primarily based on t-butylamine groups, as well as other bulkyamino groups like piperazine, isopropylamino, pirazole, and phenylamino groups, into various polymeric thermoset materials. The synthesis of HUB-bearing networks of poly(urethane-urea) (PUU) and polyurea (PUa) are extensively explored through a step-growth polyaddition process, involving the reaction of polyisocyanates with polyols and/or polyamines along with polybulkyamines. The HUBs are formed either on the backbones of the polymers or as dynamic crosslinks within the networks. Similarly, HUB networks have been prepared for epoxy resins, polysulfides, and polymethacrylates through chemical routes and the design and synthesis of reactive precursors that incorporate HUBs. These reactive precursors include HUB-bearing amines for epoxy networks, HUB-bearing (meth)acrylates for polysulfide networks, and HUB-bearing methacrylates for polymethacrylate networks. The resulting networks exhibit dynamic behavior, undergoing reversible exchange reactions through the dissociation and association of the corresponding isocyanate and bulkyamino groups. As a result, they possess self-healing and reprocessing capabilities. These developed network materials have been employed in various applications that demand dynamic properties, including energy harvesting and storage, sensors, flexible and wearable electronics, and surface coatings.

In **Chapter 3,** a dynamic poly(hindered urea) (PHU) network crosslinked with bulky urea linkages was developed by a step-growth polymerization process. This involved a two-step polyaddition process at ambient temperature, utilizing a reactive mixture containing a

diisocyanate, PDMS diamine, and 4-arm star t-butylamine, without the need for a catalyst. The resulting networks exhibited reversible exchange of hindered urea linkages in response to temperature changes, allowing for rapid void filling and self-healing of micron-sized cracks on film surfaces under ambient conditions. These networks demonstrated flexibility along with enhanced mechanical properties, including a tensile strength at break as high as 1.7 MPa. Moreover, the films could be reprocessed, and the mechanical and viscoelastic properties could be recovered by up to 95%. Leveraging these advantageous properties of self-healing, transparency, and reprocessability, we successfully fabricated robust TENG devices using these vitrimeric PHU films. These devices exhibited excellent interfacial polarization-induced triboelectric performance. Additionally, they demonstrated rapid recovery through effective self-healing. These results highlight the versatility of our approach in developing advanced TENG materials with high triboelectric output, as well as outstanding self-healing and reprocessability, contributing to increased lifetime and reduced dependence on fossil fuels. Furthermore, this approach holds promise for other energy-harvesting applications such as artificial skins, flexible sensors, nanorobotics, and portable/wearable devices.

In **Chapter 4**, a novel method was developed to create a self-healing TENG using ionic PHU network materials crosslinked with bulky urea groups using a reactive fluorinated block copolymer (FBCP). The FBCP was synthesized through a well-established reversible addition-fragmentation chain transfer polymerization technique, resulting in a controlled copolymer with a narrow molecular weight distribution and predetermined molecular weight. The copolymer consisted of a reactive block with a pendant t-butylamino group covalently attached to a TENG block with fluorinated pendants. This copolymer served as a reactive crosslinker in a two-step step-growth polymerization process under mild conditions. By incorporating an ionic liquid, the fabrication of ionic FBCP-PHU network materials was achieved. These materials exhibited high transparency, flexibility, and toughness, with a high Young's modulus of 17.4 MPa. Notably, they demonstrated excellent self-healing properties at elevated temperatures. Surface cracks at the micron scale were recovered by more than 95% within 10 minutes at 90 °C, as confirmed by non-contact scanning force microscopy (NST-SFM) measurements. Furthermore, these materials exhibited enhanced triboelectric output and served as effective negative triboelectric materials. Remarkably, the TENG output was fully restored upon the healing of surface cracks.

In **Chapter 5,** a new strategy utilizing ATRP was used to synthesize a methacrylate homopolymer with t-butylaminoethyl pendants as a multifunctional crosslinker. A range of dynamic hybrid networks combining PHU with different amounts of polymethacrylate crosslinker were prepared to investigate the relationship between structure and properties. These networks were evaluated with their optical, thermal, and mechanical characteristics. Additionally, their self-healability and reprocessability were assessed.

6.2 Future Works

6.2.1 Design of Novel PHU Networks

Stimuli-responsive (or smart) copolymers have emerged as a promising building blocks of choice in the development of advanced nanomaterials for various applications in nanoscience, nanotechnology, and pharmaceutic science. Upon being responsive to external stimuli, the smart copolymers and their nanomaterials undergo either a physical or chemical transition, depending on the nature of stimuli-responsive moieties (or groups) within the structures. Chemical transition utilizes the incorporation of cleavable (or labile) covalent bonds into the design of copolymers. The formed degradable copolymers degrade to their appropriate products upon the cleavage of labile linkages when chemical or biological stimuli present. Further to such single-directional cleavage, the use of dynamic labile bonds (or reversible bond) allows for the development of novel crosslinked nanomaterials or networks exhibiting self-healing (i.e. reversibility for bond formation and dissociation) autonomously or in response to external stimuli.[250, 251] Hindered urea chemistry has been explored for the development of self-healable networks utilizing the dynamic nature of the urea bonds with bulky substituents. We have seen 100% healablility at temperatures above 50°C but only 50% recovery at ambient temperature.[4]

In order to achieve full recovery at room temperature, it is proposed to incorporate dual stimuli response by embedding reversible disulfide linkages into PHU network. This dual crosslinked network would be promising materials for extremely healable at ambient temperature. This proposed study will allow the creation of a new strategy for synthesizing PHU networks with disulfide incorporation to develop dual stimuli-responsive networks allowing self-healing at lower temperatures. This project will increase the durability and lifetime of polymer material.

Although past research has demonstrated the impressive mechanical and recycling properties of HUB-bearing networks, the hydrolysis reaction of these bonds under ambient conditions poses a significant challenge and requires further investigation. Additionally, the chemical stability of the reagents used in this dynamic polymer plays a crucial role in its future industrialization, and improvements in this aspect are still necessary. Conducting molecular dynamics studies and materials aging tests would provide valuable insights. Moreover, the insights gained from studying dynamic HUBs would make significant contributions to the field of materials science.

6.2.2 Further Application-Self-healable Li Batteries

Further possible applications for the use of polyhindered urea networks should be explored for instance, in lithium-ion batteries (LIBs) which are rechargeable batteries that rely on the movement of lithium ions between a positive electrode and a negative electrode to function. They are widely used as the primary power source for various portable electronic devices like smartphones, laptops, and wearable electronics, as well as power tools and electric vehicles. However, it is crucial to avoid overcharging or overdischarging LIBs as it can lead to battery damage or even destruction. Currently, LIB technology still faces challenges in meeting the increasing demands for long cycle lives and high energy densities. Unlike self-healing supercapacitors, implementing self-healing capabilities in LIBs is more challenging due to the susceptibility of the materials used to environmental conditions such as water and oxygen. Combining the self-healing abilities of the PHU as a polymer binder in LIB should be further explored to obtain longer charge cycles, enhanced safety, improved reliability, increased energy efficiency, cost-effectiveness, and sustainability. These benefits will contribute to the development of more durable and efficient LIB systems for various applications, ranging from consumer electronics to electric vehicles and renewable energy storage.

6.2.3 Improvements of TENG

The underlying mechanism of charge transfer in triboelectricity has not been definitively determined. The charge transfer mechanism may vary depending on the materials involved. While several promising charge transfer mechanisms have been proposed for certain materials, the number of identified mechanisms is significantly lower than the wide range of materials used in

TENGs. The lack of clarity regarding the charge transfer mechanism poses challenges in accurately predicting the performance of fabricated TENGs during the design phase, making commercialization difficult. To facilitate the design of TENGs and gain a competitive edge, comprehensive research on the charge transfer mechanism is essential. Understanding the charge transfer mechanism in-depth will provide significant advantages, necessitating further investigations in this area.

One of the major challenges in the commercialization of TENG is the insufficient energy harvesting efficiency (EHE) to power electronic devices. Studies have proposed TENGs with high EHE rates of around 80%. However, achieving these high rates required careful optimization of the applied external mechanical energy specific to the proposed TENG configuration. To achieve high EHE in practical applications, a higher level of output charge density (σ) is necessary. Recent research efforts have focused on enhancing EHE, and circuitry designs such as charge-pumping or charge-excitation types have shown more promise, compared to the conventional structure that stores static charges in a dielectric thin layer.[252, 253] Therefore, there should be active research in enhancing σ through investigation of new designs.

Despite not having reached the stage of commercialization, TENG has made significant advancements considering its relatively short history. In the present technological landscape, there is a clear demand for energy harvesters to power the Internet of Things (IoT), and the TENG stands out as a promising contender due to its numerous advantages. Given the existence of various unknown aspects concerning triboelectrification, there is ample room for further development through comprehensive research in order to unlock its full potential.

References

1. Kim, W.-G.; Kim, D.-W.; Tcho, I.-W.; Kim, J.-K.; Kim, M.-S.; Choi, Y.-K. *ACS Nano* **2021,** 15, (1), 258-287.
2. Li, T.; Wang, Y.; Li, S.; Liu, X.; Sun, J. *Adv Mater* **2020,** 32, (32), e2002706.
3. Wang, S.; Yang, Y.; Ying, H.; Jing, X.; Wang, B.; Zhang, Y.; Cheng, J. *ACS Appl. Mater. Interfaces* **2020**.
4. Patel, T.; Kim, M. P.; Park, J.; Lee, T. H.; Nellepalli, P.; Noh, S. M.; Jung, H. W.; Ko, H.; Oh, J. K. *ACS Nano* **2020,** 14, (9), 11442-11451.
5. Nellepalli, P.; Kim, M. P.; Park, J.; Noh, S. M.; Ye, Z.; Jung, H. W.; Ko, H.; Oh, J. K. *ACS Appl. Mater. Interfaces* **2022,** 14, (15), 17806-17817.
6. Sun, W.; Zhang, L.; Wang, S.; Mao, J.; Luo, J.; Chen, Y.; Cheng, Y. *J. Mater. Chem. C* **2021,** 9, (27), 8579-8588.
7. Lu, X.; Zhang, L.; Zhang, J.; Wang, C.; Zhang, A. *ACS Appl. Mater. Interfaces* **2022,** 14, (36), 41421-41432.
8. Elizalde, F.; Amici, J.; Trano, S.; Vozzolo, G.; Aguirresarobe, R.; Versaci, D.; Bodoardo, S.; Mecerreyes, D.; Sardon, H.; Bella, F. *J. Mater. Chem. A* **2022,** 10, (23), 12588-12596.
9. Jiang, L.; Liu, Z.; Lei, Y.; Yuan, Y.; Wu, B.; Lei, J. *ACS Appl. Polym. Mater.* **2019,** 1, (12), 3261-3268.
10. Li, Y.; Wang, Y.; Wang, S.; Ye, Z.; Bian, C.; Xing, X.; Hong, T.; Jing, X. *Macromolecules* **2022,** 55, (20), 9091-9102.
11. Liu, W. X.; Yang, Z.; Qiao, Z.; Zhang, L.; Zhao, N.; Luo, S.; Xu, J. *Nat. Commun.* **2019,** 10, (1), 4753.
12. Zhou, Z.; Wang, X.; Yu, H.; Yu, C.; Zhang, F. *Macromolecules* **2022,** 55, (6), 2193-2201.
13. Choi, D.; Lee, Y.; Lin, Z.-H.; Cho, S.; Kim, M.; Ao, C. K.; Soh, S.; Sohn, C.; Jeong, C. K.; Lee, J.; Lee, M.; Lee, S.; Ryu, J.; Parashar, P.; Cho, Y.; Ahn, J.; Kim, I.-D.; Jiang, F.; Lee, P. S.; Khandelwal, G.; Kim, S.-J.; Kim, H. S.; Song, H.-C.; Kim, M.; Nah, J.; Kim, W.; Menge, H. G.; Park, Y. T.; Xu, W.; Hao, J.; Park, H.; Lee, J.-H.; Lee, D.-M.; Kim, S.-W.; Park, J. Y.; Zhang, H.; Zi, Y.; Guo, R.; Cheng, J.; Yang, Z.; Xie, Y.; Lee, S.; Chung, J.; Oh, I.-K.; Kim, J.-S.; Cheng, T.; Gao, Q.; Cheng, G.; Gu, G.; Shim, M.; Jung, J.; Yun, C.; Zhang, C.; Liu, G.; Chen, Y.; Kim, S.; Chen, X.; Hu, J.; Pu, X.; Guo, Z. H.; Wang, X.; Chen, J.; Xiao, X.; Xie, X.; Jarin, M.; Zhang, H.; Lai, Y.-C.; He, T.; Kim, H.; Park, I.; Ahn, J.; Huynh, N. D.; Yang, Y.; Wang, Z. L.; Baik, J. M.; Choi, D. *ACS Nano* **2023**.
14. Zhu, G.; Peng, B.; Chen, J.; Jing, Q.; Lin Wang, Z. *Nano Energy* **2015,** 14, 126-138.
15. Wang, Z. L.; Song, J., (1095-9203 (Electronic)).
16. Song, Y.; Shi, Z.; Hu, G.-H.; Xiong, C.; Isogai, A.; Yang, Q. *J. Mater. Chem. A* **2021,** 9, (4), 1910-1937.
17. Dong, K.; Peng, X.; Wang, Z. L. *Adv. Mater.* **2020,** 32, (5), 1902549.
18. Zhou, L.; Liu, D.; Li, S.; Zhao, Z.; Zhang, C.; Yin, X.; Liu, L.; Cui, S.; Wang, Z. L.; Wang, J. *Adv. Energy Mater.* **2020,** 10, (24), 2000965.
19. Zhang, C.; Liu, Y.; Zhang, B.; Yang, O.; Yuan, W.; He, L.; Wei, X.; Wang, J.; Wang, Z. L. *ACS Energy Lett.* **2021,** 6, (4), 1490-1499.
20. Yuan, M.; Li, C.; Liu, H.; Xu, Q.; Xie, Y. *Nano Energy* **2021,** 85, 105962.
21. Chen, F.; Wu, Y.; Ding, Z.; Xia, X.; Li, S.; Zheng, H.; Diao, C.; Yue, G.; Zi, Y. *Nano Energy* **2019,** 56, 241-251.

22. Guo, H.; Pu, X.; Chen, J.; Meng, Y.; Yeh, M.-H.; Liu, G.; Tang, Q.; Chen, B.; Liu, D.; Qi, S.; Wu, C.; Hu, C.; Wang, J.; Wang, Z. L. *Sci. Robot.* **2018,** 3, (20), eaat2516.
23. Chen, J.; Wang, Z. L. *Joule* **2017,** 1, (3), 480-521.
24. Yang, W.; Chen, J.; Zhu, G.; Wen, X.; Bai, P.; Su, Y.; Lin, Y.; Wang, Z. *Nano Res.* **2013,** 6, (12), 880-886.
25. Jin, L.; Zhang, S. L.; Xu, S.; Guo, H.; Yang, W.; Wang, Z. L. *Adv. Mater. Technol.* **2021,** 6, (3), 2000918.
26. Du, Y.; Tang, Q.; He, W.; Liu, W.; Wang, Z.; Wu, H.; Li, G.; Guo, H.; Li, Z.; Peng, Y.; Hu, C. *Nano Energy* **2021,** 90, 106543.
27. Parida, K.; Xiong, J.; Zhou, X.; Lee, P. S. *Nano Energy* **2019,** 59, 237-257.
28. Wang, H.; Han, M.; Song, Y.; Zhang, H. *Nano Energy* **2021,** 81, 105627.
29. Yuan, W.; Zhang, C.; Zhang, B.; Wei, X.; Yang, O.; Liu, Y.; He, L.; Cui, S.; Wang, J.; Wang, Z. L. *Adv. Mater. Technol.* **2022,** 7, (6), 2101139.
30. Ghosh, S. K.; Kim, J.; Kim, M. P.; Na, S.; Cho, J.; Kim, J. J.; Ko, H. *ACS Nano* **2022,** 16, (7), 11415-11427.
31. Wang, Z. L. *Materials Today* **2017,** 20, (2), 74-82.
32. Jiang, T.; Chen, X.; Han, C. B.; Tang, W.; Wang, Z. L. *Adv. Funct. Mater.* **2015,** 25, (19), 2928-2938.
33. Wang, Z. L.; Wang, A. C. *Materials Today* **2019,** 30, 34-51.
34. Fan, F.-R.; Tian, Z.-Q.; Lin Wang, Z. *Nano Energy* **2012,** 1, (2), 328-334.
35. Lowell, J.; Rose-Innes, A. C. *Adv. Phys.* **1980,** 29, (6), 947-1023.
36. Xu, C.; Zi, Y.; Wang, A. C.; Zou, H.; Dai, Y.; He, X.; Wang, P.; Wang, Y.-C.; Feng, P.; Li, D.; Wang, Z. L. *Adv. Mater.* **2018,** 30, (15), 1706790.
37. McCarty, L. S.; Winkleman, A.; Whitesides, G. M. *J. Am. Chem. Soc.* **2007,** 129, (13), 4075-4088.
38. McCarty, L. S.; Whitesides, G. M. *Angew. Chem. Int. Ed.* **2008,** 47, (12), 2188-2207.
39. Clint, J. H.; Dunstan, T. S. *Europhys. Lett.* **2001,** 54, (3), 320.
40. Baytekin, H. T.; Patashinski, A. Z.; Branicki, M.; Baytekin, B.; Soh, S.; Grzybowski, B. A. *Sci.* **2011,** 333, (6040), 308-312.
41. Xia, X.; Chen, J.; Liu, G.; Javed, M. S.; Wang, X.; Hu, C. *Carbon* **2017,** 111, 569-576.
42. Zhou, Y.; Deng, W.; Xu, J.; Chen, J. *Cell Rep.* **2020,** 1, (8), 100142.
43. Lee, K. Y.; Chun, J.; Lee, J.-H.; Kim, K. N.; Kang, N.-R.; Kim, J.-Y.; Kim, M. H.; Shin, K.-S.; Gupta, M. K.; Baik, J. M.; Kim, S.-W. *Adv. Mater.* **2014,** 26, (29), 5037-5042.
44. Mule, A. R.; Dudem, B.; Yu, J. S. *Energy* **2018,** 165, 677-684.
45. Park, C.; Song, G.; Cho, S. M.; Chung, J.; Lee, Y.; Kim, E. H.; Kim, M.; Lee, S.; Huh, J.; Park, C. *Adv. Funct. Mater.* **2017,** 27, (27), 1701367.
46. Hedau, B.; Kang, B.-C.; Ha, T.-J. *ACS Nano* **2022,** 16, (11), 18355-18365.
47. Shin, S.-H.; Bae, Y. E.; Moon, H. K.; Kim, J.; Choi, S.-H.; Kim, Y.; Yoon, H. J.; Lee, M. H.; Nah, J. *ACS Nano* **2017,** 11, (6), 6131-6138.
48. Fang, H.; Wang, X.; Li, Q.; Peng, D.; Yan, Q.; Pan, C. *Adv. Energy Mater.* **2016,** 6, (18), 1600829.
49. Yang, H. J.; Lee, J.-W.; Seo, S. H.; Jeong, B.; Lee, B.; Do, W. J.; Kim, J. H.; Cho, J. Y.; Jo, A.; Jeong, H. J.; Jeong, S. Y.; Kim, G.-H.; Lee, G.-W.; Shin, Y.-E.; Ko, H.; Han, J. T.; Park, J. H. *Nano Energy* **2021,** 86, 106083.

50. Shi, L.; Jin, H.; Dong, S.; Huang, S.; Kuang, H.; Xu, H.; Chen, J.; Xuan, W.; Zhang, S.; Li, S.; Wang, X.; Luo, J. *Nano Energy* **2021,** 80, 105599.
51. Kubisa, P. *Prog. Polym. Sci.* **2009,** 34, (12), 1333-1347.
52. Parida, K.; Kumar, V.; Jiangxin, W.; Bhavanasi, V.; Bendi, R.; Lee, P. S. *Adv. Mater.* **2017,** 29, (37), 1702181.
53. Darnell, M. C.; Sun, J.-Y.; Mehta, M.; Johnson, C.; Arany, P. R.; Suo, Z.; Mooney, D. J. *Biomater.* **2013,** 34, (33), 8042-8048.
54. Parida, K.; Thangavel, G.; Cai, G.; Zhou, X.; Park, S.; Xiong, J.; Lee, P. S. *Nat. Commun.* **2019,** 10, (1), 2158.
55. Xu, W.; Huang, L.-B.; Hao, J. *Nano Energy* **2017,** 40, 399-407.
56. Sun, J.; Pu, X.; Liu, M.; Yu, A.; Du, C.; Zhai, J.; Hu, W.; Wang, Z. L. *ACS Nano* **2018,** 12, (6), 6147-6155.
57. Han, X.; Jiang, D.; Qu, X.; Bai, Y.; Cao, Y.; Luo, R.; Li, Z. *Materials* **2021,** 14, (7), 1689.
58. Deng, J.; Kuang, X.; Liu, R.; Ding, W.; Wang, A. C.; Lai, Y. C.; Dong, K.; Wen, Z.; Wang, Y.; Wang, L.; Qi, H. J.; Zhang, T.; Wang, Z. L. *Adv Mater* **2018,** 30, (14), e1705918.
59. Lehn, J.-M. *Angew. Chem. Int. Ed.* **2015,** 54, (11), 3276-3289.
60. Lehn, J.-M. *Chem. Soc. Rev.* **2007,** 36, (2), 151-160.
61. Chen, X.; Dam, M. A.; Ono, K.; Mal, A.; Shen, H.; Nutt, S. R.; Sheran, K.; Wudl, F. *Sci.* **2002,** 295, (5560), 1698-1702.
62. Wang, Z.; Tian, H.; He, Q.; Cai, S. *ACS Appl. Mater. Interfaces* **2017,** 9, (38), 33119-33128.
63. Ji, S.; Cao, W.; Yu, Y.; Xu, H. *Angew. Chem. Int. Ed.* **2014,** 53, (26), 6781-5.
64. Yang, Y.; Du, F.-S.; Li, Z.-C. *ACS Appl. Polym. Mater.* **2020,** 2, (12), 5630-5640.
65. Hu, J.; Mo, R.; Sheng, X.; Zhang, X. *Polym. Chem.* **2020,** 11, (14), 2585-2594.
66. Chen, X.; Dam, M. A.; Ono, K.; Mal, A.; Shen, H.; Nutt, S. R.; Sheran, K.; Wudl, F. *Sci.* **2002,** 295, (5560), 1698-702.
67. Lei, Z. Q.; Xiang, H. P.; Yuan, Y. J.; Rong, M. Z.; Zhang, M. Q. *Chem. Mater.* **2014,** 26, (6), 2038-2046.
68. Li, C.; Madsen, J.; Armes, S. P.; Lewis, A. L. *Angew. Chem. Int. Ed.* **2006,** 45, (21), 3510-3513.
69. Tsarevsky, N. V.; Matyjaszewski, K. *Macromolecules* **2005,** 38, (8), 3087-3092.
70. Kildahl, N. K. *J. Chem. Educ.* **1995,** 72, (5), 423.
71. Ying, H.; Zhang, Y.; Cheng, J. *Nat. Commun.* **2014,** 5, 4218/1-4218/9.
72. Denissen, W.; Winne, J. M.; Du Prez, F. E. *Chem. Sci.* **2016,** 7, (1), 30-38.
73. Roy, N.; Bruchmann, B.; Lehn, J.-M. *Chem. Soc. Rev.* **2015,** 44, (11), 3786-3807.
74. Zhao, Q.; Zou, W.; Luo, Y.; Xie, T. *Sci. Adv.* 2, (1), e1501297.
75. Pei, Z.; Yang, Y.; Chen, Q.; Wei, Y.; Ji, Y. *Adv. Mater.* **2015,** 28.
76. Denissen, W.; Winne, J. M.; Du Prez, F. E. *Chem. Sci.* **2016,** 7, (1), 30-38.
77. Bowman, C. N.; Kloxin, C. J. *Angew. Chem. Int. Ed.* **2012,** 51, (18), 4272-4.
78. Kloxin, C. J.; Bowman, C. N. *Chem. Soc. Rev.* **2013,** 42, (17), 7161-7173.
79. Van Zee, N. J.; Nicolaÿ, R. *Prog. Polym. Sci.* **2020,** 104.
80. Samanta, S.; Kim, S.; Saito, T.; Sokolov, A. P. *J Phys Chem B* **2021,** 125, (33), 9389-9401.
81. Van Lijsebetten, F.; Holloway, J. O.; Winne, J. M.; Du Prez, F. E. *Chem. Soc. Rev.* **2020,** 49, (23), 8425-8438.
82. Montarnal, D.; Capelot, M.; Tournilhac, F.; Leibler, L. *Sci.* **2011,** 334, (6058), 965-968.

83. Dahlke, J.; Zechel, S.; Hager, M. D.; Schubert, U. S. *Adv. Mater. Interfaces* **2018,** 5, (17).
84. Bednarek, M.; Kubisa, P. *Polym. Chem.* **2019,** 10, (15), 1848-1872.
85. Zhao, X.-L.; Li, Y.-D.; Zeng, J.-B. *Polym. Chem.* **2022,** 13, (48), 6573-6588.
86. Wu, D. Y.; Meure, S.; Solomon, D. *Prog. Polym. Sci.* **2008,** 33, (5), 479-522.
87. Nellepalli, P.; Patel, T.; Oh, J. K. *Macromol. Rapid Commun.* **2021**, Ahead of Print.
88. Willocq, B.; Odent, J.; Dubois, P.; Raquez, J.-M. *RSC Adv.* **2020,** 10, (23), 13766-13782.
89. Aguirresarobe, R. H.; Nevejans, S.; Reck, B.; Irusta, L.; Sardon, H.; Asua, J. M.; Ballard, N. *Prog. Polym. Sci.* **2021,** 114.
90. Roy, N.; Bruchmann, B.; Lehn, J.-M. *Chem. Soc. Rev.* **2015,** 44, (11), 3786-3807.
91. Zheng, N.; Xu, Y.; Zhao, Q.; Xie, T. *Chem Rev* **2021,** 121, (3), 1716-1745.
92. Wanasinghe, S. V.; Dodo, O. J.; Konkolewicz, D. *Angew. Chem.* **2022,** 61, (50), e202206938.
93. Liu, T.; Zhao, B.; Zhang, J. *Polymer* **2020,** 194.
94. An, S. Y.; Arunbabu, D.; Noh, S. M.; Song, Y. K.; Oh, J. K. *Chem. Comm.* **2015,** 51, (66), 13058-13070.
95. Liguori, A.; Hakkarainen, M. *Macromol. Rapid Commun.* **2022,** 43, (13), e2100816.
96. Zhang, Q.; Wang, S.; Rao, B.; Chen, X.; Ma, L.; Cui, C.; Zhong, Q.; Li, Z.; Cheng, Y.; Zhang, Y. *React. Funct. Polym.* **2021,** 159.
97. Jung, S.; Patel, T.; Oh, J. K. *Macromol. Rapid Commun.* **2018,** 39, (5), 1700575.
98. Zhou, Q.; Gardea, F.; Sang, Z.; Lee, S.; Pharr, M.; Sukhishvili, S. A. *Adv. Funct. Mater.* **2020,** 30, (30).
99. Berto, P.; Pointet, A.; Le Coz, C.; Grelier, S.; Peruch, F. *Macromolecules* **2018,** 51, (3), 651-659.
100. Kang, D. H.; Cho, S.; Sung, S.; Kim, Y. R.; Lee, H.; Choe, A.; Yeom, J.; Kim, M. P.; Kim, J. C.; Noh, S. M.; Ko, H. *ACS Appl. Mater. Interfaces* **2020,** 12, (47), 53184-53192.
101. Zhao, B.; Ding, H.; Xu, S.; Zheng, S. *ACS Appl. Polym. Mater.* **2019,** 1, (11), 3174-3184.
102. Zhang, J.; Zhang, C.; Song, F.; Shang, Q.; Hu, Y.; Jia, P.; Liu, C.; Hu, L.; Zhu, G.; Huang, J.; Zhou, Y. *J. Chem. Eng.* **2022,** 429.
103. Jia, Y.; Ying, H.; Zhang, Y.; He, H.; Cheng, J. *Macromol. Chem. Phys.* **2019,** 220, (12).
104. Fang, Z.; Zheng, N.; Zhao, Q.; Xie, T. *ACS Appl. Mater. Interfaces* **2017,** 9, (27), 22077-22082.
105. Son, D. H.; Bae, H. E.; Bae, M. J.; Lee, S.-H.; Cheong, I. W.; Park, Y. I.; Jeong, J.-E.; Kim, J. C. *ACS Appl. Polym. Mater.* **2022,** 4, (5), 3802-3810.
106. Ying, H.; Cheng, J. *J. Am. Chem. Soc.* **2014,** 136, (49), 16974-16977.
107. Wang, Y.; Pan, Y.; Zheng, Z.; Ding, X. *Macromol. Rapid. Commun.* **2018,** 39, (10), e1800128.
108. Zhang, L.; Rowan, S. J. *Macromolecules* **2017,** 50, (13), 5051-5060.
109. Zhang, Y.; Ying, H.; Hart, K. R.; Wu, Y.; Hsu, A. J.; Coppola, A. M.; Kim, T. A.; Yang, K.; Sottos, N. R.; White, S. R.; Cheng, J. *Adv. Mater.* **2016,** 28, (35), 7646-7651.
110. Chiefari, J.; Chong, Y. K.; Ercole, F.; Krstina, J.; Jeffery, J.; Le, T. P. T.; Mayadunne, R. T. A.; Meijs, G. F.; Moad, C. L.; Moad, G.; Rizzardo, E.; Thang, S. H. *Macromolecules* **1998,** 31, (16), 5559-5562.
111. Perrier, S.; Takolpuckdee, P. *J. Polym. Sci., Part A: Polym. Chem.* **2005,** 43, (22), 5347-5393.

112. McCormick, C. L.; Sumerlin, B. S.; Lokitz, B. S.; Stempka, J. E. *Soft Matter.* **2008,** 4, (9), 1760-1773.
113. Boyer, C.; Bulmus, V.; Davis, T. P.; Ladmiral, V.; Liu, J.; Perrier, S. *Chemical Reviews (Washington, DC, United States)* **2009,** 109, (11), 5402-5436.
114. Boyer, C.; Stenzel, M. H.; Davis, T. P. *J. Polym. Sci., Part A: Polym. Chem.* **2011,** 49, (3), 551-595.
115. Nellepalli, P.; Patel, T.; Kim, M. P.; Park, J.; Ye, Z.; Jung, H. W.; Ko, H.; Oh, J. K. *Polym. Chem.* **2022,** 13, (29), 4343-4351.
116. Park, J. I.; Choe, A.; Kim, M. P.; Ko, H.; Lee, T. H.; Noh, S. M.; Kim, J. C.; Cheong, I. W. *Polym. Chem.* **2018,** 9, (1), 11-19.
117. Lee, H. M.; Perumal, S.; Kim, G. Y.; Kim, J. C.; Kim, Y.-R.; Kim, M. P.; Ko, H.; Rho, Y.; Cheong, I. W. *Polym. Chem.* **2020,** 11, (22), 3701-3708.
118. Xie, S.; Wang, D.; Zhang, S.; Xu, J.; Fu, J. *J. Mater. Chem. A* **2022,** 10, (17), 9457-9467.
119. Wang, F.-Z.; Wang, H.-Q.; Gao, W.-T.; Li, C.-H. *Materials Chemistry Frontiers* **2022,** 6, (4), 473-481.
120. Sun, W.; Luo, J.; Zhang, L.; Chen, Y.; Li, P.; Zheng, Y.; Cheng, Y. *ACS Appl. Polym. Mater.* **2021,** 3, (11), 5622-5631.
121. Xie, D.-M.; Zhao, X.-L.; Li, Y.-D.; Weng, Y.; Zeng, J.-B. *Industrial Crops and Products* **2022,** 188.
122. Jiang, L.; Lei, Y.; Xiao, Y.; Fu, X.; Kong, W.; Wang, Y.; Lei, J. *J. Mater. Chem. A* **2020,** 8, (42), 22369-22378.
123. Wang, X.-Z.; Xie, D.-M.; Zhao, X.-L.; Li, Y.-D.; Zeng, J.-B. *Macromolecules* **2022,** 55, (6), 2243-2251.
124. Erice, A.; Ruiz de Luzuriaga, A.; Matxain, J. M.; Ruipérez, F.; Asua, J. M.; Grande, H.-J.; Rekondo, A. *Polymer* **2018,** 145, 127-136.
125. Chen, B.; Liu, X.; Liu, J.; Feng, Z.; Zheng, X.; Wu, X.; Yang, C.; Liang, L. *React. Funct. Polym.* **2022,** 172.
126. Zhou, Z.; Zeng, Y.; Yu, C.; Li, Q.; Zhang, F. *Mater. Chem. Phys.* **2021,** 267.
127. Peng, S.; Wang, Z.; Lin, J.; Miao, J. T.; Zheng, L.; Yang, Z.; Weng, Z.; Wu, L. *Adv. Funct. Mater.* **2020,** 31, (10).
128. Zhou, Z.; Zeng, Y.; Yu, C.; Chen, H.; Zhang, F. *Smart Mater Struct.* **2020,** 29, (11).
129. Jun, S.; Kim, S. O.; Lee, H.-J.; Han, C. J.; Lee, C.-J.; Yu, Y.-T.; Lee, C.-R.; Ju, B.-K.; Kim, Y.; Kim, J.-W. *J. Mater. Chem. A* **2019,** 7, (7), 3101-3111.
130. Zhao, B.; Li, L.; Hu, J.; Wang, H.; Mei, H.; Zheng, S. *Polymer* **2022,** 242.
131. Bin Rusayyis, M. A.; Torkelson, J. M. *ACS Macro Lett.* **2022,** 11, (4), 568-574.
132. Zhu, G.; Su, Y.; Bai, P.; Chen, J.; Jing, Q.; Yang, W.; Wang, Z. L. *ACS Nano* **2014,** 8, (6), 6031-6037.
133. Qin, Y.; Wang, X.; Wang, Z. L. *Nature* **2008,** 451, (7180), 809-813.
134. Wang, S.; Lin, L.; Wang, Z. L. *Nano Lett.* **2012,** 12, (12), 6339-6346.
135. Mackanic, D. G.; Chang, T. H.; Huang, Z.; Cui, Y.; Bao, Z. *Chem. Soc. Rev.* **2020,** 49, (13), 4466-4495.
136. Wu, C.; Wang, A. C.; Ding, W.; Guo, H.; Wang, Z. L. *Adv. Energy Mater.* **2019,** 9, (1), 1802906.
137. Wang, Z. L.; Zhu, G.; Yang, Y.; Wang, S.; Pan, C. *Mater. Today* **2012,** 15, (12), 532-543.

138. Wang, Z. L.; Chen, J.; Lin, L. *Energy Environ. Sci.* **2015,** 8, (8), 2250-2282.
139. Wang, S.; Xie, Y.; Niu, S.; Lin, L.; Wang, Z. L. *Adv. Mater.* **2014,** 26, (18), 2818-2824.
140. Zhang, M.; Gao, T.; Wang, J.; Liao, J.; Qiu, Y.; Yang, Q.; Xue, H.; Shi, Z.; Zhao, Y.; Xiong, Z. *Nano Energy* **2015,** 13, 298-305.
141. Lin, L.; Wang, S.; Niu, S.; Liu, C.; Xie, Y.; Wang, Z. L. *ACS Appl. Mater. Interfaces* **2014,** 6, (4), 3031-3038.
142. Pu, X.; Li, L.; Song, H.; Du, C.; Zhao, Z.; Jiang, C.; Cao, G.; Hu, W.; Wang, Z. L. *Adv. Mater.* **2015,** 27, (15), 2472-2478.
143. Lai, Y. C.; Deng, J.; Zhang, S. L.; Niu, S.; Guo, H.; Wang, Z. L. *Adv. Funct. Mater.* **2017,** 27, (1), 1604462.
144. Guo, H.; Yeh, M.-H.; Zi, Y.; Wen, Z.; Chen, J.; Liu, G.; Hu, C.; Wang, Z. L. *ACS Nano* **2017,** 11, (5), 4475-4482.
145. Yang, Y.; Zhang, H.; Liu, Y.; Lin, Z. H.; Lee, S.; Lin, Z.; Wong, C. P.; Wang, Z. L. *ACS Nano* **2013,** 7, (3), 2808-2813.
146. Cheng, G.; Lin, Z. H.; Du, Z. L.; Wang, Z. L. *ACS Nano* **2014,** 8, (2), 1932-1939.
147. Wang, Z. L. *Nature* **2017,** 542, (7640), 159-160.
148. Zhang, L. M.; Han, C. B.; Jiang, T.; Zhou, T.; Li, X. H.; Zhang, C.; Wang, Z. L. *Nano Energy* **2016,** 22, 87-94.
149. Maitra, A.; Paria, S.; Karan, S. K.; Bera, R.; Bera, A.; Das, A. K.; Si, S. K.; Halder, L.; De, A.; Khatua, B. B. *ACS Appl. Mater. Interfaces* **2019,** 11, (5), 5022-5036.
150. Chen, D.; Wang, D.; Yang, Y.; Huang, Q.; Zhu, S.; Zheng, Z. *Adv. Energy Mater.* **2017,** 7, (23), 1700890.
151. Parida, K.; Thangavel, G.; Cai, G.; Zhou, X.; Park, S.; Xiong, J.; Lee, P. S. *Nat. Commun.* **2019,** 10, (1), 2158.
152. Lai, Y. C.; Wu, H. M.; Lin, H. C.; Chang, C. L.; Chou, H. H.; Hsiao, Y. C.; Wu, Y. C. *Adv. Funct. Mater.* **2019,** 29, (40), 1904626.
153. Guan, Q. B.; Dai, Y. H.; Yang, Y. Q.; Bi, X. Y.; Wen, Z.; Pan, Y. *Nano Energy* **2018,** 51, 333-339.
154. Xu, W.; Wong, M.-C.; Guo, Q.; Jia, T.; Hao, J. *J. Mater. Chem. A* **2019,** 7, (27), 16267-16276.
155. Guan, Q.; Lin, G.; Gong, Y.; Wang, J.; Tan, W.; Bao, D.; Liu, Y.; You, Z.; Sun, X.; Wen, Z.; Pan, Y. *J. Mater. Chem. A* **2019,** 7, (23), 13948-13955.
156. Chen, Y.; Pu, X.; Liu, M.; Kuang, S.; Zhang, P.; Hua, Q.; Cong, Z.; Guo, W.; Hu, W.; Wang, Z. L. *ACS Nano* **2019,** 13, (8), 8936-8945.
157. Dai, X. Y.; Huang, L. B.; Du, Y. Z.; Han, J. C.; Zheng, Q. Q.; Kong, J.; Hao, J. H. *Adv. Funct. Mater.* **2020,** 30, (16), 1910723.
158. Capelot, M.; Unterlass, M. M.; Tournilhac, F.; Leibler, L. *ACS Macro Lett.* **2012,** 1, (7), 789-792.
159. Zou, H.; Zhang, Y.; Guo, L.; Wang, P.; He, X.; Dai, G.; Zheng, H.; Chen, C.; Wang, A. C.; Xu, C.; Wang, Z. L. *Nat. Commun.* **2019,** 10, (1), 1427.
160. Menon, A. V.; Madras, G.; Bose, S. *Polym. Chem.* **2019,** 10, (32), 4370-4388.
161. Van Zee, N. J.; Nicolaÿ, R. *Prog. Polym. Sci.* **2020,** 104.
162. Jiang, L.; Liu, Z.; Lei, Y.; Yuan, Y.; Wu, B.; Lei, J. *ACS Appl Polym Mater* **2019,** 1, (12), 3261-3268.

163. Fang, Z.; Zheng, N.; Zhao, Q.; Xie, T. *ACS Appl Mater Interfaces* **2017,** 9, (27), 22077-22082.
164. Wang, Y.; Pan, Y.; Zheng, Z.; Ding, X. *Macromol Rapid Commun* **2018,** 39, (10), e1800128.
165. Han, F.; Xu, B.; Shah, S. A. A.; Zhang, J.; Cheng, J. *Macromol. Mater. Eng.* **2020**, 1900782.
166. Pistone, A.; Ferlazzo, A.; Lanza, M.; Milone, C.; Iannazzo, D.; Piperno, A.; Piperopoulos, E.; Galvagno, S. *J Nanosci Nanotechno* **2012,** 12, (6), 5054-5060.
167. Zhang, L.; Rowan, S. J. *Macromolecules* **2017,** 50, (13), 5051-5060.
168. Chen, J.; Guo, H. Y.; He, X. M.; Liu, G. L.; Xi, Y.; Shi, H. F.; Hu, C. G. *ACS Appl. Mater. Interfaces* **2016,** 8, (1), 736-744.
169. Fang, Z. G.; Chan, K. H.; Lu, X.; Tan, C. F.; Ho, G. W. *J. Mater. Chem. A* **2018,** 6, (1), 52-57.
170. Harnchana, V.; Ngoc, H. V.; He, W.; Rasheed, A.; Park, H.; Amornkitbamrung, V.; Kang, D. J. *ACS Appl. Mater. Interfaces* **2018,** 10, (30), 25263-25272.
171. Xia, X. N.; Chen, J.; Liu, G. L.; Javed, M. S.; Wang, X.; Hu, C. G. *Carbon* **2017,** 111, 569-576.
172. Ago, H.; Kugler, T.; Cacialli, F.; Salaneck, W. R.; Shaffer, M. S. P.; Windle, A. H.; Friend, R. H. *J. Phys. Chem. B* **1999,** 103, (38), 8116-8121.
173. Van Trinh, P.; Anh, N. N.; Tam, N. T.; Hong, N. T.; Hong, P. N.; Minh, P. N.; Thang, B. H. *RSC Adv.* **2017,** 7, (79), 49937-49946.
174. Sun, H. B.; Zhang, H. L.; Liu, S. T.; Ning, N. Y.; Zhang, L. Q.; Tian, M.; Wang, Y. *Compos Sci Technol* **2018,** 154, 145-153.
175. Ning, N. Y.; Bai, X.; Yang, D.; Zhang, L. Q.; Lu, Y. L.; Nishi, T.; Tian, M. *RSC Adv.* **2014,** 4, (9), 4543-4551.
176. Lee, J. W.; Cho, H. J.; Chun, J.; Kim, K. N.; Kim, S.; Ahn, C. W.; Kim, I. W.; Kim, J. Y.; Kim, S. W.; Yang, C.; Baik, J. M. *Sci Adv* **2017,** 3, (5), e1602902.
177. Kim, M. P.; Lee, Y.; Hur, Y. H.; Park, J.; Kim, J.; Lee, Y.; Ahn, C. W.; Song, S. W.; Jung, Y. S.; Ko, H. *Nano Energy* **2018,** 53, 37-45.
178. Baer, E.; Zhu, L. *Macromolecules* **2017,** 50, (6), 2239-2256.
179. Zhu, L. *J Phys Chem Lett* **2014,** 5, (21), 3677-3687.
180. Xu, W.; Huang, L. B.; Hao, J. H. *Nano Energy* **2017,** 40, 399-407.
181. Feng, Y. G.; Zheng, Y. B.; Zhang, G.; Wang, D. A.; Zhou, F.; Liu, W. M. *Nano Energy* **2017,** 38, 467-476.
182. Liu, Y.; Zheng, Y.; Li, T.; Wang, D.; Zhou, F. *Nano Energy* **2019,** 61, 454-461.
183. Niu, H.; Du, X.; Zhao, S.; Yuan, Z.; Zhang, X.; Cao, R.; Yin, Y.; Zhang, C.; Zhou, T.; Li, C. *RSC Adv.* **2018,** 8, (54), 30661-30668.
184. Zhu, G.; Lin, Z.-H.; Jing, Q.; Bai, P.; Pan, C.; Yang, Y.; Zhou, Y.; Wang, Z. L. *Nano Lett.* **2013,** 13, (2), 847-853.
185. Zhong, J.; Zhong, Q.; Fan, F.; Zhang, Y.; Wang, S.; Hu, B.; Wang, Z. L.; Zhou, J. *Nano Energy* **2013,** 2, (4), 491-497.
186. Zhu, G.; Chen, J.; Zhang, T.; Jing, Q.; Wang, Z. L. *Nat. Commun.* **2014,** 5, (1), 3426.
187. Guo, H.; Chen, J.; Tian, L.; Leng, Q.; Xi, Y.; Hu, C. *ACS Appl. Mater. Interfaces* **2014,** 6, (19), 17184-17189.
188. Cao, X.; Jie, Y.; Wang, N.; Wang, Z. L. J. A. E. M. **2016,** 6, (23), 1600665.
189. Wang, Z. L. *Nano Energy* **2018,** 54, 477-483.

190. Lai, Y.-C.; Hsiao, Y.-C.; Wu, H.-M.; Wang, Z. L. *Adv. Sci.* **2019,** 6, (5), 1801883.
191. Luo, J.; Wang, Z. L. *Energy Storage Mater.* **2019,** 23, 617-628.
192. Zhang, C.; Chen, J.; Xuan, W.; Huang, S.; You, B.; Li, W.; Sun, L.; Jin, H.; Wang, X.; Dong, S.; Luo, J.; Flewitt, A. J.; Wang, Z. L. *Nat. Commun.* **2020,** 11, (1), 58.
193. Zhang, Y.; Khanbareh, H.; Roscow, J.; Pan, M.; Bowen, C.; Wan, C. *Matter* **2020,** 3, (4), 989-1008.
194. Deng, J.; Kuang, X.; Liu, R.; Ding, W.; Wang, A. C.; Lai, Y.-C.; Dong, K.; Wen, Z.; Wang, Y.; Wang, L.; Qi, H. J.; Zhang, T.; Wang, Z. L. *Adv. Mater.* **2018,** 30, (14), 1705918.
195. Guan, Q.; Dai, Y.; Yang, Y.; Bi, X.; Wen, Z.; Pan, Y. *Nano Energy* **2018,** 51, 333-339.
196. Dang, C.; Shao, C.; Liu, H.; Chen, Y.; Qi, H. *Nano Energy* **2021,** 90, 106619.
197. Zhang, M.; Tao, X.; Yu, R.; He, Y.; Li, X.; Chen, X.; Huang, W. *J. Mater. Chem. A* **2022**.
198. Yang, D.; Ni, Y.; Kong, X.; Li, S.; Chen, X.; Zhang, L.; Wang, Z. L. *ACS Nano* **2021,** 15, (9), 14653-14661.
199. Dai, X.; Huang, L.-B.; Du, Y.; Han, J.; Zheng, Q.; Kong, J.; Hao, J. *Adv. Funct. Mater.* **2020,** 30, (16), 1910723.
200. Yang, D.; Ni, Y.; Su, H.; Shi, Y.; Liu, Q.; Chen, X.; He, D. *Nano Energy* **2021,** 79, 105394.
201. Zhang, P.; Guo, W.; Guo, Z. H.; Ma, Y.; Gao, L.; Cong, Z.; Zhao, X. J.; Qiao, L.; Pu, X.; Wang, Z. L. J. A. M. *Adv. Mater.* **2021,** 33, (31), 2101396.
202. Zhou, Z.; Zeng, Y.; Yu, C.; Chen, H.; Zhang, F. *Smart Mater Struct.* **2020,** 29, (11), 115041.
203. Wu, J.; Wang, X.; He, J.; Li, Z.; Li, L. *J. Mater. Chem. A* **2021,** 9, (10), 6583-6590.
204. Liang, Q.; Yan, X.; Gu, Y.; Zhang, K.; Liang, M.; Lu, S.; Zheng, X.; Zhang, Y. *Sci. Rep.* **2015,** 5, (1), 9080.
205. Li, X.; Tao, J.; Wang, X.; Zhu, J.; Pan, C.; Wang, Z. L. *Adv. Energy Mater.* **2018,** 8, (21), 1800705.
206. Nie, J.; Chen, X.; Wang, Z. L. J. A. F. M. *Adv. Funct. Mater.* **2019,** 29, (41), 1806351.
207. Yao, C.; Hernandez, A.; Yu, Y.; Cai, Z.; Wang, X. *Nano Energy* **2016,** 30, 103-108.
208. Xiao, T. X.; Liang, X.; Jiang, T.; Xu, L.; Shao, J. J.; Nie, J. H.; Bai, Y.; Zhong, W.; Wang, Z. L. *Adv. Funct. Mater.* **2018,** 28, (35), 1802634.
209. Bai, P.; Zhu, G.; Zhou, Y. S.; Wang, S.; Ma, J.; Zhang, G.; Wang, Z. L. *Nano Res.* **2014,** 7, (7), 990-997.
210. Lee, J. W.; Cho, H. J.; Chun, J.; Kim, K. N.; Kim, S.; Ahn, C. W.; Kim, I. W.; Kim, J.-Y.; Kim, S.-W.; Yang, C. J. S. a. *Sci Adv* **2017,** 3, (5), e1602902.
211. Cao, Y.; Morrissey, T. G.; Acome, E.; Allec, S. I.; Wong, B. M.; Keplinger, C.; Wang, C. J. A. M. *Adv Mater* **2017,** 29, (10), 1605099.
212. Kim, Y.; Lee, D.; Seong, J.; Bak, B.; Choi, U. H.; Kim, J. *Nano Energy* **2021,** 84, 105925.
213. Cao, Y.; Morrissey, T. G.; Acome, E.; Allec, S. I.; Wong, B. M.; Keplinger, C.; Wang, C. *Adv. Mater.* **2017,** 29, (10), 1605099.
214. Li, H.; Xu, F.; Guan, T.; Li, Y.; Sun, J. *Nano Energy* **2021,** 90.
215. Jazani, A. M.; Oh, J. K. *Macromolecules* **2017,** 50, (23), 9427-9436.
216. Jazani, A. M.; Arezi, N.; Shetty, C.; Hong, S. H.; Li, H.; Wang, X.; Oh, J. K. *Polym. Chem.* **2019,** 10, (22), 2840-2853.
217. Jung, S.; Kim, S. Y.; Kim, J. C.; Noh, S. M.; Oh, J. K. *RSC Adv.* **2017,** 7, (42), 26496-26506.
218. Li, H.; Tuo, L.; Yang, K.; Jeong, H.-K.; Dai, Y.; He, G.; Zhao, W. *J. Membr. Sci.* **2016,** 511, 130-142.

219. Plamus, T.; Savest, N.; Viirsalu, M.; Harz, P.; Tarasova, E.; Krasnou, I.; Vassiljeva, V.; Kallavus, U.; Krumme, A. *Polymer Testing* **2018,** 71, 335-343.
220. Kim, M. P.; Um, D.-S.; Shin, Y.-E.; Ko, H. *Nanoscale Res. Lett.* **2021,** 16, (1), 35.
221. Xu, Y.; Min, G.; Gadegaard, N.; Dahiya, R.; Mulvihill, D. M. *Nano Energy* **2020,** 76, 105067.
222. Kim, M. P.; Ahn, C. W.; Lee, Y.; Kim, K.; Park, J.; Ko, H. *Nano Energy* **2021,** 82, 105697.
223. Kloxin, C. J.; Bowman, C. N. *Chem. Soc. Rev.* **2013,** 42, (17), 7161-73.
224. Canadell, J.; Goossens, H.; Klumperman, B. *Macromolecules* **2011,** 44, (8), 2536-2541.
225. Pepels, M.; Filot, I.; Klumperman, B.; Goossens, H. *Polym. Chem.* **2013,** 4, (18), 4955-4965.
226. Lafont, U.; van Zeijl, H.; van der Zwaag, S. *ACS Appl. Mater. Interfaces* **2012,** 4, (11), 6280-6288.
227. Zhang, Z. P.; Rong, M. Z.; Zhang, M. Q.; Yuan, C. e. *Polym. Chem.* **2013,** 4, (17), 4648-4654.
228. Imato, K.; Nishihara, M.; Kanehara, T.; Amamoto, Y.; Takahara, A.; Otsuka, H. *Angew. Chem. Int. Ed.* **2012,** 51, (5), 1138-1142.
229. Cromwell, O. R.; Chung, J.; Guan, Z. *J. Am. Chem. Soc.* **2015,** 137, (20), 6492-6495.
230. Cash, J. J.; Kubo, T.; Bapat, A. P.; Sumerlin, B. S. *Macromolecules* **2015,** 48, (7), 2098-2106.
231. Ying, H.; Zhang, Y.; Cheng, J., (2041-1723 (Electronic)).
232. Liu, W.-X.; Yang, Z.; Qiao, Z.; Zhang, L.; Zhao, N.; Luo, S.; Xu, J. *Nat. Commun.* **2019,** 10, (1), 4753.
233. Jiang, L.; Lei, Y.; Xiao, Y.; Fu, X.; Kong, W.; Wang, Y.; Lei, J. *J. Mater. Chem. A* **2020,** 8, (42), 22369-22378.
234. Zechel, S.; Geitner, R.; Abend, M.; Siegmann, M.; Enke, M.; Kuhl, N.; Klein, M.; Vitz, J.; Gräfe, S.; Dietzek, B.; Schmitt, M.; Popp, J.; Schubert, U. S.; Hager, M. D. *NPG Asia Materials* **2017,** 9, (8), e420-e420.
235. Bin Rusayyis, M. A.; Torkelson, J. M. *ACS Macro Lett.* **2022,** 11, (4), 568-574.
236. Zhou, Z.; Chen, S.; Xu, X.; Chen, Y.; Xu, L.; Zeng, Y.; Zhang, F. *Prog. Org. Coat.* **2021,** 154, 106213.
237. Jung, S.; Kim, S. Y.; Kim, J. C.; Noh, S. M.; Oh, J. K. *RSC Adv.* **2017,** 7, (42), 26496-26506.
238. Jakubowski, W.; Min, K.; Matyjaszewski, K. *Macromolecules* **2006,** 39, (1), 39-45.
239. Matyjaszewski, K.; Jakubowski, W.; Min, K.; Tang, W.; Huang, J.; Braunecker, W. A.; Tsarevsky, N. V. *Proceedings of the National Academy of Sciences of the United States of America* **2006,** 103, (42), 15309-15314.
240. Matyjaszewski, K.; Xia, J. *Chem. Rev.***2001,** 101, (9), 2921-2990.
241. Kamigaito, M.; Ando, T.; Sawamoto, M. *Chem. Rev.* **2001,** 101, (12), 3689-3745.
242. Wang, S.; Yang, Y.; Ying, H.; Jing, X.; Wang, B.; Zhang, Y.; Cheng, J. *ACS Appl. Mater. Interfaces* **2020,** 12, (31), 35403-35414.
243. Zhang, Z. P.; Rong, M. Z.; Zhang, M. Q. *Adv. Funct. Mater.* **2018,** 28, (11), 1706050.
244. Jia, Y.; Ying, H.; Zhang, Y.; He, H.; Cheng, J. *Macromol. Chem. Phys.* **2019,** 220, (12), 1900148.
245. Xie, D.-M.; Zhao, X.-L.; Li, Y.-D.; Weng, Y.; Zeng, J.-B. *Industrial Crops and Products* **2022,** 188, 115739.

246. Liu, W.-X.; Yang, Z.; Qiao, Z.; Zhang, L.; Zhao, N.; Luo, S.; Xu, J. *Nat. Commun.* **2019,** 10, (1), 4753.
247. Chen, B.; Liu, X.; Liu, J.; Feng, Z.; Zheng, X.; Wu, X.; Yang, C.; Liang, L. *React. Funct. Polym.* **2022,** 172, 105184.
248. Zhou, Z.; Zeng, Y.; Yu, C.; Li, Q.; Zhang, F. *Mater. Chem. Phys.* **2021,** 267, 124642.
249. Jiang, L.; Liu, Z.; Lei, Y.; Yuan, Y.; Wu, B.; Lei, J. *ACS Appl. Polym. Mater.* **2019,** 1, (12), 3261-3268.
250. Jud, K.; Kausch, H. H.; Williams, J. G. *J. Mater. Sci.* **1981,** 16, (1), 204-210.
251. Malinskii, Y. M.; Prokopenko, V. V.; Ivanova, N. A.; Kargin, V. S. *Polymer Mechanics* **1970,** 6, (3), 382-384.
252. Liang, X.; Jiang, T.; Feng, Y.; Lu, P.; An, J.; Wang, Z. L. *Adv. Energy Mater.* **2020,** 10, (40), 2002123.
253. Li, Y.; Guo, Z.; Zhao, Z.; Gao, Y.; Yang, P.; Qiao, W.; Zhou, L.; Wang, J.; Wang, Z. L. *Appl. Energy.* **2023,** 336, 120792.

Publications

1. **T. Patel**, J. K. Oh. Dynamic Covalent Adaptive Polymer Network Materials based on Hindered Urea Bonds. ***Journal of Macromolecular Science, Part A*** *2023. (Review)*

2. P. Nellepalli, **T. Patel**, M. Kim, J. Park, Z. Ye, H. Jung, H. Ko, J. K. Oh. Self-healable triboelectric nanogenerators based on ionic poly(hindered urea) network materials cross-linked with fluorinated block copolymers. ***Polymer Chemistry*** 2022. 13, 4343-4351

3. P. Nellepalli, **T. Patel**, J. K. Oh. Dynamic covalent polyurethane materials: synthesis and self-healability. ***Macromolecular Rapid Communications*** 2021. 42, 2100391 (Review)

4. G. Zhang, **T. Patel**, P. Nellepalli, S. Bhagat, H. Hase, A. M. Jazani, I. Salzmann, Z. Ye, J. K. Oh. Macromolecularly-engineered thermoreversible heterogeneous self-healable networks encapsulating reactive multidentate block copolymer-stabilized carbon nanotubes. ***Macromolecular Rapid Communications*** 2021. *42*, 2000514.

5. **T. Patel**, M. P. Kim, J. Park, T. H. Lee, P. Nellepalli, S. M. Noh, H. W. Jung, H. Ko, J. K. Oh. Self-healable reprocessable triboelectric nanogenerators fabricated with vitrimeric poly(hindered urea) networks. ***ACS Nano***, 2020, *14*, 11442–11451

6. S. H. Hong, **T. Patel**, S. Ip, S. Garg, J. K. Oh. Microfluidic assembly to synthesize dual enzyme/oxidation-responsive polyester-based nanoparticulates with controlled sizes for drug delivery**,** ***Langmuir*** 2018, *34*, 3316-3325.

7. S. Jung, **T. Patel**, J. K. Oh Thermally-labile self-healable branched gel networks fabricated by new macromolecular engineering approach utilizing thermoreversibility, ***Macromolecular Rapid Communications*** 2017.

Oral poster and presentation

1. Twinkal Patel, J.K. Oh. Development of Poly(hindered Urea) Networks for self-healable triboelectric nanogenerators. Canadian Chemistry Conference and Exhibition, Vancouver, BC, Canada, June, 2023 **(oral)**

2. Twinkal Patel, Jun Young Park, Hyun Wook Jung, J. K. Oh. Healable and re-processable hindered polyurea: synthesis and application. 103nd Canadian Chemistry Conference and Exhibition, Winnipeg, MB, Canada, May, 2020 **(oral)**

3. Twinkal Patel, Jun Young Park, Hyun Wook Jung, J. K. Oh. Healable and re-processable hindered polyurea: synthesis and application. Quebec Center for Advanced Materials Student Symposium, Montreal, QC, Canada, November 2019 **(Poster)**

4. Twinkal Patel, J. Y. Park, H. W. Jung, J. K. Oh. Exploration of hindered urea chemistry to synthesize dynamic crosslinked networks self-healable at ambient temperature. 30th Quebec/Ontario Mini-Symposium for Synthesis and Bioorganic Chemsitry, Ottawa, ON, Canada, Novemeber 2019 **(Poster)**

5. Twinkal Patel, J.K.Oh. New Macromolecular Engineering Approach Utilizing Thermoreversibility: Development of Thermally-Labile Networks with Robust Self-Healability. CSCAC-CQMF Advanced Materials Annual Conference 2017, Sherbrooke, QC, Canada, October 2017. **(Poster)**

Awards and Honours

1. CU Grad Incentive Fellow FAS ($54,000), Concordia University, QC, Canada (2020-2024)
2. Concordia conference and exposition award ($ 750), Concordia University, QC, Canada (2023).
3. Faculty of Arts and Science graduate student conferment award ($ 300), Concordia University, QC, Canada (2023)
4. Concordia conference and exposition award ($ 111.87), Concordia University, QC, Canada (2021).
5. Mitacs Globalink research award ($ 6,000), Mitacs Canada, South Korea (2020).